TECHNISCHE UNIVERSITÄT MÜNCHEN

Lehrstuhl für Molekulare Ernährungsmedizin

The Contribution of Liver-secreted Factors to Tissue Wasting in Cancer Cachexia

Claudia-Eveline Molocea

Vollständiger Abdruck der von der TUM School of Life Sciences der Technischen Universität München zur Erlangung des akademischen Grades eines

Doktors der Naturwissenschaften

genehmigten Dissertation.

Vorsitzender:	Prof. Dr. Dirk Haller
Prüfer der Dissertation:	1. Prof. Dr. Martin Klingenspor
	2. Prof. Dr. Stephan Herzig

Die Dissertation wurde am bei 29.06.2020 der Technischen Universität München eingereicht und durch die TUM School of Life Sciences am 24.11 .2020 angenommen.

"And though the course may change sometimes

Rivers always reach the sea"

-Led Zeppelin, 1975, Ten years gone

Dedicated to Vlad

(1987 - 2019)

Abstract

Cancer cachexia is a devastating multi-factorial condition observed in up to 70% of cancer patients, markedly reducing the quality of life, and estimated to be the direct cause of more than 20% of cancer-related deaths in humans. Cachexia is associated with massive loss of adipose tissue and skeletal muscle mass, but at the molecular level the etiology is incompletely understood and currently no effective therapeutic measures against cachexia exist. Cachexia represents an integrative, global metabolic response to tumor stimuli, characterized by defective energy utilization, increased catabolism, and systemic inflammation.

Traditionally, skeletal muscle and adipose tissue have been the focus of cachexia research, but recent studies suggest that cancer cachexia is a multi-organ syndrome. The functionality of multiple organs is affected during cachexia progression and these changes could further contribute to tissue wasting. Despite its central role as a metabolic regulator, the liver has received little attention in the context of cancer cachexia. However, hepatic metabolic dysfunction has been reported in cachexia and it is thought to contribute to inefficient energy utilization. Moreover, the hepatic activation of the Acute Phase Response (APR) is well documented in cachectic patients. The APR refers to an unspecific, early-defense mechanism that serves to clear potential pathogens, initiate inflammatory processes, and contribute to resolution and healing. A direct contribution of APR proteins to tissue wasting still needs to be formally proven.

The work presented in this thesis aimed at identifying liver/hepatocyte-secreted factors that are upregulated in cancer cachexia and to address their potential contribution to cachexia development. The first part addressed the contribution of three liver-secreted factors to wasting, while focusing on SAA 1/2, one of the main APR proteins. SAA 1/2 was upregulated in the serum of cachectic mice and humans, and treatment with recombinant SAA 1/2 led to decreased myotube width, *in vitro.* The contribution of SAA 1/2 to cachexia development *in vivo* was addressed by using a hepatocyte-specific knock-down (KD) approach in C26 tumor-bearing mice, which normally develop cachexia upon tumor cell implantation. Despite a significant reduction in circulating levels, SAA 1/2 was still highly upregulated in tumor-bearing mice relative to healthy controls and no effects on body weight (BW) loss were observed. The second part of the thesis focused on hepatocyte-secreted factors and identified twenty-four candidates which were strongly upregulated in cachectic mice. A number of these factors have been associated with the APR. Experiments using candidate-conditioned media (CM) showed that seven factors contributed to adipocyte-lipolysis, while five factors led to decreased myotube width. Studies in primary hepatocytes demonstrated that lipolysis factors are mainly under the control of STAT3 and Nf-KB, while, interestingly, GR activation seemed to be particularly important for the upregulation of the factors responsible for myotube-atrophy. Lastly, most of these candidates were downregulated after restoration of a transcriptional repressor, Rev-erbα, which rescued the BW loss in C26 mice. These results support the contribution of a hepatic cachectic program to cachexia development, that can be successfully targeted, to some extent, by interfering with the transcriptional regulators of hepatocyte-secreted factors.

Zusammenfassung

Tumorkachexie ist ein multifaktorielles Syndrom, das bei bis zu 70% der Krebspatienten vorkommt. Tumorkachexie ist durch einen ausgeprägten Verlust von Fettgewebe und Skelettmuskelmasse charakterisiert und wirkt sich negativ auf die Lebensqualität der betroffenen Krebspatienten aus. Schätzungen zufolge stellt Kachexie die direkte Ursache für mehr als 20% der krebsbedingten Todesfälle dar. Die Ursachen der Enstehung von Tumorkachexie sind auf molekularer Ebene nur unvollständig geklärt und es gibt derzeit keine effektive therapeutische Maßnahme. Kachexie ist durch eine systemische, metabolische Reaktion auf Tumorsignale bedingt, die durch gestörte Energienutzung, erhöhten Katabolismus und chronischer Entzündung charakterisiert ist.

Traditionell wurden in der Kachexieforschung vornehmlich Skelettmuskeln und Fettgewebe untersucht. Neuere Studien weisen jedoch darauf hin, dass Tumorkachexie ein Multiorgansyndrom darstellt. Die Funktionalität mehrerer Organe ist durch die Kachexie betroffen und diese Änderungen können zum Gewebeverlust beitragen. Trotz ihrer zentralen Rolle in der Regulation des Stoffwechsels hat die Leber bisher wenig Aufmerksamkeit im Kontext von Tumorkachexie erhalten. Hepatische Stoffwechselstörungen bei Kachexie sind jedoch bekannt und es wird angenommen, dass diese zur ineffizienten Energienutzung beitragen. Außerdem ist die Aktivierung der hepatischen Akute-Phase-Reaktion (APR) bei Kachexie-Patienten bereits gut dokumentiert. Die APR bezeichnet einen unspezifischen und akute Abwehrmechanismus, der dazu dient, potenzielle Krankheitserreger zu beseitigen, weitere Entzündungsprozesse auszulösen, sowie zur Beendigung von Entzündung und zu Heilungsprozesse beizutragen. Ein direkter Beitrag von APR-Proteinen zum Gewebeverlust bei Kachexie ist formal aber noch nicht nachgewiesen worden.

Das Ziel dieser Doktorarbeit war die Identifizierung von bei Tumorkachexie hochregulierten Leber- und Hepatozyten-sezernierte Proteinfaktoren, sowie die Bestimmung ihres potenziellen Beitrags zur Entwicklung der Kachexie. Der erste Teil der Arbeit behandelte den Beitrag von vier Leber-sezernierten Faktoren zur ungewollten Gewichtsabnahme, mit Fokus auf SAA 1/2, eines der wichtigsten APR-Proteine. Die Spiegel von SAA 1/2 waren im Serum von kachektischen Mäusen und Menschen erhöht und die Behandlung mit rekombinantem SAA 1/2 führte in vitro zu einer Verringerung der Myotubendurchmessern. Der Beitrag von SAA 1/2 zur Entwicklung der Kachexie in vivo wurde unter Verwendung eines Hepatozyten-spezifischen Knock-down-Ansatzes (KD) bei C26-tumortragenden Mäusen untersucht, die bedingt durch die Implantation von C26-Tumorzellen eine Kachexie entwickeln. Trotz einer deutlichen Verringerung der zirkulierenden Spiegel von SAA 1/2 bei tumortragenden Mäusen nach Hepatozyten-spezifischen KD, waren SAA1/2-Spiegel im Vergleich zu gesunden Kontrollen immer noch stark erhöht, so dass keine Auswirkung auf den Verlust des Körpergewichts beobachtet wurde.

Der zweite Teil der Arbeit konzentrierte sich auf Hepatozyten-spezifischen Proteinfaktoren und identifizierte vierundzwanzig Kandidaten, die bei kachektischen Mäusen stark hochreguliert waren. Einige dieser Faktoren konnten mit der APR in Verbindung gebracht werden. Experimente mit konditionierten Medien (CM) für einzelnen Kandidaten zeigten, dass sieben der Faktoren zur Adipozytenlipolyse beitrugen, während fünf Faktoren zu einer verringerten Myotubendicke führten. Untersuchungen an primären Hepatozyten zeigten, dass Lipolysefaktoren hauptsächlich unter der Kontrolle von STAT3 und Nf-KB stehen, während interessanterweise die Glukokortikoid Rezeptor (GR)-Aktivierung für die Hochregulation der für die Myotubenatrophie verantwortlichen Faktoren besonders wichtig zu sein schien. Schließlich wurden die meisten dieser Kandidaten nach Wiederherstellung des Transkriptionsrepressors Rev-erbα, die dem Körpergewichtsverlust bei C26-Mäusen entgegen wirkte, signifikant herunterreguliert. Diese Ergebnisse stützen die

Hypothese, dass ein Tumorkachexie-assoziiertes hepatisches Programm zur Kachexieentwicklung beiträgt. Diesem hepatischen Tumorkachexie-Programm kann , bis zu einem gewissen Grad, durch die Manupulation der an der Regulation der Leber-sezernierten Faktoren beteiligten Transkriptionsfaktoren entgegen gewirkt werden.

Acknowledgments

This work could not have been possible without the support, guidance, and contribution of so many people that I wish to acknowledge here.

Firstly, I would like to thank Prof. Dr. Stephan Herzig and Dr. Mauricio Berriel Diaz for giving me the opportunity to work on this project under their supervision. I appreciate their guidance and commitment. I would also like to thank the members of my TAC committee, Prof. Dr. Martin Klingenspor and Prof. Dr Achim Krüger for helpful comments and discussions and Prof. Dr. Dirk Haller for being the chair of my examination. Special thanks to Dr. Sören Fisker-Schmidt for mentoring me. I am grateful for his patience and guidance, and for all the fruitful discussions that instilled great scientific excitement.

I would also like to acknowledge all the current and past members of the IDC, and particularly the MAC division, for great input and help and for creating such a nice work atmosphere. Special thanks to Victor, Juliano, Adriano, Miriam, Susi and Phivos for always providing a helpful hand, to Götz for always pushing me to challenge myself and grow and to Katarina for all the helpful input on my thesis.

I am grateful for all the friends that I made during my time at the IDC. Coffee breaks with Ana, Asrar, Katarina and Phivos were a great way to get helpful input on my project, to discuss ideas and to get philosophical about the role of science in society. Christina's willingness to always listen and advise me was incredibly valuable, especially in the beginning of my PhD. Your friendship means the world to me!

My deepest gratitude goes to my friends and family, who supported me through the most difficult times of my life: Vlad's family-Veronica, Dan, and Roxana-, my parents-Nicoleta and Robert-, and my dearest friend, Manuela.

Lastly, but most importantly, I would not be where I am today without Vlad's unconditional love and support. When I was unsure about moving to Munich for my Master's, he wrote a song encouraging me to "Take a chance while it's here/ Brush off all your fears". When I was not sure if I should pursue a PhD, he listed all my accomplishments and relentlessly told me how smart I am. He listened and comforted me every time I was frustrated or disappointed and he always believed in me, even when I doubted myself. Thank you! I will miss you forever!

Table of Contents

ABSTRACT I
ZUSAMMENFASSUNG II
ACKNOWLEDGMENTS IV
LIST OF FIGURES ..... - 1 -
LIST OF TABLES ..... - 3 -
LIST OF ABBREVIATIONS ..... - 4 -
1. INTRODUCTION ..... - 6 -
CANCER CACHEXIA: PREVALENCE AND PATHOPHYSIOLOGY ..... - 6 -
Skeletal muscle atrophy ..... - 6 -
Adipose tissue atrophy ..... - 8 -
MOUSE MODELS OF CANCER CACHEXIA ..... - 8 -
CANCER CACHEXIA: A MULTI-ORGAN SYNDROME ..... - 9 -
Hepatic dysfunction in cachexia ..... - 9 -
SELECTION OF THE INITIAL LIVER-SECRETED CANDIDATES ..... - 11 -
SELECTION OF THE HEPATOCYTE-SECRETED FACTORS ..... - 12 -
AIMS OF THE STUDY ..... - 13 -
Establishment of the screening pipeline using SAA 1/2, LCN2 and PAI-1 ..... - 13 -
Screening pipeline optimization and functional characterization of hepatocyte-secreted factors in vitro - 14 -
2. RESULTS ..... - 15 -
2.1 LIVER-SECRETED FACTORS SCREEN ..... - 15 -
Murine serum levels of liver-secreted factors ..... - 15 -
Serum levels of liver-secreted factors in human patients ..... - 16 -
Functional investigation in vitro: 3T3-L1 adipocyte lipolysis ..... - 17 -
Functional investigation in vitro: C2C12 myotube atrophy ..... - 17 -
Hepatocyte-specific SAA 1/2 KD in vivo ..... - 18 -
2.2 HEPATOCYTE-SECRETED FACTORS SCREEN ..... - 23 -
Functional investigation in vitro: 3T3-L1 adipocyte lipolysis ..... - 23 -
Functional investigation in vitro: C2C12 myotube atrophy ..... - 26 -
Upstream regulation of hepatocyte-secreted factors ..... - 29 -
3. DISCUSSION ..... - 35 -
3.1 MULTIPLE LIVER/HEPATOCYTE-SECRETED FACTORS CONTRIBUTE TO CACHEXIA DEVELOPMENT ..... - 35 -
3.2 UPSTREAM REGULATORS OF THE HEPATIC "CACHECTIC PROGRAM" ..... - 37 -
4. MATERIAL AND METHODS ..... - 40 -
4.1 MATERIAL ..... - 40 -
Chemicals ..... - 40 -
Primers ..... - 40 -
Antibodies ..... - 42 -
Plasmids ..... - 42 -
miRNA SAA sequences ..... - 42 -
Cytokines and recombinant proteins ..... - 43 -
Kits ..... - 43 -
Instruments ..... - 44 -
Consumables ..... - 45 -
4.2 METHODS ..... - 47 -
Cell culture ..... - 47 -
Molecular biology & biochemistry ..... - 49 -
ANNEX ..... - 52 -
PUBLICATIONS ..... - 54 -
REFERENCES ..... - 55 -

List of figures

Figure 1. Signaling pathways involved in skeletal muscle protein synthesis and degradation in cancer cahexia. ..... - 7 -

Figure 2. The contribution of hepatic dysfunction to cancer cachexia. Futile metabolic cycles and nutrient exchange between the liver and the tumor contribute to inefficient energy utilization. ..... - 11 -

Figure 3. Schematic representation of the generation of Alb-INTACT mice that allow for the isolation of hepatocyte nuclei. ..... - 13 -

Figure 4. Steps involved in the liver-secreted factors screen ..... - 14 -

Figure 5. Steps involved in the hepatocyte-secreted factors screen. ..... - 14 -

Figure 6. Liver-secreted factors identified in RNA-seq are upregulated in the serum of cachectic mice. ..... - 15 -

Figure 7. (A, B) SAA 1/2 and (C, D) LCN2 are upregulated in the serum of cancer patients. ..... - 16 -

Figure 8. 3T3-L1 glycerol release in culture media upon treatment with (A) SAA 1/2, (B) LCN2 and for 24hrs ..... - 17 -

Figure 9. C2C12 myotube diameter upon treatment with (A) SAA 1/2, (B) LCN2 for 48hrs ..... - 18 -

Figure 10. Intracellular FLAG protein levels upon miRNA mediated KD in HEK 293A cells expressing either (A) SAA 1 or (B) SAA 2. ..... - 19 -

Figure 11. Schematic representation miR-LP1-AAV-SAA 1/2 KD *in vivo* experimental design ..... - 19 -

Figure 12. SAA 1/2 KD *in vivo* does not affect cachexia development ..... - 21 -

Figure 13. Tumor size progression over the course of the experiment ..... - 22 -

Figure 14. SAA 1/2 treatment does not affect C26 proliferation *in vitro* ..... - 22 -

Figure 15. (A) CM generation in HEK293A cells and (B) quantification of FLAG protein in concentrated candidate-CM ..... - 23 -

Figure 16. 3T3-L1 lipolysis optimization ..... - 24 -

Figure 17. 3T3-L1 lipolysis upon candidate-CM treatment ..... - 25 -

Figure 18. C2C12 myotube-atrophy optimization ..... - 27 -

Figure 19. C2C12 myotube-atrophy upon candidate-CM treatment ..... - 28 -

Figure 20. Cachexia-signature genes respond to STAT3 (IL-6), NF-kb (IL-1β) and GR (Corticosterone) activation in primary hepatocyte ..... - 29 -

Figure 21. pre-mRNA expression of adipocyte-lipolysis hits upon STAT3 (IL-6), NF-kb (IL-1β) and GR (Corticosterone) activation in primary hepatocytes ..... - 30 -

Figure 22. Mature mRNA expression of adipocyte-lipolysis hits upon STAT3 (IL-6), NF-kb (IL-1β) and GR (Corticosterone) activation in primary hepatocytes. ..... - 31 -

Figure 23. pre-mRNA expression of myotube-atrophy hits upon STAT3 (IL-6), NF-kb (IL-1β) and GR (Corticosterone) activation in primary hepatocytes ..... - 31 -

Figure 24. Mature mRNA expression of myotube-atrophy hits upon STAT3 (IL-6), NF-kb (IL-1β) and GR (Corticosterone) activation in primary hepatocytes. ..... - 32 -

Figure 25. Overview of transcriptional regulation of adipocyte-lipolysis and myotube-atrophy hits ..... - 32 -

Figure 26. Hepatic NR1D1 expression upon AAV-mediated hepatocyte-specific overexpression ..... - 33 -

Figure 27. mRNA regulation of adipocyte-lipolysis hits upon Rev-erbα OE in C26 mice ..... - 34 -

Figure 28. mRNA regulation of myotube-atrophy hits upon Rev-erbα OE in C26 mice. ..... - 34 -

List of tables

Table 1. Protocols used for 3T3-L1 differentiation in 96-well plates. - 23 -
Table 2. Chemicals - 40 -
Table 3. qPCR primers - 40 -
Table 4. Antibodies - 42 -
Table 5. Plasmids - 42 -
Table 6. Sequences of miRNAs targeting SAA - 42 -
Table 7. Cytokines and recombinant proteins - 43 -
Table 8. Kits - 43 -
Table 9. Instruments - 44 -
Table 10. Consumables - 45 -
Table 11. Media used for cell culture - 47 -
Table 12. Murine and human serum dilutions - 50 -

List of abbreviations

AA	Amino acids
AAV	Adeno-associated virus
ActRI/II	Activin Receptor type I/II
AKT	Protein Kinase B
ALS	Autophagy-lysosome system
APC	Adenomatous polyposis coli
APR	Acute phase response
ATGL	Adipose triglyceride lipase
ATP	Adenosine triphosphate
BAT	Brown adipose tissue
BW	Body weight
cAMP	Cyclic adenosine monophosphate
cGMP	Cyclic guanosine monophosphate
CM	Conditioned media
CNS	Central nervous system
CPR	C-reactive protein
CRC	Colorectal cancer
Dex	Dexamethasone
ECM	Extracellular matrix
ELISA	Enzyme-linked immunosorbent assay
FFA	Free fatty acid
FOXO	Forkhead box transcription factors
GC	Glucocorticoid
GC muscle	Gastrocnemius
GDF-15	Growth differentiation factor-15
GEMM	Genetically engineered mouse models
GI	Gastrointestinal tract
GR	Glucocorticoid receptor
HSL	Hormone sensitive lipase
IBMX	3-Isobutyl-1-methylxanthine
IFNγ	Interferon gamma
IGF-1	Insulin-like growth factor 1

IL-1	Interleukin 1
IL-6	Interleukin 6
JAK	Janus Kinase
KD	Knock-down
KPC	Kras; p53; Cre
KPP	Kras; p48; Pten
LCN2	Lipocalin 2
LP1 promoter	Liver promoter 1
LPL	Lipoprotein lipase
LPS	Lipopolysaccharide
mRNA	messenger RNA
miRNA	micro RNA
mTOR	mammalian target of rapamycin
Nf-KB	Nuclear Factor kappa-light-chain-enhancer of activated B cells
PAI-1	Plasminogen activator inhibitor-1
PDAC	Pancreatic ductal adenocarcinoma
PI3K	Phosphatidylinositol 3-kinase
PIF	Proteolysis-inducing factor
PKA	Protein Kinase A
PKG	Protein Kinase G
PPARα	Peroxisome proliferator-activated receptor alpha
Rosi	Rosiglitazone
RT	Room temperature
SAA	Serum amyloid A
SR-B1	Scavenger receptor class B type 1
STAT3	Signal transducer and activator of transcription 3
TG	Triglycerides
TGF-β	Transforming growth factor beta
TLR	Toll like receptor
TNFα	Tumor necrosis factor α
UCP1	Uncoupling protein 1
UPS	Ubiquitin proteasome system
WAT	White adipose tissue
ZAG	Zinc-α2-glycoprotein

1. Introduction

Cancer cachexia: prevalence and pathophysiology

Cancer is the second leading cause of death worldwide, accounting for approximately 9.6 million deaths in 2018 [1]. Cancer cachexia refers to a multifactorial syndrome characterized by ongoing loss of muscle mass (with or without loss of adipose tissue) which cannot be fully reversed by nutritional support alone [2]. It affects up to 50-80% of cancer patients and it is associated with reduced quality of life, decreased tolerance to therapy and reduced survival [3]. Cachexia is not usually listed as a cause of death so exact numbers are lacking, but approximately half of the total number of cancer related deaths are due to cancers that are most frequently associated with cachexia, such as pancreatic ductal adenocarcinoma (PDAC), esophageal, gastric, pulmonary, hepatic and colorectal cancer (CRC) [4]. Clinical management of cachexia is challenging and to date no standard of care in terms of pharmacotherapy exists. The complexity of the disease and the late stage diagnosis contribute to the low success rates of current therapies [5].

Clinically, cachexia is diagnosed as involuntary weight loss ≥ 5%, and three disease stages have been proposed: pre-cachexia, cachexia, and refractory cachexia. Not all patients go through all stages and the ones diagnosed with refractory cachexia have a life expectancy of less than 3 months [2]. Pathophysiologically, cachexia is characterized by a negative protein and energy balance regulation driven both by inadequate food intake as well as abnormal metabolism. In cachectic patients, energy intake is usually lower than the resting energy expenditure, and resistance to anabolic signals and an overall catabolic state have been documented [4]. However, unlike starvation, where mostly adipose tissue is affected, in cachexia skeletal muscle is one of the main tissues affected by wasting, suggesting that anorexia alone cannot account for the decrease in weight [6]. The energetic cost of the tumor, which can range from 190 to 470 kcal/kg tumor/day [7] is also an important contributor to elevated energy expenditure, although tumor size has not been correlated with the severity of cachexia, in contrast to tumor stage and localization [8]. Further contributors to high energy demands are also represented by inflammation and futile substrate cycles such as an increase in Cori cycle in the liver and increased glucose and triacylglycerol/fatty acids flux [4, 8] which lead to ATP depletion. Moreover, decreased mitochondrial production of ATP in skeletal muscle has also been documented in animal models, but still needs to be formally proven in humans [3, 4]. Beyond the energy imbalance and metabolic dysfunction aspects of cancer cachexia, several cytokines and secreted factors, derived both from tumor and host cells, have been described to be directly involved in tissue wasting [4].

Skeletal muscle atrophy

Loss of skeletal muscle mass is one of the key features of cancer cachexia and is generally ascribed to reduced protein synthesis, increased degradation, or a relative imbalance of these processes [8]. Under physiological condition, activation of the PI3K/AKT signaling pathway, by insulin or IGF-1, simultaneously leads to increased protein synthesis via mTOR activation and inhibition of protein degradation via FOXO phosphorylation (Figure 1) [9]. However, anabolic signaling is perturbed in cancer cachexia since insulin resistance and decreased levels of IGF-1 have been reported in both cancer patients and animal models [6].

Together with Nf-KB and STAT3, the FOXO family of transcription factors regulate the key players of skeletal muscle degradation: the E3 ligases Atrogin-1 and MuRF-1 (Figure 1) [9]. These proteins

trigger the polyubiquitination of myofibrillar proteins targeted for degradation in the ubiquitin-proteasome system (UPS) [10]. Although the UPS is the best described process involved in protein degradation, the autophagy-lysosomal system (ALS) is getting more and more attention in the context of cancer cachexia as autophagy-related genes are upregulated in atrophic muscle [9]. FOXO3 and SMAD protein complexes are reported to activate the ALS in cachexia conditions (Figure 1) [9, 11]. Moreover, FOXO3 has also been linked to apoptosis [12], which could constitute another mechanism of skeletal muscle loss.

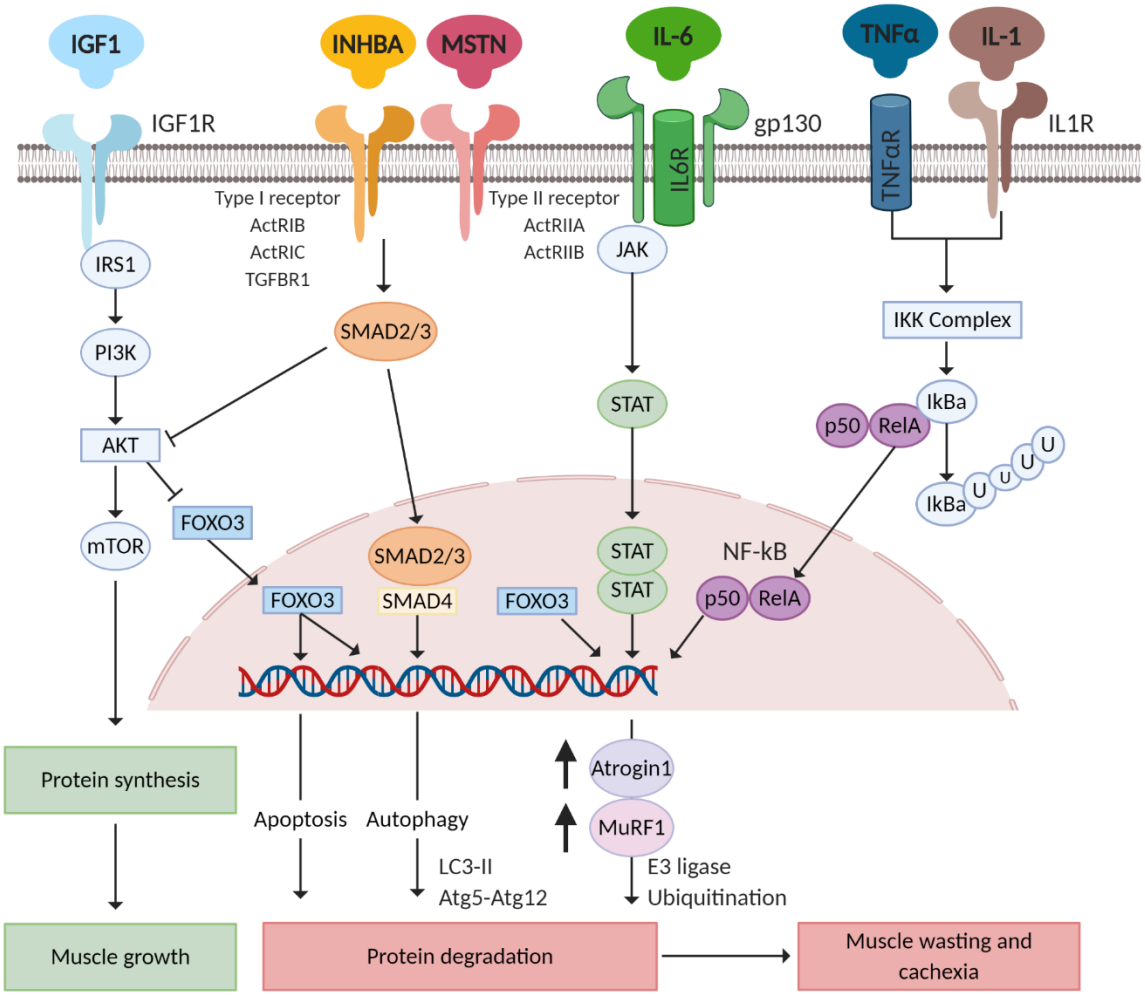

Figure 1. Signaling pathways involved in skeletal muscle protein synthesis and degradation in cancer cahexia. Inflammatory cytokines and members of the TGF-β family activate pathways that lead to proteolysis while inhibiting signals that lead to muscle growth. Adapted from [13]. Abbreviations: IHBA, Activin A; MSTN, Myostatin.

The complex regulatory network that maintains skeletal muscle homeostasis is heavily disrupted in cancer cachexia by several tumor and host-derived factors and cytokines [6]. Systemic inflammation plays a crucial role in mediating these effects since TNFα, IL-6 and IL-1 are important inducers of skeletal muscle atrophy (Figure 1) [8]. By binding to their respective receptors, TNFα and IL-1 allow translocation of Nf-KB to the nucleus where it activates transcription of Atrogin-1 and MuRF-1 [13]. Similarly, IL-6 receptor binding activates the JAK/STAT3 pathway which also activates the transcription of E3 ligases [14]. Particular attention has been given to members of the TGF-β family. The roles of TGF-β, Myostatin, Activin A and GDF-15 in mediating muscle wasting have been well described in cachexia [8, 9]. For instance, the myokines Myostatin and

Activin bind ActRI and ActRII receptors and activate SMAD2/3 which translocates to the nucleus and induces transcriptional changes that lead to muscle wasting [13]. Moreover, Myostatin negatively regulates AKT signaling therefore contributing to both reduced protein synthesis and increased protein degradation [15]. Although Myostatin is predominantly expressed in skeletal muscle, tumor cells have also been reported to secrete it [9]. In fact, tumor cells are also a source of inflammatory cytokines, as well as tumor-specific factors, such as Proteolysis-inducing factor (PIF), which were associated with skeletal muscle atrophy in animal models [8].

Adipose tissue atrophy

Traditionally, skeletal muscle wasting has been the focus of cancer cachexia research, but a substantial amount of weight loss in patients is attributed to fat mass wasting [4]. Fat loss develops more rapidly than lean mass loss and can be a predictor of survival in cachectic patients [16]. Murine studies have also demonstrated that fat loss might predispose muscle to wasting, since inhibition of lipolysis showed protective effects on muscle mass [17]. Furthermore, increased deposition of intramyocellular lipid droplets has also been reported in cachectic patients and associated with weight loss [18], and it has been shown that the presence of free fatty acids (FFAs) and ceramides in muscle inhibit protein synthesis and promote breakdown [19].

The depletion of adipose tissue occurs mainly due to lipolysis, and not apoptosis of fat cells [4] and results from a combination of decreased food intake, tumor derived factors and systemic inflammatory cytokines that lead to lipolysis and/or reduce lipogenesis [8]. Lipolysis occurs when triglycerides (TGs) are hydrolyzed to FFAs and glycerol which are released in the circulation. ATGL and HSL are the enzymes that mediate intracellular lipolysis of stored TGs, while LPL is responsible for cleaving circulating lipoprotein-incorporated TGs [20]. While in animal models of cachexia FA uptake and TG synthesis are decreased in the adipose tissue, in humans cachexia is mostly associated with normal lipid synthesis but increased lipolysis [21], suggesting that lipid catabolism is more relevant than a reduction in lipid synthesis. Indeed, increased HSL activity, plasma FFAs and glycerol were documented in cachectic patients, together with a 2-3-fold enhanced lipolytic activity in response to lipolytic stimuli [22]. Furthermore, genetic ablation of ATGL and HSL prevented lipolysis in a cachectic mouse model and preserved fat mass [17].

In adipocytes, lipolysis is mediated by hormones or mediators (e.g. adrenaline, norepinephrine, and glucagon) that lead to an increase in cAMP levels. cAMP binds and activates PKA which activates ATGL [23] and HSL [20], leading to TG hydrolysis. Brain and atrial natriuretic peptides can also activate lipolysis, via a cGMP/PKG pathway that also leads to HSL phosphorylation and activation [24]. Insulin inhibits lipolysis by activating PI3K and depleting cAMP levels, and insulin resistance is a common feature of cancer cachexia which further contributes to increased rates of lipolysis [8]. In the context of cancer cachexia, lipolysis can be induced by multiple tumor and host derived factors such as hormones (glucocorticoids and catecholamines), cytokines (TNFα, IL-1β and IL-6) and Zinc-α2-glycoprotein (ZAG), an adipokine that can also be secreted by tumors [21].

Mouse models of cancer cachexia

Several murine models for the study of cancer cachexia are available, either as tumor cell implantation or genetically engineered mouse models (GEMM). C26 tumor-bearing mice represent a well characterized and used subcutaneous model of CRC associated with cachexia. Upon C26 tumor growth, mice develop body and skeletal muscle weight loss, particularly due to increased fat and muscle catabolism [25]. Generally, a tumor that accounts for up to 10% of the total BW leads to 20-25% decrease in muscle mass and a severe depletion of fat mass [26].

Cachectic C26 mice also display hepato- and splenomegaly along with increased activation of the APR and circulating levels of pro-inflammatory cytokines [27]. In contrast, subcutaneous implantation of MC38 CRC cells has no impact on BW, fat and skeletal muscle loss [28], and is used as non-cachectic controls for C26 cells. Mice with mutations in the tumor suppressor Adenomatous polyposis coli (APC) develop multiple intestinal adenomatous polyps [28]. ApcMUT mice are commonly used to study cancer cachexia in a GEMM since the development of polyps is accompanied by BW, fat and skeletal mass loss, as well as anemia [28, 29]. As opposed to the C26 model, where cachexia develops rapidly, largely three weeks after tumor implantation [26], cachexia progression is slower in ApcMUT mice that lose 20-25% of their BW 10-15 weeks after the polyps develop [29]. Although PDAC is one of the most aggressive cancers, highly associated with cachexia, widely accepted mouse models are still lacking [30]. Genetically modified KPC mice exhibit features of cachexia and, recently, a subcutaneous model that uses KPC cells has also been developed and shown to recapitulate the cachectic phenotype [31]. However, it has been argued that the muscle gene expression observed in C26 mice does not resemble that of human patients, and that severity of the pancreatic diseases of KPC mice does not correlate with the degree of BW loss [32]. A new genetically engineered PDAC mouse model, KPP, appears to overcome this issue [32], but there is still a need for the generation of both implantation and GEMM models that better recapitulate the molecular aspects of human cachexia. Therefore, it is important to employ multiple cachexia models to avoid studying model-specific changes.

Cancer cachexia: a multi-organ syndrome

As early as the 1950s, cancer cachexia has been recognized as a standalone entity that was independent of the effects of reduced food intake or the mechanical interference of tumors on surrounding tissues and was associated with systemic inflammation [21]. In the early 1980s, IL-1 was shown to induce protein breakdown in skeletal muscle and Cachectin/TNFα was the first identified mediator of cancer cachexia [33]. The majority of research, from that point on, has focused on the mechanisms of skeletal muscle wasting [21]. However, in recent years it has been increasingly recognized that cachexia is a multifactorial disease that involves the cooperation of several tumor and host derived signals and that targets multiple organs [34]. Alterations to the cardiac muscle are often present in mouse models of cachexia, where cardiac atrophy and dysfunction have been documented [4]. The circulatory system is also affected as increased thrombin generation and increased platelet counts have been reported in mouse models [35]. This can lead to hypercoagulability and increase the risk of thrombosis. Perturbances in the CNS and GI tract further contribute to anorexia and inflammation and support energy imbalance [36]. The activation of brown adipose tissue (BAT) has also been proposed to contribute to increased energy expenditure in cachexia [37] since increased expression of UCP1 leads to heat generation by uncoupling oxidative phosphorylation from ATP production [36]. However, mice lacking UCP1 are not protected against cachexia and mice housed at thermoneutrality develop cachexia at the same rate as mice kept at room temperature (RT), therefore questioning the role of BAT in cachexia development [38].

Hepatic dysfunction in cachexia

The liver is at the center of multiple physiological processes, including macronutrient metabolism, endocrine control of growth factors, lipid homeostasis, blood volume regulation, metabolization of xenobiotics and immune system support [39]. Hepatocytes (parenchymal cells) represent 60% of the liver's cellular composition while multiple sinusoidal cells account for the rest [40]. The

non-parenchymal cell fraction is divided into sinusoidal endothelial cells (44%), Kupffer cells (33%), stellate cells (10-25%) and hepatic NK cells (5%) [40].

Despite its central role as a metabolic mediator, the liver has received little attention in the context of cancer cachexia. However, the liver undergoes multiple histological and metabolic changes during cachexia progression [41]. Hepatic metabolic dysfunction can contribute to energy imbalance in cancer cachexia in several different ways (Figure 2). Firstly, decreased hepatic oxidative phosphorylation and increased Cori cycle activity can contribute to energy loss [34]. Secondly, hepatic steatosis has been documented in cachectic patients and pre-clinical studies suggest that hepatic mobilization of TG stores is impaired in cachexia [21]. Additionally, it has been recently shown that ketogenesis is reduced in cachectic mice in response to food depravation due to a decrease in Peroxisome proliferator-activated receptor alpha (PPARα), which leads to an increase in glucocorticoid (GC) levels that can further contribute to skeletal muscle wasting [42].

Besides the metabolic changes, cachexia is also associated with increased activation of APR in the liver [8]. The APR refers to an acute and unspecific inflammatory response to infection, tissue injury, tumor growth or immunological disorders, consisting in the synthesis, primarily by hepatocytes, and release into circulation of a plethora of proteins with diverse functions [34]. APR proteins serve to clear potential pathogens, initiate inflammatory processes, and contribute to resolution and healing. IL-6 is the main cytokine responsible for the APR activation in the hepatocytes, but IL-1, TNFα and IFNγ can also elicit this response [43]. Kupffer cells acts as intermediators of the APR since, upon pro-inflammatory stimulation, they secrete and present IL-6 to hepatocytes [44]. Normal liver protein synthesis can be divided into fixed (including structural cytoplasmic and mitochondrial proteins) and export proteins (such as APR proteins) whose production takes place in an even fashion [45]. However, in cachectic patients the rate of the fixed hepatic protein synthesis is decreased by approximately 30% while the rate of export protein synthesis is increased [46]. As the body prioritizes the production of export proteins in cancer cachexia, protein mobilization from peripheral tissues, such as muscle, might be employed in order to provide sufficient substrate for the APR (Figure 2) [8]. Individual APR proteins, such as Serum Amyloid A (SAA) and fibrinogen, have been shown to contribute to muscle atrophy in other disease models and increased hepatic production of coagulation factors can contribute to hypercoagulability in murine models [35, 47]. This suggest that APR proteins could also have a more direct role in cachexia development but considering the number and the diverse roles of APR proteins, this is yet to be formally proven (Figure 2).

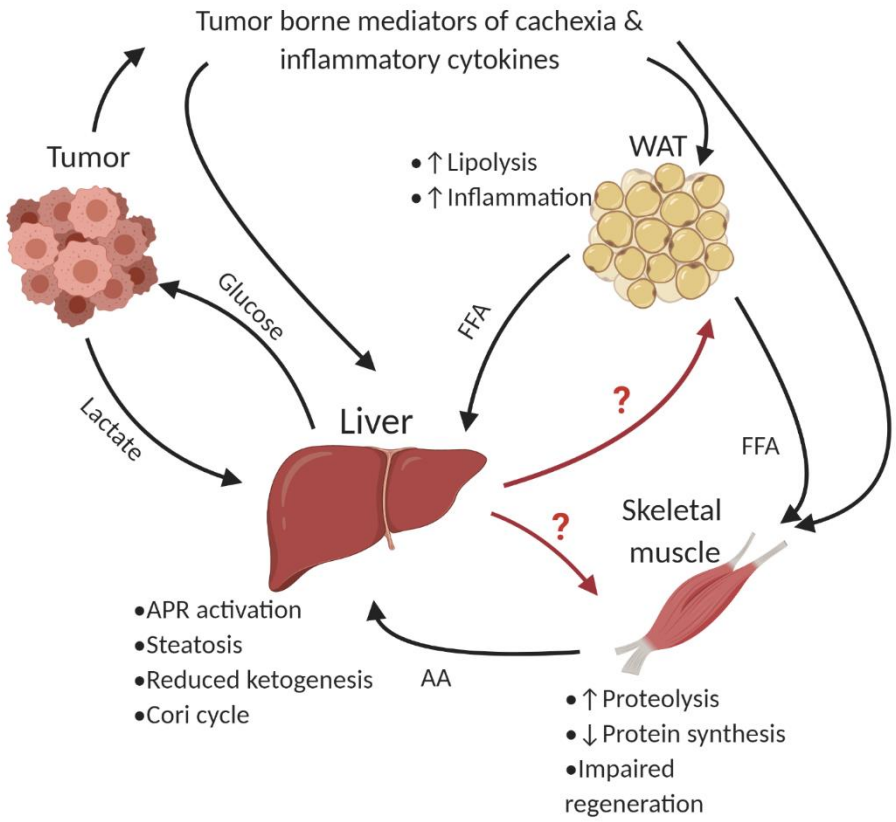

Figure 2. The contribution of hepatic dysfunction to cancer cachexia. Futile metabolic cycles and nutrient exchange between the liver and the tumor contribute to inefficient energy utilization. Systemic alterations in response to tumors lead to white adipose tissue (WAT) and skeletal muscle atrophy, which feedback to the liver and contribute to hepatic dysfunction. Formal proof of the direct contribution on liver-derived factors to tissue wasting is still required. Abbreviations: FAA, Free-fatty acids; AA, Amino acids.

Selection of the initial liver-secreted candidates

To study the role of liver-secreted factors in mediating cancer cachexia, an initial data set was generated by performing RNA-seq analysis on whole liver tissues from multiple cachectic (CRC: C26 and ApcMUT, PDAC: 8025) and non-cachectic (CRC: MC38) tumor models. A preliminary list of candidates was created by selecting genes that were highly upregulated in cachectic conditions. This list was cross-referenced with public data from healthy mice to allow selection of liver specific factors that are predicted to be secreted. Published literature on APR supported the idea that circulating levels of the selected factors were mainly hepatocyte-derived [48]. These analyses were performed by Sören Fisker-Schmidt and led to the selection of Serum Amyloid A 1/2 (SAA 1/2), Lipocalin-2 (LCN2) and Plasminogen activator inhibitor-1 (PAI-1) for further functional characterization, none of which have been described in the context of cancer cachexia so far.

Together with C-reactive protein (CRP), SAA are the main APR proteins. SAAs are a family of apolipoproteins, highly conserved in mammals and birds. Four isoforms exist with SAA 1 and SAA 2 showing 96% homology over their entire length [49]. During inflammation, IL-1 and IL-6 synergistically act to induce SAA, which is upregulated up to 1000x, and GCs were also reported to enhance its activation [50]. The liver is the major site of SAA production, but extrahepatic tissues have also been shown to contribute to its release. The roles of SAA are not yet completely clear and its contribution to amyloid formation is one of the best characterized function. However,

multiple roles for SAA have been proposed, including lipid metabolism/ transport, induction of ECM-degrading enzymes and chemotactic recruitment of inflammatory cells [50]. This is further supported by the fact that SAA can bind at least eight receptors, including Toll-like receptors (TLRs) and SR-B1, suggesting a diverse functional area for SAA [49]. Interestingly, by binding to TLR2 and inducing IL-6 and TNFα production in C2C12 myotubes, SAA led to decreased myotube width [51].

LCN2 is also an APR protein, highly upregulated during injury, infection, and other inflammatory stimuli [52]. LCN2 is an important part of the innate immune system as it sequesters siderophores, small molecules secreted by bacteria to scavenge soluble ferric iron for vital bacterial cellular processes [53]. Increased LCN2 levels have been associated with inflammatory and metabolic disease progression [54], but its role in cancer progression is still unclear. Studies show that LCN2 can promote proliferation and dissemination of endometrial, breast cancer and pancreatic cancer [53, 55], but it has also been reported that LCN2 can suppress metastatic potential of CRC cancer cells [56]. Experiments performed in renal cancer suggest that the iron load of LCN2 defines its pro-tumor function [57]. LCN2 is expressed in multiple tissues (kidney, tumor, adipose tissue, bone, immune cells) [53], but hepatocyte-specific LCN2 knock-out (KO) models demonstrated that during infection 90% of circulating levels of LCN2 are hepatocyte-derived and that the IL-6/STAT3 pathway is crucial for its induction [58].

PAI-1 is a serine protease inhibitor that acts as the principal inhibitor of the tissue-type and the urinary-type plasminogen activator [59]. Plasminogen activation is required for the degradation of blood clots, therefore increased PAI-1 levels can contribute to fibrin deposition and tissue damage [59]. As with SAA 1/2 and LCN2, PAI-1 is also a part of the APR [60] and its levels have been reported to be increased in cancer, thrombosis, atherosclerosis [61]. Although PAI-1 is expressed in multiple cells types, such as platelets, adipocytes, smooth muscle cells and monocytes, the liver is the main contributor to PAI-1 circulating levels [62].

Selection of the hepatocyte-secreted factors

To be able to distinguish hepatocyte-derived factors from factors secreted from non-parenchymal cells, the generation of a novel mouse model was employed. This work was performed, in the context of a parallel study in the lab, by Sören Fisker-Schmidt. This model was based on the INTACT mouse model that allows cell-type-specific GFP labeling of nuclei [63] (Figure 3). The original INTACT mice were bred with mice expressing Cre recombinase under the hepatocyte-specific Albumin (Alb) promoter [64] which would therefore allow GFP expression in hepatocytes' nuclei. Consequently, GFP-labeled nuclei can be isolated using an affinity-purification method from tissue homogenates. By using the Alb-INTACT-tumor bearing mice (Cachectic CRC: C26, PDAC: 8025 and non-cachectic CRC: NC26 and MC38) we were able to select factors enriched in the hepatocyte versus non-hepatocyte fraction, which allowed us to identify hepatocyte-selectively expressed factors. By integrating these data with C26 serum proteomics (Annex 1A) we identified twenty-eight hepatocyte-secreted factors, highly upregulated in cachectic conditions (Annex 2B). C26 serum proteomics was performed by a collaborator, while RNA-seq data analysis and integration with the secretome were performed by Sören Fisker-Schimdt.

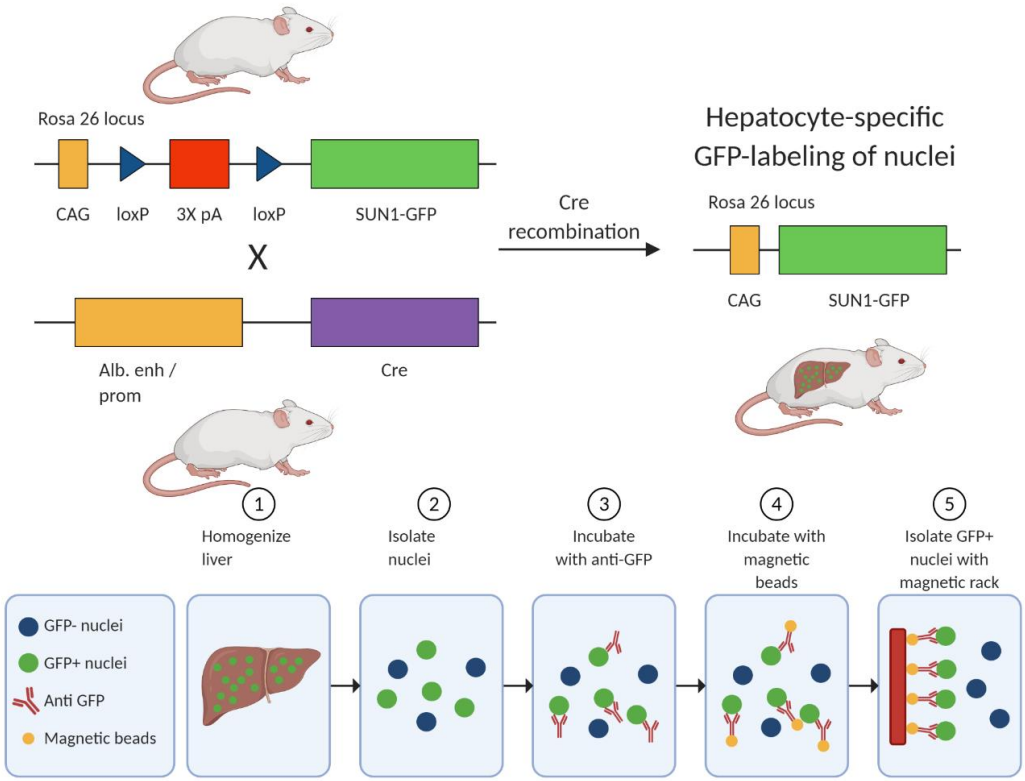

Figure 3. Schematic representation of the generation of Alb-INTACT mice that allow for the isolation of hepatocyte nuclei. Adapted from [63].

Aims of the study

Cancer cachexia is a multifactorial syndrome in which multiple tumor and host-derived signals lead to multi-organ dysfunction that translates into severe tissue wasting [34]. The liver is an essential organ that has multiple functions in maintaining homeostasis, but the nature and extent of liver dysfunction has received little attention in the context of cancer cachexia [21]. Several metabolic processes involved in lipid homeostasis and energy utilization are disrupted in the liver in cachectic conditions, and the APR activation has been reported in both human patients and multiple animal models [4]. However, functional investigations that address the direct contribution of liver-derived factors to tissue wasting in cancer cachexia are still largely missing. Therefore, the aim of this thesis was to elucidate the contribution of liver-secreted factors to tissue wasting in cancer cachexia.

Establishment of the screening pipeline using SAA 1/2, LCN2 and PAI-1

The first objective of this study is to develop a screening pipeline (Figure 4) which would allow the functional assessment of potential tissue wasting effects of liver-secreted candidates. To begin with, the increase in gene expression of the factors identified through whole-liver RNA-seq analysis from multiple cachectic versus non-cachectic models will be confirmed at protein level in both murine and human serum. For the ones confirmed to be upregulated in the serum, the effects on 3T3-L1 adipocyte-lipolysis and C2C12 myotube-atrophy will be addressed *in vitro.* Lastly, to confirm the contribution to the murine cachectic phenotype, a hepatocyte specific KD *in vivo* will be performed for the candidate that showed promising effects during the functional assessment. The first chapter of the Results section describes the establishment of the screening pipeline using the initial liver-secreted candidates, i.e. SAA 1/2, LCN2 and PAI-1.

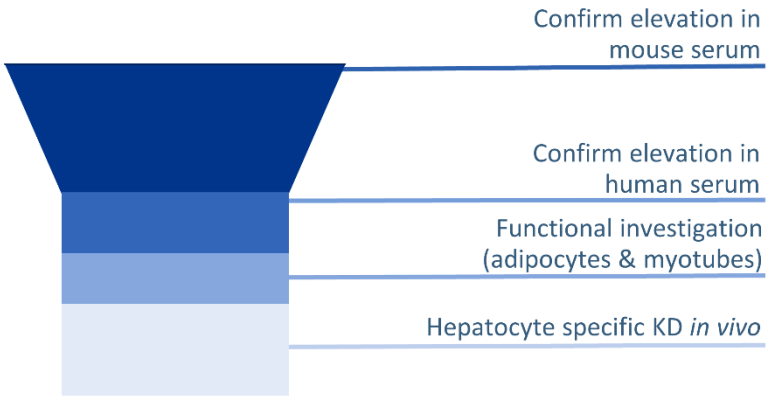

Figure 4. Steps involved in the liver-secreted factors screen

Screening pipeline optimization and functional characterization of hepatocyte-secreted factors *in vitro*

The second objective of this work is to address the contribution of hepatocyte-secreted factors, derived from the experiments performed with the Alb-INTACT tumor bearing mice, to tissue wasting *in vitro.* In the second part of the Results the pipeline (Figure 5) will be further optimized for the screening of a larger number of candidates. Firstly, functional assessment of 3T3-L1 lipolysis and C2C12 myotube atrophy will be performed. Secondly, the characterization of upstream regulators of adipocyte-lipolysis and myotube-atrophy hits will be addressed in primary hepatocytes.

Figure 5. Steps involved in the hepatocyte-secreted factors screen.

2. Results

2.1 Liver-secreted factors screen

Murine serum levels of liver-secreted factors

In an initial assessment, the circulating levels of the liver-secreted factors were measured in serum from healthy control versus C26 cachectic mice by ELISA. SAA 1/2 (Figure 6A) and LCN2 (Figure 6B) were upregulated by up to 1000-fold and 64-fold, respectively, in cachectic animals, while PAI-1 levels were not different than in control healthy animals (Figure 6C).

To further confirm the observed upregulation of SAA 1/2 and LCN2, two more ELISAs were performed using samples from three different CRC mouse models: the cachectic C26 and the non-cachectic MC38 control, both xenograft models, and the genetic ApcMUT mouse model that also develops cachexia. PBS-injected mice were included as healthy controls for each animal experiment. Neither SAA 1/2, nor LCN2 were upregulated in the non-cachectic tumor model (Figure 6 D,E) relative to PBS control mice. Both SAA 1/2 and LCN2 were significantly induced in both cachectic models. While LCN2 levels were upregulated to a similar extent between C26 and ApcMUT mice, SAA 1/2 levels were markedly higher in the C26 model (1000-fold vs PBS) as compared to the ApcMUT model (13-fold vs ApcWT).

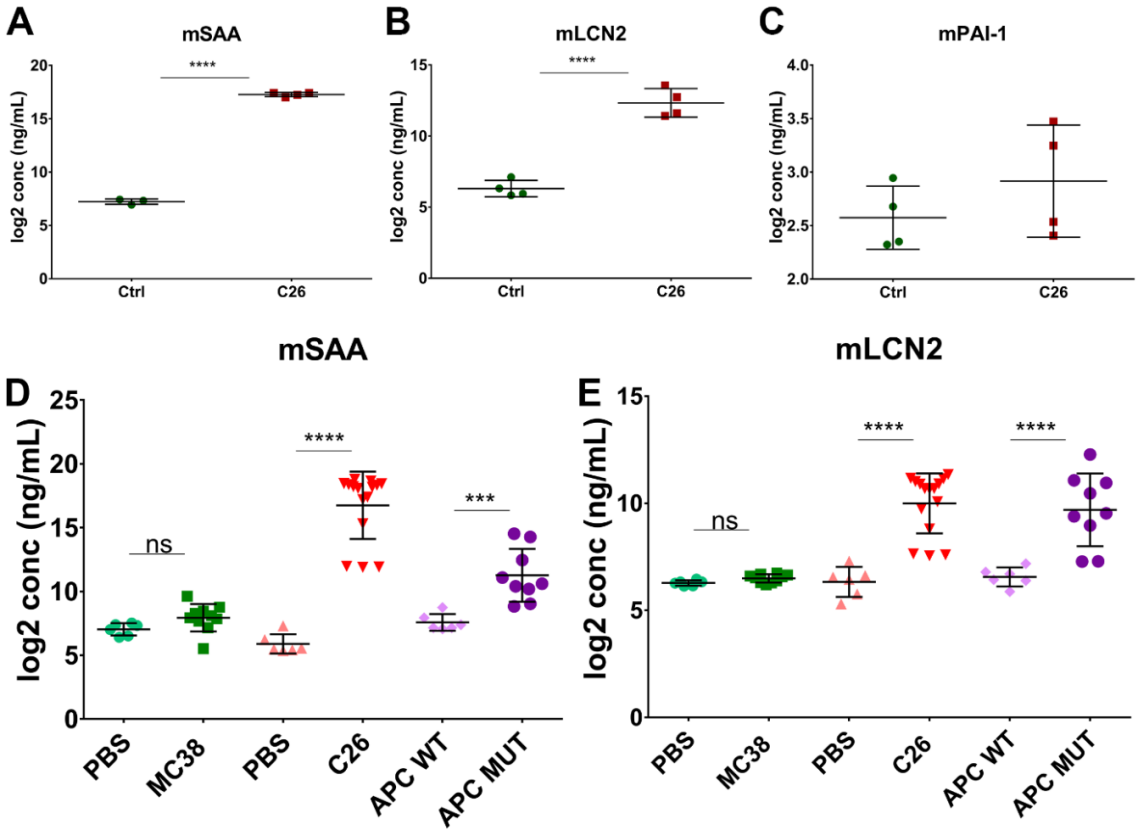

Figure 6. Liver-secreted factors identified in RNA-seq are upregulated in the serum of cachectic mice. Circulating levels of **(A)** SAA 1/2, **(B)** LCN2 and **(C)** PAI-1 in healthy vs C26 cachectic mice. Circulating levels of **(D)** SAA 1/2 and **(E)** LCN2 in multiple mouse models. For the xenograft models, mice were injected with either PBS, MC38 or C26 cells. Controls for the ApcMUT mice were represented by wild-type littermates (APC WT). Data are represented as log2 mean ± SD. Statistics were performed by using a t.test for A,B,C and one way ANOVA for D and E. * p≤ 0.5, ** p≤ 0.01, *** p≤ 0.001 and **** p≤ 0.0001. (A,B,C) Ctrl: n=4, C26: n=4. (D,E) PBS: n=6, MC38: n=10, C26: n=15, ApcWT: n=6, ApcMUT: n=9.

Serum levels of liver-secreted factors in human patients

Since the upregulation of SAA 1/2 and LCN2 was confirmed in the serum of cachectic mice, the next step was to assess their levels in human serum from cancer patients. For this purpose, ELISAs were performed on a small cohort of CRC (9 non-cachectic, 4 cachectic) and PDAC (10 non-cachectic, 6 cachectic) patients. Cachectic patients were defined by a weight loss >5%, while non-cachectic patients were defined by the absence of weight loss in the last 3 months prior to blood sampling.

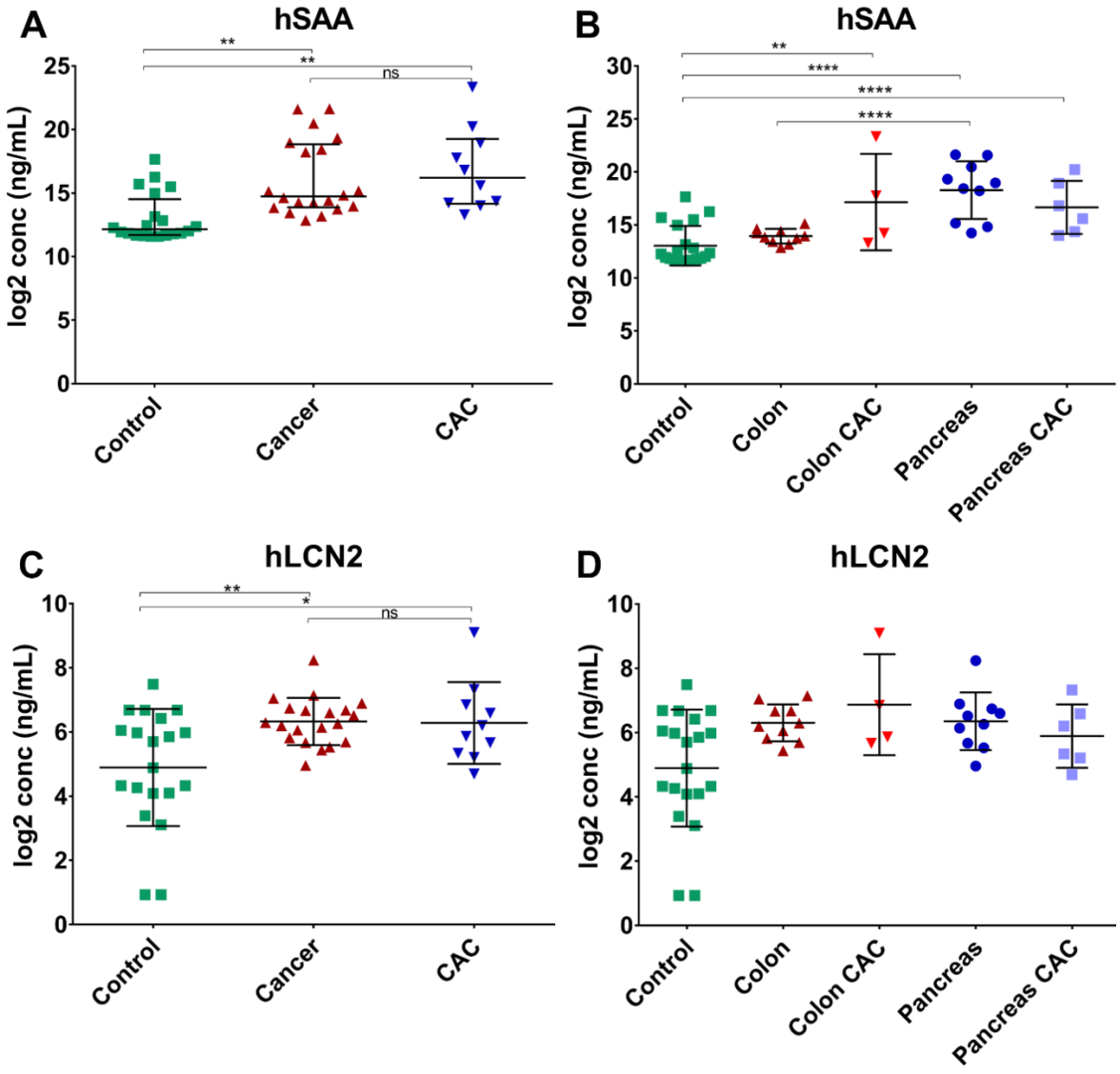

Figure 7. (A, B) SAA 1/2 and (C, D) LCN2 are upregulated in the serum of cancer patients. Depicted are circulating levels in healthy controls, non-cachectic cancer patients (cancer) and cachectic cancer patients (CAC). Data are represented as log2 mean ± SD, one-way ANOVA, * p≤ 0.5, ** p≤ 0.01, *** p≤ 0.001 and **** p≤ 0.0001. (A,C) Control: n=20, Cancer: n=20, CAC: n=10. (B,D) Control: n=20, Colon: n=10, Colon CAC: n=4, Pancreas: n=10, Pancreas CAC: n=6.

As seen in Figure 7A and C, both SAA 1/2 and LCN2 were upregulated in cancer patients as compared to healthy controls, by 8-fold in the case of SAA 1/2, and 3-fold for LCN2. However, no differences were observed between non-cachectic and cachectic patients for either of the two proteins. When stratification based on tumor entity was applied, a 9-fold increase in cachectic vs

non-cachectic CRC was observed for SAA 1/2, but this was not statistically significant possibly due to the small number of cachectic samples (Figure 7B). Similarly, a 1.5-fold increase of LCN2 levels in cachectic CRC was also observed, but this was again not statistically significant (Figure 7D). In the case of PDAC, for both SAA 1/2 and LCN2 small, non-significant effects were observed, with non-cachectic patients having higher circulating levels than the cachectic ones. Interestingly, non-cachectic patients with PDAC had 20-fold higher levels of SAA 1/2 than non-cachectic CRC patients (Figure 7B), which indicates that acute systemic inflammation was more prevalent in PDAC patients.

The BW loss data in this cohort was self-reported, which could indicate that the patients classified as non-cachectic might have been, to some extent, pre-cachectic. This is be supported by the fact that PDAC is the cancer entity most often associated with cachexia development and that most PDAC patients are diagnosed in very advanced disease stages [4]. Therefore, the lack of difference in circulating levels between cachectic and non-cachectic patients could have been affected by the reporting of the BW loss which served as exclusion criteria. For both SAA 1/2 and LCN2 a trend was observed in the CRC cohort, with increased levels in cachectic patients, but due to the small number of patients this was not statistically significant. However, taking together these data, and the high upregulation in murine cachectic serum, SAA 1/2 and LCN2 were selected for further functional assessment of potential tissue wasting properties *in vitro.*

Functional investigation *in vitro*: 3T3-L1 adipocyte lipolysis

To investigate if SAA 1/2 and LCN2 could contribute to lipolysis, 3T3-L1 differentiated adipocytes were treated with recombinant proteins and glycerol release was quantified. Medium conditioned by C26 cells was collected and used as a positive control (C26-CM). Four different concentrations of SAA 1/2 were tested (Figure 8A), with the highest concentration reflecting the circulating levels observed in ApcMUT cachectic mice. However, an increase in lipolysis was not observed at any of the tested concentrations. Similarly, treatment of 3T3-L1 adipocytes with concentrations of LCN2 that mimic the cachectic state also did not lead to an increase in lipolysis rates (Figure 8B).

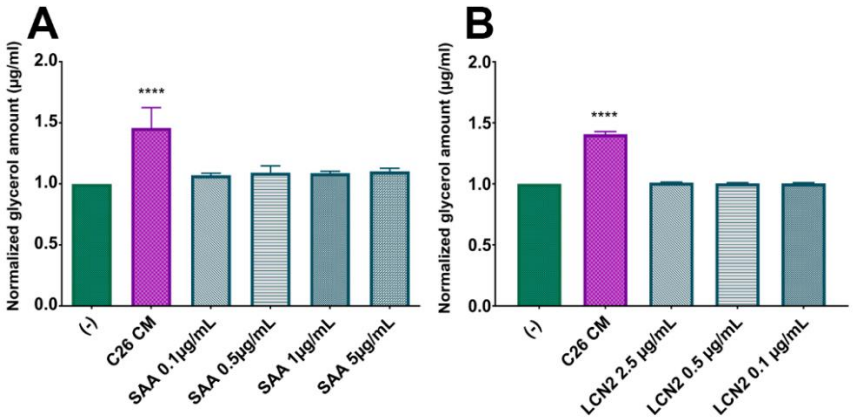

Figure 8. 3T3-L1 glycerol release in culture media upon treatment with (A) SAA 1/2, (B) LCN2 and for 24hrs. Data are represented as mean ± SD, n=3 independent experiments, one way ANOVA, **** p≤ 0.0001, normalized to (-). Significance is shown relative to (-).

Functional investigation *in vitro*: C2C12 myotube atrophy

The second aspect addressed during functional investigations was the ability of the selected liver-secreted factors to induce C2C12 myotube-atrophy *in vitro*. For this purpose, mature myotubes

were treated with the aforementioned concentrations (Functional investigation *in vitro*: 3T3-L1 adipocyte lipolysis) of SAA 1/2 and LCN2 and their width was measured. Myotube treatment with C26-CM led to a 21% decrease in width, on average, and SAA 1/2 was the only candidate that was able to induce myotube-atrophy *in vitro*, by leading to a 15% decrease in width (Figure 9A) at concentrations reflecting circulating levels in cachexia. LCN2 treatment lowered myotube width by 12% (Figure 9B), but this was not statistically significant.

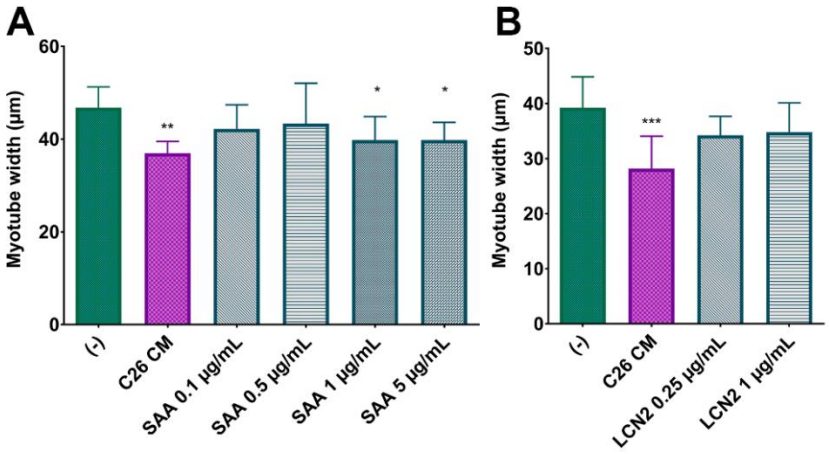

Figure 9. C2C12 myotube diameter upon treatment with (A) SAA 1/2, (B) LCN2 for 48hrs. Data are represented as mean ± SD, n=3 independent experiments, one way ANOVA, * p≤ 0.5, ** p≤ 0.01, *** p≤ 0.001, normalized to (-). Significance is shown relative to (-).

Hepatocyte-specific SAA 1/2 KD *in vivo*

After running all the initial liver-secreted factors through the screening pipeline, SAA 1/2 was the only one that fulfilled all the selection criteria. Therefore, the contribution of SAA 1/2 to cancer cachexia development *in vivo* was assessed by using an Adeno-associated virus (AAV)-mediated hepatocyte specific KD approach [65].

To select the optimal miRNA constructs that would successfully downregulate both SAA 1 and SAA 2, several constructs that target either SAA 1/2 or each isoform specifically, were tested. Each SAA isoform was overexpressed in HEK 293A cells after which the cells were transfected with the different miRNA constructs. Since the overexpression constructs contain a FLAG tag, the protein lysates were analyzed via dot blot using a FLAG-antibody. As seen in Figure 10A, construct A, targeting both SAA 1 and SAA 2, and construct 1F, targeting SAA 1 specifically, led to a significant decrease in FLAG levels in cells overexpressing SAA 1, compared to a negative control (NC) miRNA construct. Similarly, construct A and construct 2F had the strongest effect in cells overexpressing SAA 2 (Figure 10B). Therefore, construct SAA 1/2 A was selected and cloned into an AAV vector, downstream of the hepatocyte specific LP1 promoter. A LP1-AAV vector containing the NC miRNA construct was generated as a negative control.

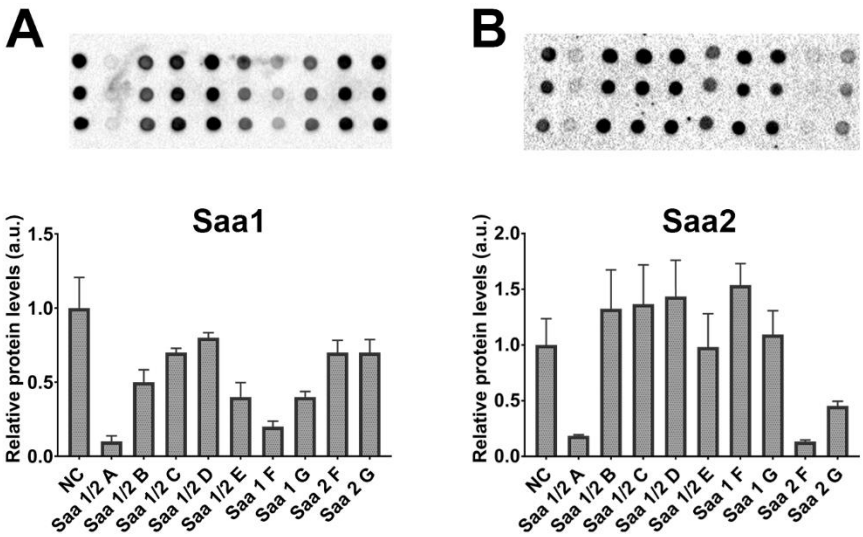

Figure 10. Intracellular FLAG protein levels upon miRNA mediated KD in HEK 293A cells expressing either (A) SAA 1 or (B) SAA 2. Dot blots were quantified and normalized to negative control miRNA (NC).

The experimental setup of the Hepatocyte-specific SAA 1/2 KD *in vivo* is described in Material and methods (LP1-AAV-miR SAA 1/2 KD *in vivo*) and a schematic representation is shown in Figure 11. The endpoint of the experiment was defined as 10% BW loss.

Briefly, 8 weeks old mice were divided into three different groups: PBS (6 mice), LP1-AAV-miR SAA 1/2 (10 mice) and LP1-AAV-miR Ctrl (10 mice). The two AAV groups represented experimental, tumor-bearing mice, while PBS mice were used as healthy, non-tumor bearing controls. Four weeks prior to C26 tumor cell implantation, LP1-AAV-miR Ctrl and LP1-AAV-miR SAA 1/2 were injected with the corresponding AAVs, and PBS mice were injected with PBS. Injections were performed via tail vein.

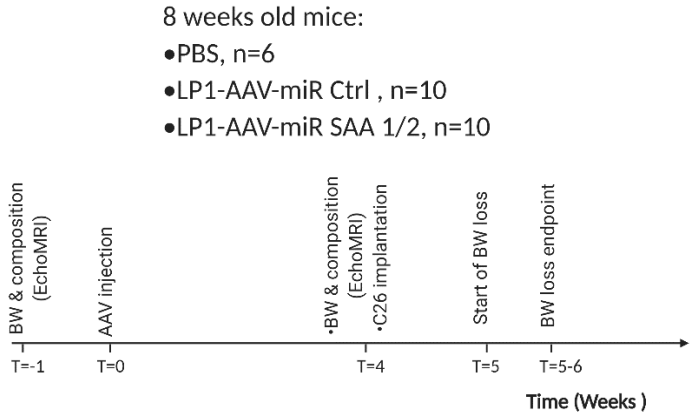

Figure 11. Schematic representation miR-LP1-AAV-SAA 1/2 KD *in vivo* experimental design

At T=4 weeks (Figure 11) there were no differences in BW and composition between the three groups (Figure 12A). As seen in Figure 12B, tumor-bearing mice started losing weight approximately one week after C26 cell injection. The pace at which mice lost BW was very heterogeneous, with some mice reaching the defined endpoint of 10% BW loss after 8 days of C26 injection, while others took up to 14 days to reach it. C26 tumor-bearing mice belonging in either LP1-AAV-miR Ctrl (Control C26) or LP1-AAV-miR SAA 1/2 (SAA KD C26) group were sacrificed in a paired fashion whenever one mouse reached ≥10% BW loss.

Due to the paired-experimental design, some mice had to be sacrificed although they had not reached 10% BW loss. By the end of the experiment, both tumor-bearing groups lost weight as compared to the PBS mice that accumulated weight (Figure 12C, left panel). The overall BW loss in the Control C26 group was 4.5%, while the SAA KD C26 mice lost on average 8.2% BW, relative to their initial BW. Both tumor-bearing mice lost significant amounts of fat mass (63% for Control C26 animals and 77% for SAA KD C26). As with BW loss, knocking down SAA 1/2 did not have any effects on fat mass loss as compared to Control C26 animals (Figure 12C, mid panel). Lastly, SAA KD C26 mice, but not Control C26 mice, lost lean mass (approximately 5%). However, in contrast to healthy PBS mice that gained lean mass over time, Control C26 animals failed to accumulate lean mass (Figure 12C, right panel).

The effects on fat and lean mass, as measured by EchoMRI, were also recapitulated at the level of tissue weight (Figure 12D). Both epididymal and inguinal fat pads weighed approximately 60% less in tumor-bearing mice as compared to healthy mice. The only effect observed in skeletal muscle mass was a 5% reduction of the gastrocnemius (GC) muscle weight in SAA KD C26 as compared to PBS mice, but triceps muscle weight was not affected by the presence of the tumor. However, both tumor-bearing groups had displayed a 10% reduction of cardiac muscle mass as compared to healthy PBS mice. Splenomegaly was documented in both tumor groups, with SAA KD C26 mice having a 23% increase in spleen weight as compared to Control C26 animals, while liver mass was not affected by the tumors (Figure 12E). Finally, SAA KD C26 animals had a 42% increase in tumor weight as compared to Control C26 animals (Figure 12F). However, the variability was relatively high in the Control C26 animals for both liver as well as for tumor mass.

The KD efficiency was addressed by measuring SAA 1/2 protein levels in the serum and the liver. Serum levels were 7.8-fold lower in SAA KD C26 vs Control C26 animals, but compared to healthy PBS mice, they were still approximately 480-fold increased (Figure 12G). Remarkably, Control C26 mice had 3700-fold higher serum SAA 1/2 levels than healthy animals. Hepatic SAA 1/2 levels were also decreased in SAA KD C26 compared to Control C26 animals by up to 4.2-fold (Figure 12H).

SAA 1/2 KD seemed to influence tumor mass development, but when sacrificed, mice were paired based on their BW loss, and not their tumor size, which could have exaggerated pre-existing minor variations in tumor growth. While significant, the differences in tumor mass were also highly variable. To be able to distinguish if this could be attributed to the experimental design consisting of BW-based pairing (and, consequently, different disease durations), tumor size over the course of the experiment was analyzed. As seen in Figure 13, at day 8, when all the mice were still alive, there was no difference in tumor size between the two groups. The difference only became apparent once mice were eliminated from groups based on their BW loss on the following days. Moreover, in contrast to the tumor weight, when mice reached the 10% BW loss endpoint there was no difference in tumor size between the two groups.

To address a potential direct effect of SAA 1/2 on tumor cell proliferation, C26 cells were treated with recombinant protein and their proliferation was assessed. However, as seen in Figure 14, SAA 1/2 treatment had no effect on cell proliferation as compared to Doxorubicin, a chemotherapeutic drug.

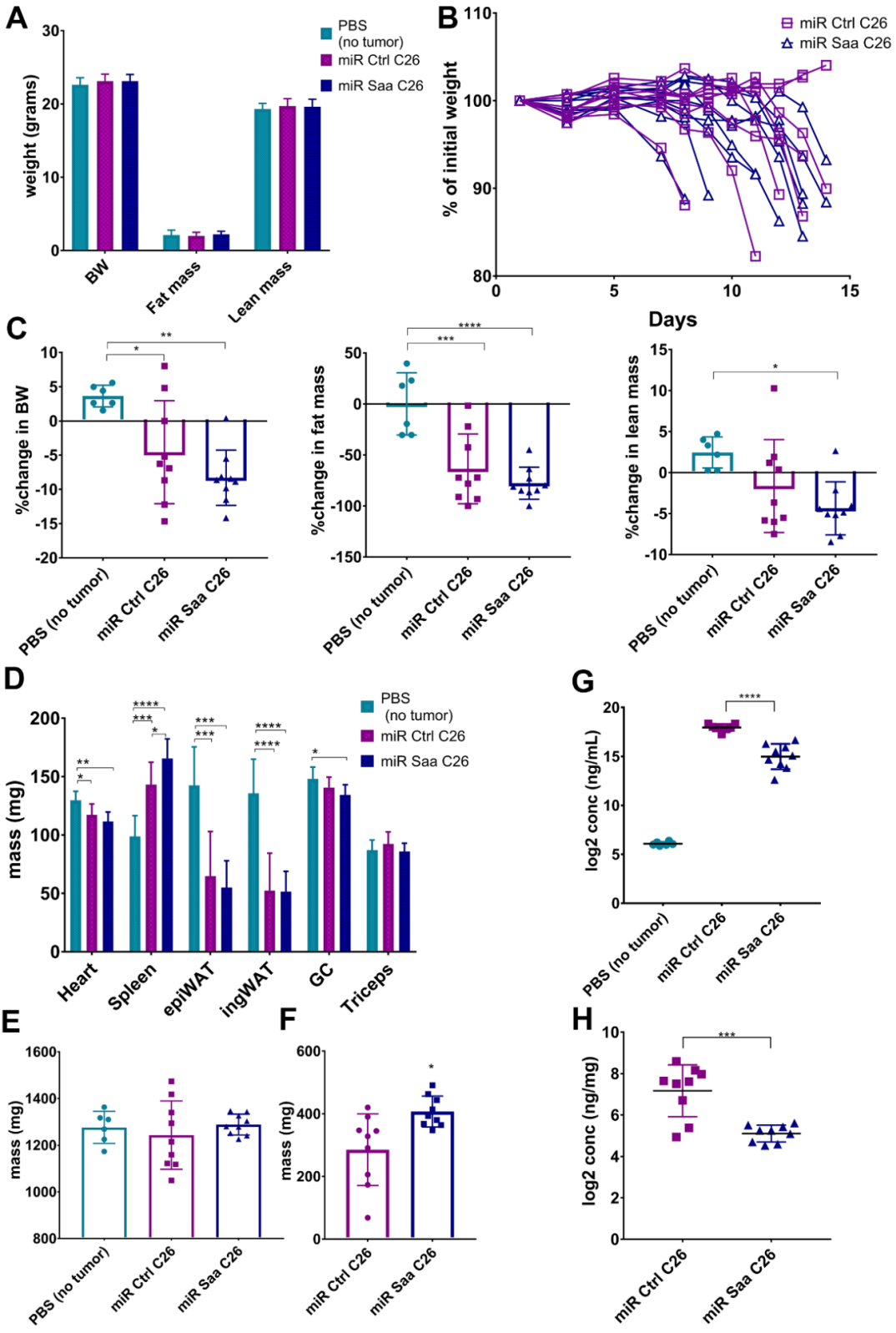

Figure 12. SAA 1/2 KD *in vivo* does not affect cachexia development. (A) BW and composition (EchoMRI) at the start of the experiment. **(B)** BW loss progression over days since C26 cell implantation. **(C)** % change in BW, fat, and lean mass at the end of the experiment relative to the initial BW and composition. **(D)** Tissue weights at BW loss endpoint (liver and tumor are shown separately in **(E)** and **(F),** respectively). **(G)** Serum and **(H)** liver protein levels of SAA 1/2 at BW loss endpoint (log2 conc ng/mL). Data are represented as mean ± SD, one-way ANOVA except for **(F)** and **(H)** where Welch's t.test was used. * p≤ 0.5, ** p≤ 0.01, *** p≤ 0.001 and **** p≤ 0.0001. Abbreviations: miR Ctrl, LP1-AAV-miR Ctrl; miR Saa, LP1-AAV-miR SAA 1/2.

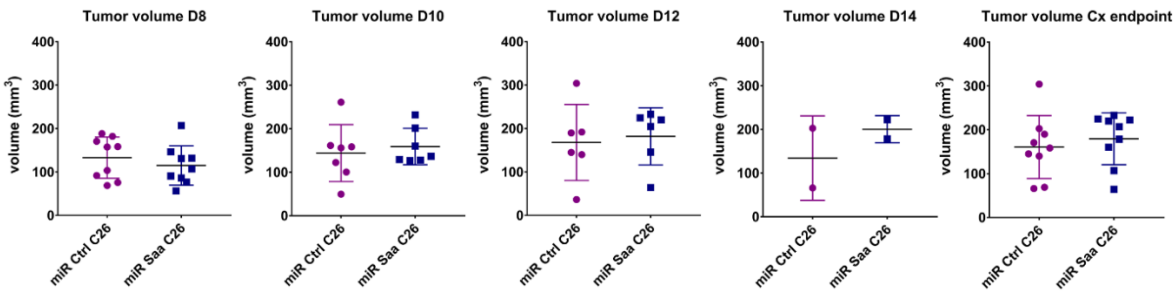

Figure 13. Tumor size progression over the course of the experiment. Data are represented as mean ± SD of tumor volume and analyzed by t.test.

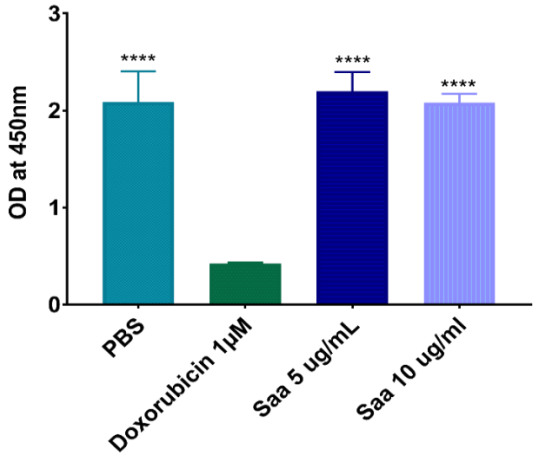

Figure 14. SAA 1/2 treatment does not affect C26 proliferation *in vitro.* Proliferation was measured using a CCK-8 assay. Data are represented as mean ±SD, one-way ANOVA, **** p≤0.0001, n=2 independent experiments. Significance is shown relative to Doxorubicin treatment.

Overall, SAA 1/2 KD did not affect cachexia development in C26 mice. As compared to Control C26 animals, SAA KD C26 mice had an increase in spleen mass, and potentially tumor mass, although, as previously mentioned, this could be attributed to the experimental design adjusted for the detection of effects on BW loss. Despite a significant downregulation of hepatic SAA 1/2 upon AAV-mediated KD, hepatic and circulating SAA 1/2 protein levels were still highly upregulated in SAA1/2 KD C26 mice as compared to a healthy state.

The experiments performed in the liver-secreted factors screen allowed the development of a screening pipeline that can successfully be used to address the contribution of the candidates to tissue wasting *in vitro*. SAA 1/2 was identified as the most promising candidate based on its high upregulation in cachectic serum and its myotube-atrophy promoting effects. However, the hepatocyte specific KD i*n vivo* failed to rescue the cachectic phenotype observed in C26 mice. Despite an 8-fold decrease of serum SAA 1/2 levels upon KD in tumor-bearing mice, SAA 1/2 remained highly upregulated in diseased vs healthy mice. This suggests that the AAV-mediated KD approach might not be sufficient to counter the expression of factors which are highly upregulated in cancer cachexia.

2.2 Hepatocyte-secreted factors screen

For twenty-four of the twenty-eight hepatocyte-secreted candidates, cDNA expression plasmids were commercially available. The plasmids were transfected into HEK 293A cells in order to generate candidate-CM that was used for the *in vitro* functional assessment of 3T3-L1 lipolysis and C2C12 myotube atrophy. Candidate-CM was generated as shown in Figure 15A and detailed in Material and methods (HEK293A transfection and candidate-CM generation). To confirm that the cells can secrete the candidate proteins into the media upon transfection, a FLAG ELISA was performed on the concentrated candidate-CM (Figure 15B).

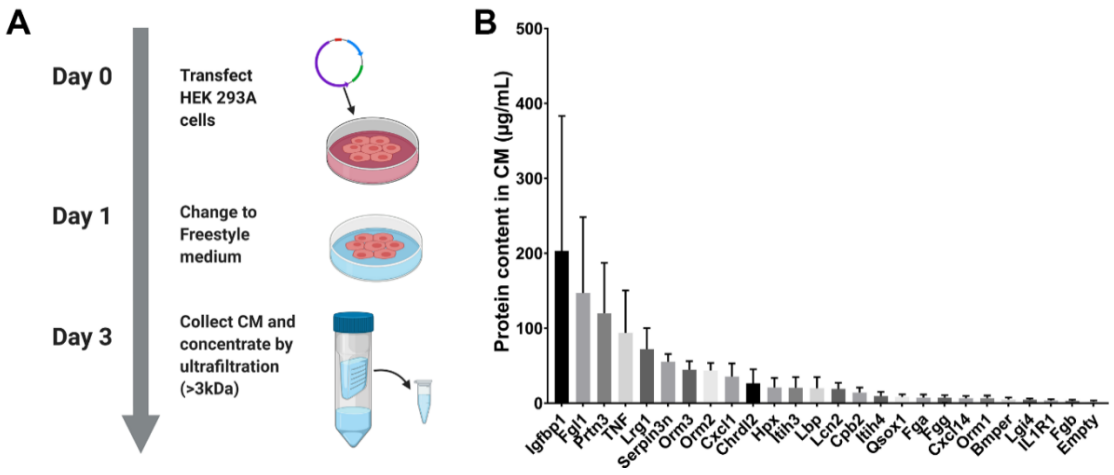

Figure 15. (A) CM generation in HEK293A cells and (B) quantification of FLAG protein in concentrated candidate-CM. Data are represented as mean ±SD, n=3 independent productions of candidate-CM.

Functional investigation *in vitro*: 3T3-L1 adipocyte lipolysis

Lipolysis optimization

To assess the candidate-CM contribution to 3T3-L1 lipolysis, a high-throughput screening analysis was developed and optimized. To define the conditions that would capture the strongest response, two different protocols (Table 1) for differentiation of 3T3-L1 cells in 96-well plates were tested, and lipolysis was measured at different time points using C26-CM as positive control and MC38-CM as negative control.

Cells differentiated with Protocol 2 and treated at day 10 had the lowest response to C26-CM treatment (Figure 16A). The strongest response to C26-CM was achieved when cells were differentiated using Protocol 1 and treated at day 6.

Table 1. Protocols used for 3T3-L1 differentiation in 96-well plates.

PROTOCOL 1	PROTOCOL 2
Day -4: Seed	
Day -2: DMEM	**Day -2**: Seed
Day 0: Insulin, Dex, Rosi, IBMX	**Day 0**: Insulin, Dex, Rosi, IBMX
Day 2: Insulin	**Day 2**: Insulin, Dex, Rosi, IBMX
Day 4: DMEM	**Day 4**: Insulin
Day 6/Day 8: treatment	**Day 6**: DMEM
	Day 8/Day 10: treatment

Insulin: 1 µg/mL, Dexamethasone: 0.25 µM, Rosiglitazone: 2µM and IBMX: 0.5mM

A second aspect that was addressed was whether cachectic factors have an effect on basal lipolysis or if concomitant β-adrenergic stimulation of lipolysis would be required to see an effect. Therefore, cells were treated with C26-CM and recombinant TNFα in basal or isoproterenol (a β-adrenergic activator) stimulated conditions (Figure 16B). In basal conditions both C26-CM and recombinant TNFα significantly induced glycerol release. However, isoproterenol treatment canceled out the effects of C26-CM, indicating that the lipolysis-inducing properties of the candidate-CM on 3T3-L1 cells need to be tested under basal conditions.

Lastly, to enrich the overexpressed protein-candidates in the CM and maximize the effects of the candidate-CM, protein concentrator spin columns were used. Consequently, this would also avoid potential effects of candidate-induced changes in the nutrient composition of the CM. Figure 16C shows that, while an effect was observed when cells were treated with 1x TNF-CM, the effect was much stronger when 4x TNF-CM was used.

Therefore, for the lipolysis screening, cells were differentiated using Protocol 1, treated at day 6 with concentrated candidate-CM and lipolysis was measured in basal conditions.

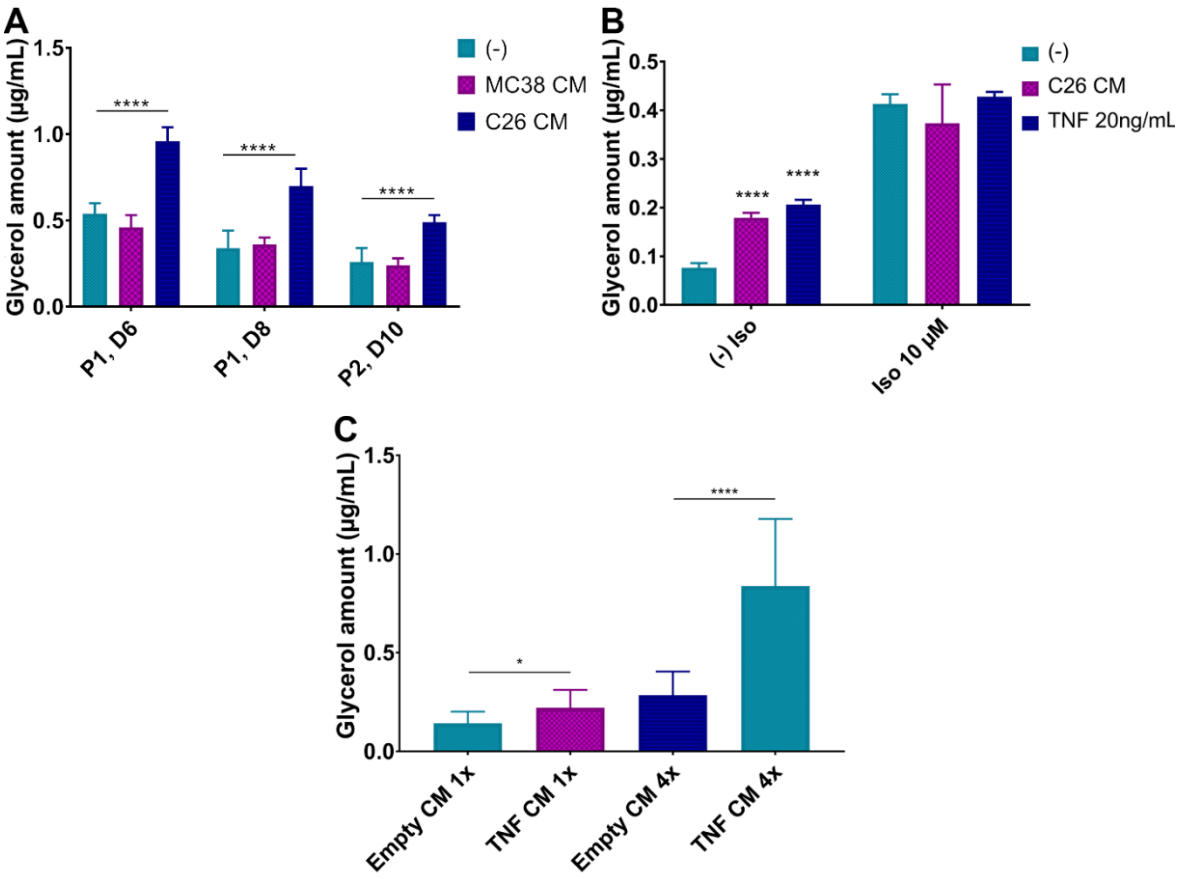

Figure 16. 3T3-L1 lipolysis optimization. (A) Glycerol release upon CM treatment. Cells were differentiated using Protocol 1 (P1) or Protocol 2 (P2) and treated with MC38-CM and C26-CM at day 6, day 8 or day 10. The amount of glycerol released in the media was measured after 24hrs. **(B)** Basal ((-) Iso) vs stimulated (Iso 10 µM) lipolysis upon C26-CM and rTNFα treatment. Significance is shown relative to (-). **(C)** Glycerol release upon treatment with non-concentrated CM (1x) vs concentrated CM (4x). Data are represented as mean ±SD, n=2 independent experiments, one-way ANOVA, * p≤0.05, **** p≤0.0001.

3T3-L1 lipolysis with candidate-CM

As mentioned before, for the generation of candidate-CM, cDNA expression plasmids were transfected in HEK 293A cells and media was collected and concentrated approximately 8x (see HEK293A transfection and candidate-CM generation). An empty expression plasmid was used as a negative control, while a TNF cDNA expression plasmid was used as positive control.

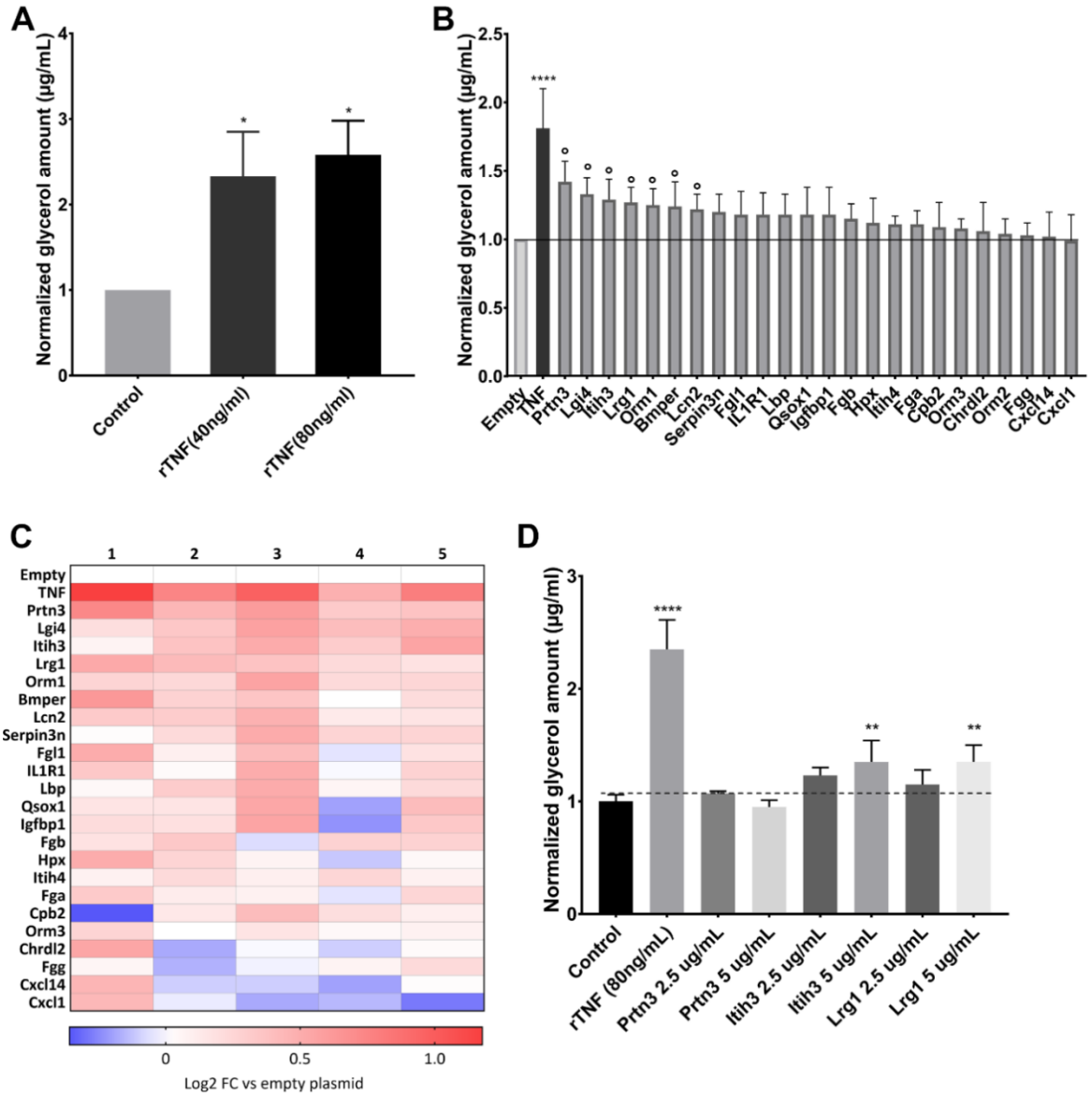

Figure 17. 3T3-L1 lipolysis upon candidate-CM treatment. (A) rTNFα induced lipolysis in 3T3-L1 cells. **(B)** Candidate-CM screening. ° marks the candidates that had an effect ≥1.5x average SD. **(C)** Heatmap representation of candidate-CM screening. **(D)** Lipolysis upon treatment with recombinant protein for a panel of selected candidates. Data are represented as mean ± SD (A, B, D) and log2 fold changes (C), normalized to control media (A,D) or empty plasmid-CM (B,C). n=5 (A-C), n=2 independent experiments (D). One-way ANOVA (A, B, D): * p≤0.05, ** p≤0.01, **** p≤0.0001 vs control (A, D) or empty plasmid-CM (B).

As depicted in Figure 17A, 3T3-L1 cells responded to rTNFα treatment which induced roughly a 2.5-fold increase in lipolysis rates. The response to TNF-CM was lower, with an approximately 1.8-fold increase in lipolysis (Figure 17B). Seven out of twenty-four candidates had an effect above the selected threshold of ≥1.5-times average SD (Figure 17B), ranging from a 1.4-fold increase in lipolysis, for Prtn3-CM, to 1.2-fold for Lcn2-CM. These candidates were selected as positive hits. Although the effects are rather moderate, overall, most candidates were able to increase lipolysis and none reduced lipolysis rates (Figure 17C). However, due to the high variability in 3T3-L1 response between biological replicates (Figure 17C), none of the effects were statistically significant after adjusting for multiple testing. Therefore, to validate the results of the screen using an independent approach, the top hits, for which recombinant protein was commercially available, were tested again for lipolysis. rPrtn3 did not have any effect at either of the two tested concentrations while both rItih3 and rLrg1 induced lipolysis in a concentration dependent manner (Figure 17D). For these two candidates, the degree of induction obtained with recombinant protein was similar to the one achieved when cells were treated with CM, namely an increase in lipolysis of about 1.3-fold.

Functional investigation *in vitro*: C2C12 myotube atrophy

C2C12 myotube atrophy optimization

In order to assess the potential effect of hepatocyte-secreted factors on skeletal muscle wasting, the C2C12 myotube atrophy assay was first optimized, due to the high number of candidates.

MitoTracker fluorescent dyes were used to stain differentiated myotubes in order to make the visualization, and subsequent quantification more reliable [66]. The difference between the two dyes is that MitoTracker Green accumulates into mitochondria regardless of mitochondrial membrane potential while MitoTracker Red is dependent on it. To test the accuracy of this method, C2C12 cells were treated with either C26-CM or rSaa 1/2 in the presence or absence of MitoTracker. Indeed, both dyes improved considerably the aspect of the myotubes and helped distinguish differentiated from undifferentiated cells (Figure 18A) As seen in Figure 18B, the staining did not affect the myotube diameter as the effect of C26-CM and rSAA remained constant across the different staining conditions.

Lastly, the assay was further optimized using 1x TNF-CM. A higher concentration of dye over a shorter time was used in order to improve the quality of the staining. As shown Figure 18C, the MitoTracker Green dye worked better in staining and visually separating myotubes that overlapped during differentiation. Therefore, for the C2C12 myotube atrophy screening all conditions were stained with MitoTracker Green and imaged for diameter quantification.

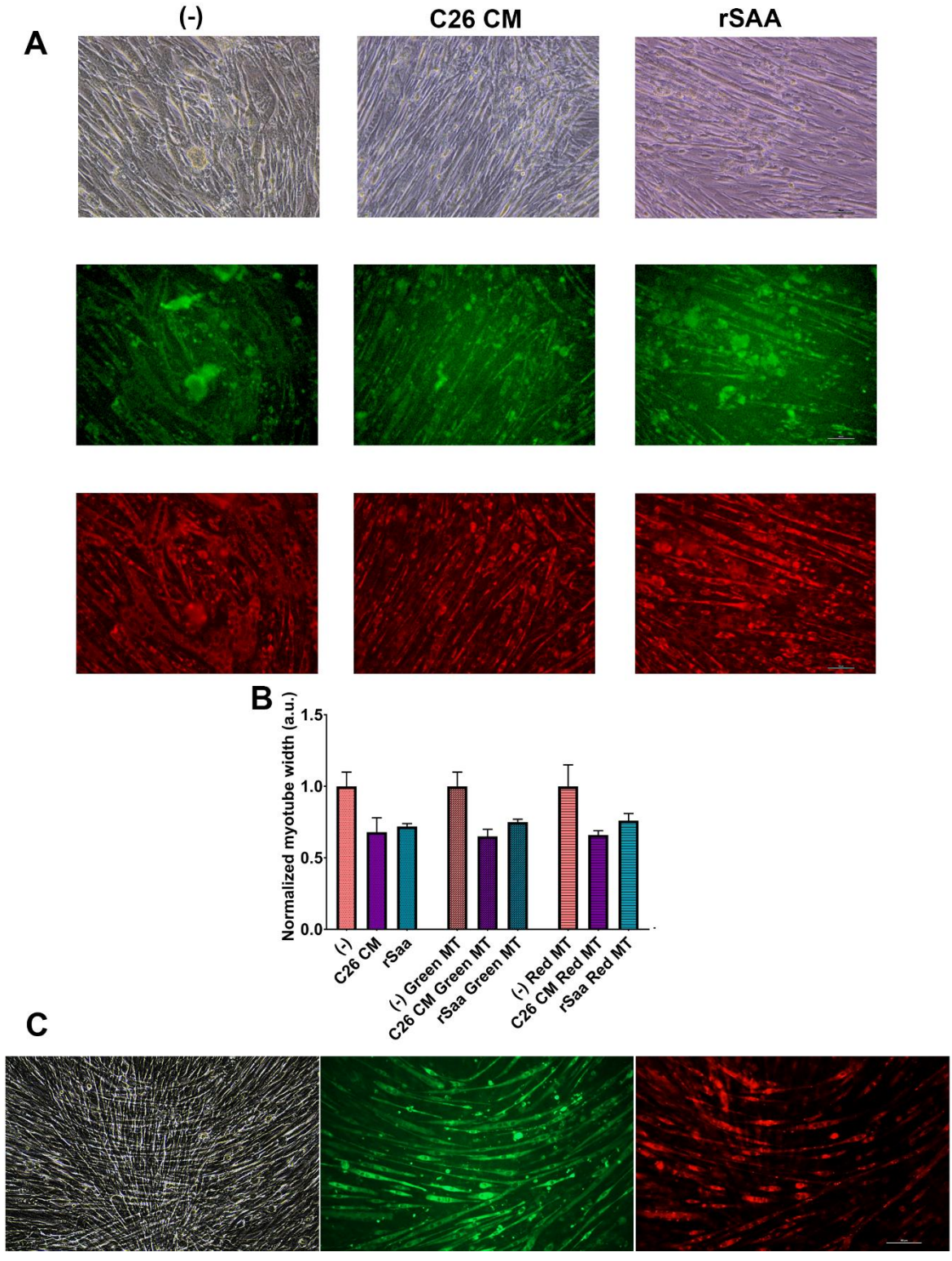

Figure 18. C2C12 myotube-atrophy optimization. (A) Example of myotube staining with MitoTracker Green or Red at 50nM for 1hr upon C26-CM or rSAA treatment. **(B)** Quantification of stained myotubes, normalized to (-) control in each condition. **(C)** Myotube staining at 250nm for 30min upon TNF-CM treatment. Scale bar indicates 100 μm.

C2C12 myotube atrophy with candidate-CM

During the optimization process it was noted that treatment with 8x candidate-CM was very harsh on the myotubes and during the MitoTracker staining protocol the cells would detach, therefore the following experiments were performed with 4x candidate-CM. However, even at this concentration TNF-CM proved to be toxic for the cells, so no data were collected for this condition. The empty expression plasmid-CM was used as a negative control

Five out of twenty-four candidates had an effect above the threshold of ≥1.5-times average SD, ranging from a 11% decrease in myotube width for Chrdl2, to a 7% decrease for Cxcl14 (Figure 19A). These candidates were selected as positive hits. As with the lipolysis assay, most candidates had a small effect on myotube-atrophy and generally no hypertrophic effects, but the variability was rather high between the experiments, particularly due to the third experiment, and thus no statistical significance was achieved (Figure 19B). Only Lrg1 was a common hit in both lipolysis and myotube-atrophy, but Bmper, Lcn2, Itih3 and Lgi4 were also just below the limit of the 1.5-times the average SD threshold, leading to a 6% decrease in myotube width. This could indicate that most of the candidates have tissue-specific effects when it comes to *in vitro* tissue wasting.

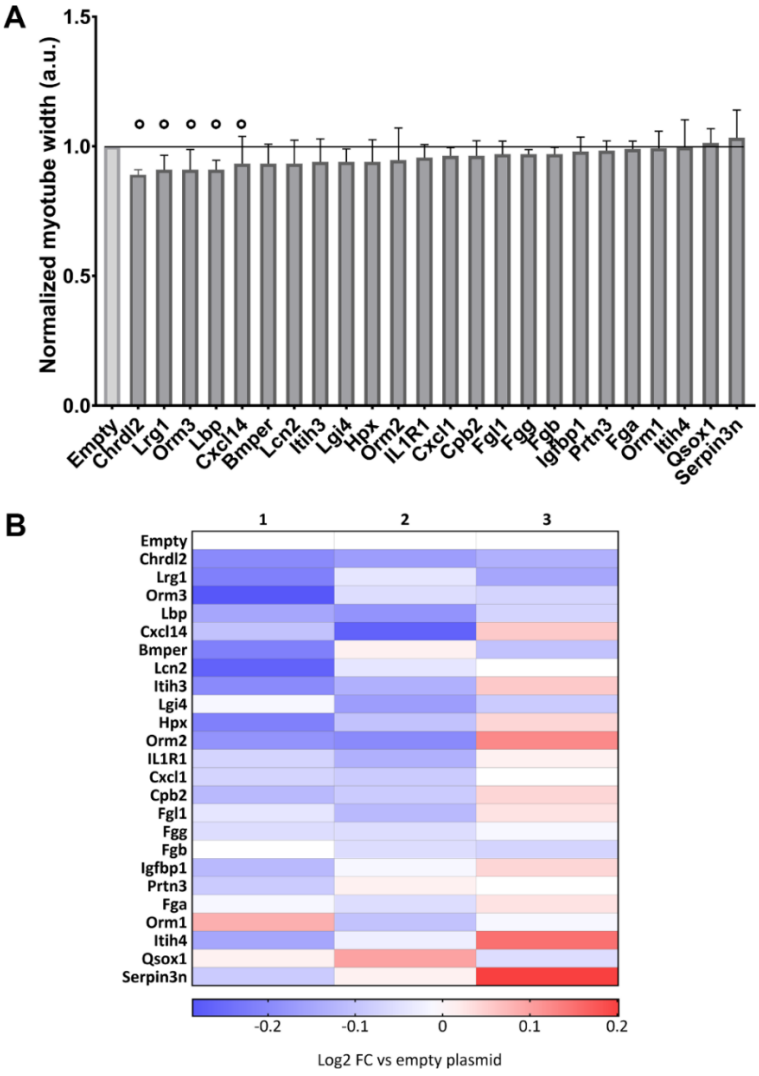

Figure 19. C2C12 myotube-atrophy upon candidate-CM treatment. (A) Candidate-CM screening. ° marks the candidates that had an effect ≥1.5x average SD. **(B)** Heatmap representation of candidate-CM screening. Data are represented as mean ± SD (A) and log2 fold changes (B), normalized to empty plasmid-CM, n=3 independent experiments.

Upstream regulation of hepatocyte-secreted factors

The role of STAT3, NF-kB and GR activation

The functional assessment of the hepatocyte-secreted factors suggested that multiple factors, with rather small effects when taken individually, contribute to tissue wasting in cancer cachexia. Therefore, targeting individual factors might not be sufficient to rescue the cachectic phenotype. Consequently, a different strategy was employed, which was to address the potential upstream regulators of the hepatic cachectic program. STAT3, NF-kB and GR are known to be involved both in the activation of the APR [48] [67], as well as in cancer cachexia [4] [68]. Therefore, to identify a potential pattern of upstream activation, the role of these three transcription factors in mediating the upregulation of the hepatocyte-secreted factors was investigated.

To help set up the assay, a panel of signature genes, reported to be upregulated in atrophic muscle of C26 cachectic mice [27], and to respond to the signals of interest were investigated. SAA 1/2 was reported to respond to IL-1β + IL-6 dual treatment, Fgg to IL-6 and Serpina3n to GC [69] [70]. IL-6, IL-1β and Corticosterone were used in different combinations to activate STAT3, NF-kB and GR, respectively [69]. Pre-mRNA levels were measured after 2hrs of treatment in order to assess a potential acute response that would more closely reflect transcriptional regulation since they are less influenced by mRNA processing and degradation. Mature mRNA levels were measured after 8hrs to assess whether the acute response contributes to the total mature mRNA pools.

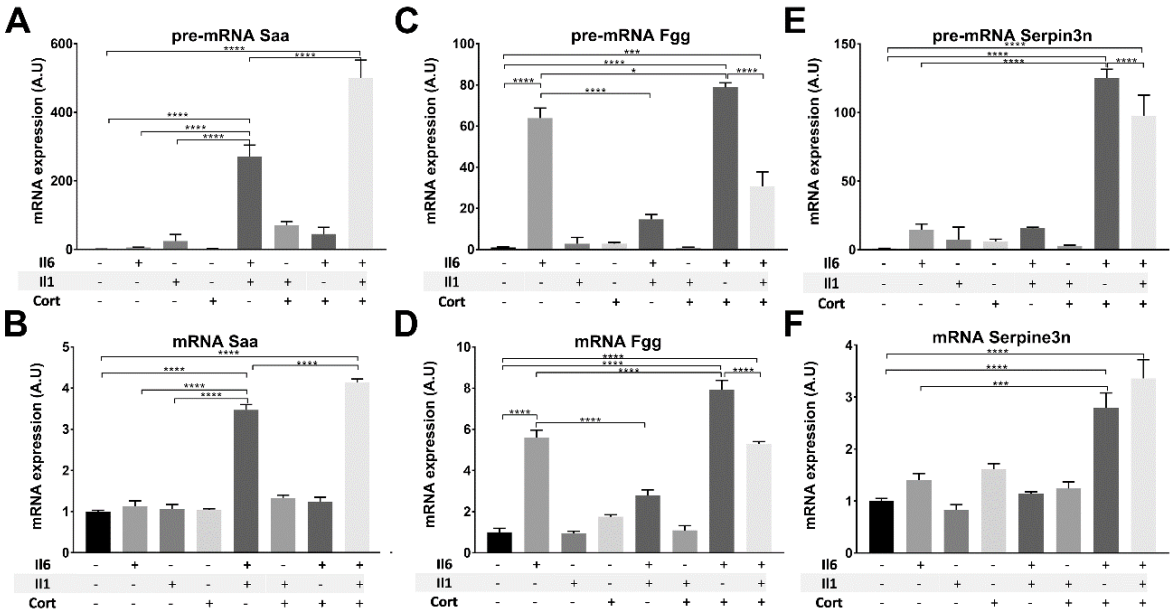

Figure 20. Cachexia-signature genes respond to STAT3 (IL-6), NF-kb (IL-1β) and GR (Corticosterone) activation in primary hepatocytes. (A,C,E) pre-mRNA levels after 2hrs of treatment. **(B,D,F)** mature mRNA levels after 8hrs of treatment. Cells were treated with 100ng/mL IL-6 and IL-1β, and 1μM Corticosterone. Data are represented as mean ± SD, normalized to untreated control, two-way ANOVA: * p≤0.05, *** p≤0.001, **** p≤0.0001, n=3 biological replicates.

Although the pattern of upstream regulation was different in the case of each gene, it seems that in general, single treatments do not significantly induce a response in gene expression. The only exception constituted the activation of Fgg transcription following IL-6 treatment (Figure 20C,D). Dual treatment with IL-6 and Corticosterone potentiated each other's effects on Serpina3n (Figure 20 E,F) and Fgg induction, while SAA 1/2 (Figure 20 A,B) responded to the combination of IL-6 and

IL-1β. This is in line with previously published studies [69] and demonstrated that primary hepatocytes respond to IL-1, IL-6 and Corticosterone treatment. Interestingly, the absolute fold induction was much higher at the pre-mRNA compared to mature mRNA levels.

After observing that cachexia-related genes respond to the upstream activation of STAT3, NF-kB and GR, the response of the seven adipocyte-lipolysis hits and the five myotube-atrophy hits was also addressed in primary hepatocytes, both at pre-mRNA levels, after 2hrs of treatment, as well as at mature mRNA levels after 8hrs of treatment. Lrg1, the common hit, was only depicted in the figures pertaining to adipocyte-lipolysis hits.

Upon 2hrs treatment, a tendency of increased pre-mRNA levels of Prtn3, Lgi4, Itih3 and Bmper was observed, but statistical significance was not reached (Figure 21A, B, C, F). Acute activation of Lrg1 was only achieved by IL-6 + Corticosterone (Figure 21D). Pre-mRNA levels of Orm1 were up by 8.5-fold upon IL-6 treatment, and the combination of IL-6 and IL-1β lead to a 23-fold upregulation in gene expression. IL-6 + Corticosterone also had an effect, although smaller, while the combination of all three treatments led to the highest increase, namely a 33-fold upregulation (Figure 21E). Although none of the single treatments had any effect on Lcn2, the combinations of either two treatments led to an upregulation of 15-18-fold in pre-mRNA levels while the triple combination led to a 31-fold increase (Figure 21G).

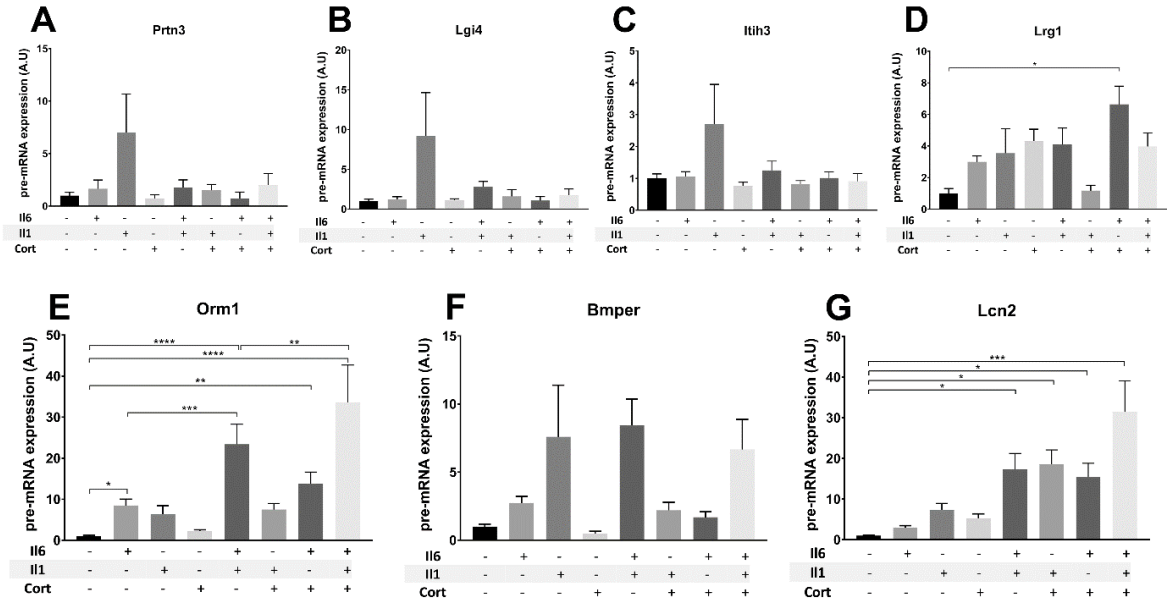

Figure 21. pre-mRNA expression of adipocyte-lipolysis hits upon STAT3 (IL-6), NF-kb (IL-1β) and GR (Corticosterone) activation in primary hepatocytes. Cells were treated with 100ng/mL IL-6 and IL-1β, and 1μM Corticosterone for 2hrs. Data are represented as mean ± SD, normalized to untreated control, two-way ANOVA: * p≤0.05, ** p≤0.01, *** p≤0.001, **** p≤0.0001, n=3 biological replicates.

As with the pre-mRNA, mature mRNA levels of Prtn3, Lgi4 and Itih3 were also not affected by any of the treatments (Figure 22 A ,B, C). Similar to the pre-mRNA, Lrg1 mature mRNA was upregulated 2.5-fold by IL-6 + Corticosterone treatment. The addition of IL-1β did not seem to significantly contribute since the combination of all three treatments had a similar effect (Figure 22D). For Orm1 and Bmper, the combination of IL-6 + IL-1β was the most potent inducer of gene expression leading to an induction of 2.6-fold and 15.6-fold, respectively, compared to control. Corticosterone, in combination to IL-6, also had a significant effect, but it did not improve the effect of IL-6 + IL-1β combination (Figure 22E, F). As with the pre-mRNA, for Lcn2 mature mRNA all

the double combinations had a similar effect of 3.5-fold increase, while the triple combination led to a 5.9-fold upregulation of gene expression (Figure 22G).

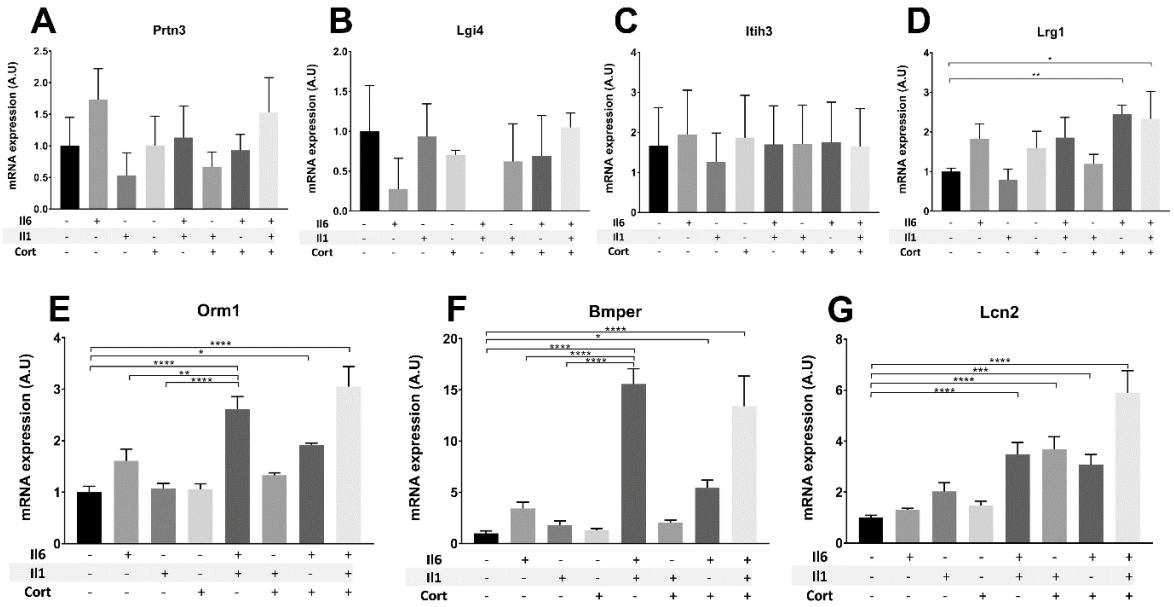

Figure 22. Mature mRNA expression of adipocyte-lipolysis hits upon STAT3 (IL-6), NF-kb (IL-1β) and GR (Corticosterone) activation in primary hepatocytes. Cells were treated with 100ng/mL IL-6 and IL-1β, and 1μM Corticosterone for 8hrs. Data are represented as mean ± SD, normalized to untreated control, two-way ANOVA: * p≤0.05, ** p≤0.01, *** p≤0.001, **** p≤0.0001, n=3 biological replicates.

Similar to the adipocyte-lipolysis hits, the myotube-atrophy hits also tended to respond mainly to IL-1β treatment at the pre-mRNA levels (Figure 23), but none of the effects were statistically significant.

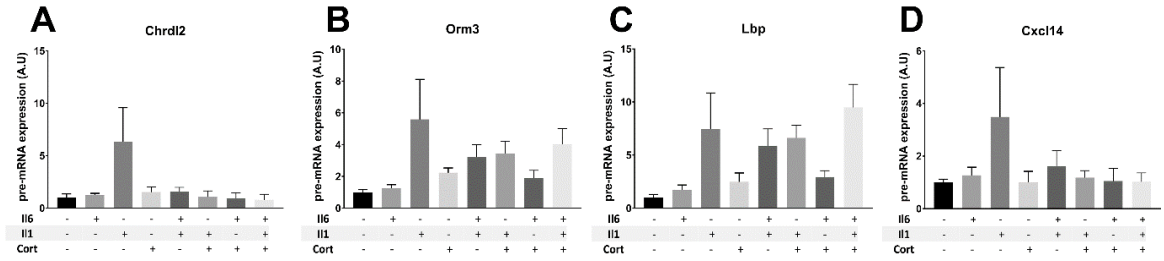

Figure 23. pre-mRNA expression of myotube-atrophy hits upon STAT3 (IL-6), NF-kb (IL-1β) and GR (Corticosterone) activation in primary hepatocytes. Cells were treated with 100ng/mL IL-6 and IL-1β, and 1μM Corticosterone for 2hrs. Data are represented as mean ± SD, normalized to untreated control, two-way ANOVA: * p≤0.05, ** p≤0.01, *** p≤0.001, n=3 biological replicates.

Mature mRNA levels of Cxcl14 were not induced in either condition (Figure 24D). Lbp mainly responded to IL-1β + Corticosterone with a 4-fold upregulation of expression (Figure 24C). Both Chrdl2 and Orm3 were upregulated upon Corticosterone treatment by 2.8-fold and 1.9-fold, respectively (Figure 24A, B) and in both cases the addition of IL-1β or IL-6 blunted the response. Except for Lbp, where double treatment with IL-1β and Corticosterone led to a 4-fold upregulation, double or triple treatment did not have any impact on the regulation of any of the other genes.

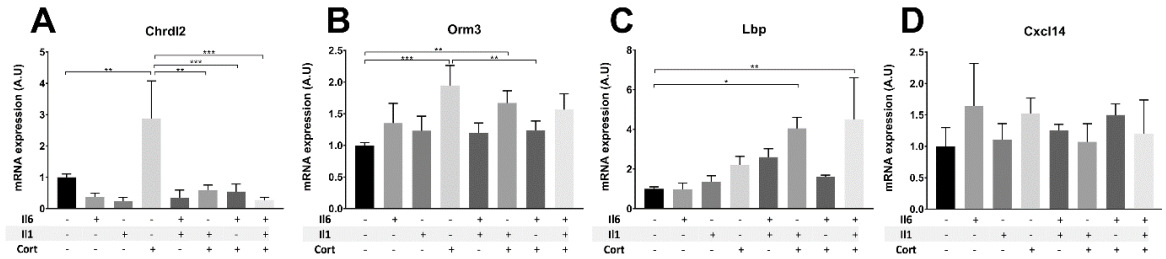

Figure 24. Mature mRNA expression of myotube-atrophy hits upon STAT3 (IL-6), NF-kb (IL-1β) and GR (Corticosterone) activation in primary hepatocytes. Cells were treated with 100ng/mL IL-6 and IL-1β, and 1μM Corticosterone for 8hrs. Data are represented as mean ± SD, normalized to untreated control, two-way ANOVA: * p≤0.05, ** p≤0.01, *** p≤0.001, n=3 biological replicates.

Overall, although IL-1β did not seem to be a strong inducer of gene expression when the mature mRNA was analyzed, when it comes to the acute setting it seemed that IL-1β was one of the main drivers of gene activation (Figure 25A). Mature mRNA levels of most of the genes were not affected by single treatments, and double treatment with either IL-6 + IL-1β or IL-6 + Corticosterone were required for an effect. Moreover, where either of the two dual combinations activated gene expression, the addition of the third treatment did not have any further effect (Figure 25B). In contrast to the adipocyte-lipolysis hits where double or triple treatments were required for gene expression induction, the myotube-atrophy hits (Chrdl2, Orm3 and Lbp) seemed to be rather Corticosterone induced when it comes to mature mRNA. Adipocyte-lipolysis-hits (Orm1, Bmper and Lcn2) seemed more responsive to IL-6 (Figure 25B). Interestingly, Lrg1, the common hit in both adipocyte-lipolysis and myotube-atrophy screenings responded mostly to the IL6 + Corticosterone treatment.

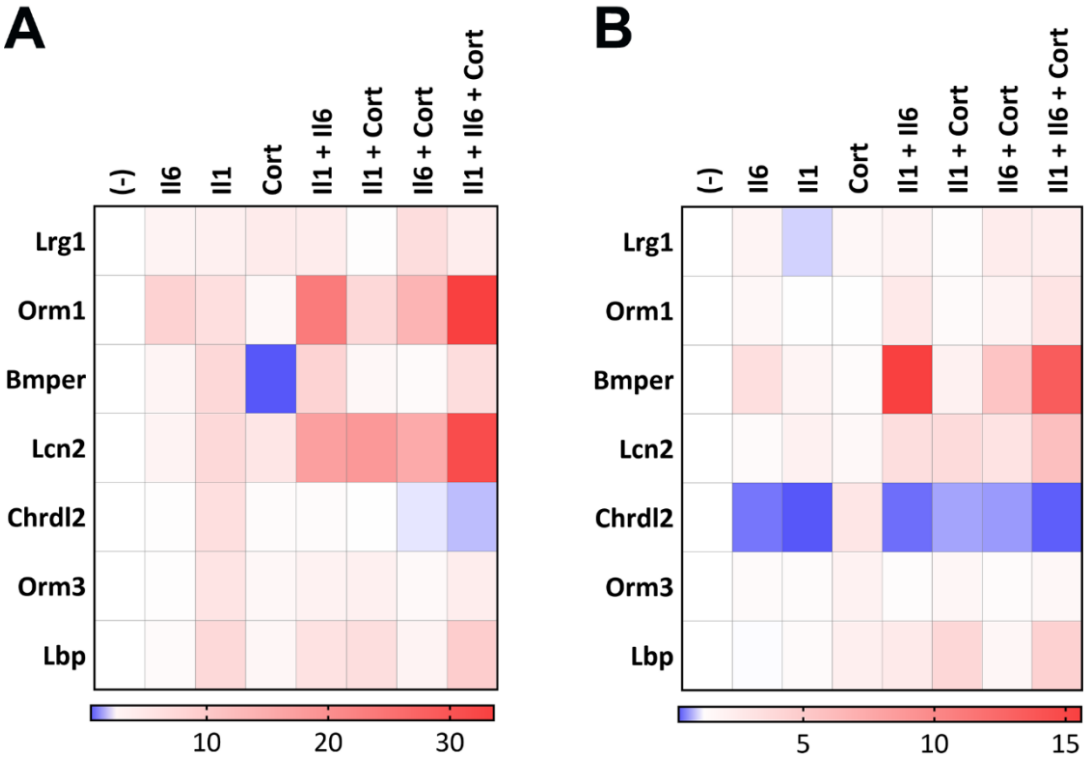

Figure 25. Overview of transcriptional regulation of adipocyte-lipolysis and myotube-atrophy hits. (A) pre-mRNA levels. **(B)** mature mRNA levels. Data are represented as mean, normalized to untreated control.

Proof of concept: *in vivo* manipulation of transcription factors can rescue the cachectic phenotype

Parallel studies in our lab explored the contribution of the transcriptional repressor Rev-erbα, encoded by the NR1D1 gene, to cachexia development. In mouse livers, Rev-erbα is a regulated in a diurnal pattern and is important for the regulation of several metabolic genes that control lipid homeostasis [71]. Experiments performed in our lab showed that Rev-erbα is downregulated in the C26 cachectic mice (unpublished data). Restoration of Rev-erbα in C26 mice (Annex 2A) led to a milder loss of body weight (Annex 2B) and protected the fat and muscle mass from wasting (Annex 2C).

As seen in Figure 26, C26 mice showed a 2.3-fold downregulation of hepatic NR1D1 expression, compared to healthy mice (C26 GFP vs PBS GFP). AAV-mediated hepatocyte-specific overexpression (OE) of NR1D1 in C26 mice resulted in expression levels similar to those of non-tumor-bearing mice (PBS Reverb), and to a 6.5-fold upregulation of mRNA levels as compared to C26 GFP mice.

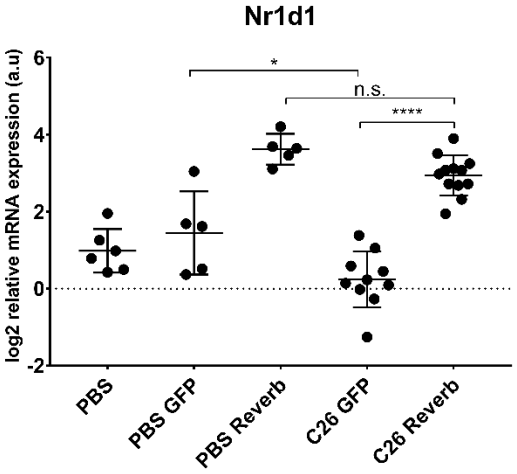

Figure 26. Hepatic NR1D1 expression upon AAV-mediated hepatocyte-specific overexpression. Data are represented as log2 mean ± SD, one-way ANOVA: * p≤0.05, **** p≤0.0001, n.s.=not significant. PBS: n=6, PBS GFP: n= 5, PBS Reverb: n= 5, C26 GFP: n=10, C26 Reverb: n=12.

To identify a potential molecular mechanism that could have contributed to the partial rescue of the BW, fat and skeletal muscle loss upon Rev-erbα restoration in C26 mice, the expression of the adipocyte-lipolysis (Figure 27) and myotube-atrophy hits (Figure 28) was addressed in the livers of these mice. The aim of this experiment was to investigate if the hits were regulated in PBS vs C26 mice in a Rev-erbα-dependent manner. Since Rev-erbα is a transcriptional repressor, the amelioration of cachexia upon Rev-erbα OE could, at least in part, be mediated by a downregulation of the adipocyte-lipolysis and myotube-atrophy hits.

Interestingly, Prtn3 was detected only in C26 mice, and not in healthy mice (Figure 27A), but there were no significant differences in its expression upon Rev-erbα OE. All the other genes were highly upregulated in C26 mice, compared to non-tumor mice (both in GFP as well as in Reverb groups). Both Lrg1 and Orm1 were upregulated between 11-14-fold in C26 mice vs healthy mice, but no difference upon Rev-erbα OE was observed (Figure 27D, E). Lgi4 and Lbp mRNA levels were increased by up to 6-8-fold in C26 mice compared to PBS mice, while Lcn2 levels were up by 1400-fold. Lgi4 (Figure 27B), Lcn2 (Figure 27G) and Lbp (Figure 28C), mRNA levels decreased by roughly 1.4-fold in C26 Reverb mice vs C26 GFP mice but these differences were not statistically

significant. Interestingly, Lcn2 levels were significantly downregulated in PBS mice by 3.4-fold, upon Rev-erbα OE, suggesting a potential regulation in basal condition, which, in cachectic conditions, is not sufficient to counter the high upregulation of Lcn2.

Itih3 (Figure 27C), Bmper (Figure 27F), Chrdl2 (Figure 28A), Orm3 (Figure 28B) and Cxcl14 (Figure 28D) were all significantly downregulated in C26 Reverb vs C26 GFP mice. The most pronounced difference was seen in Bmper (3-fold), followed by Orm3 and Cxcl14 (2.3-fold), Chrdl2 (2-fold) and, lastly, Itih3 (1.7-fold).

Overall, significant differences in C26 mice upon hepatic Rev-erbα OE were observed in 2 out of 7 adipocyte-lipolysis hits and 3 out of 5 myotube-atrophy hits. All genes were highly upregulated in cachectic mice, but some of them were expressed at rather low basal levels, i.e. Prtn3, Lgi4, Bmper and Chrdl2. Taken together, this indicates that hepatocyte clock disruption in cancer cachexia results in the upregulation of some of these factors which, in turn, suggests that they can contribute to cachexia development *in vivo.*

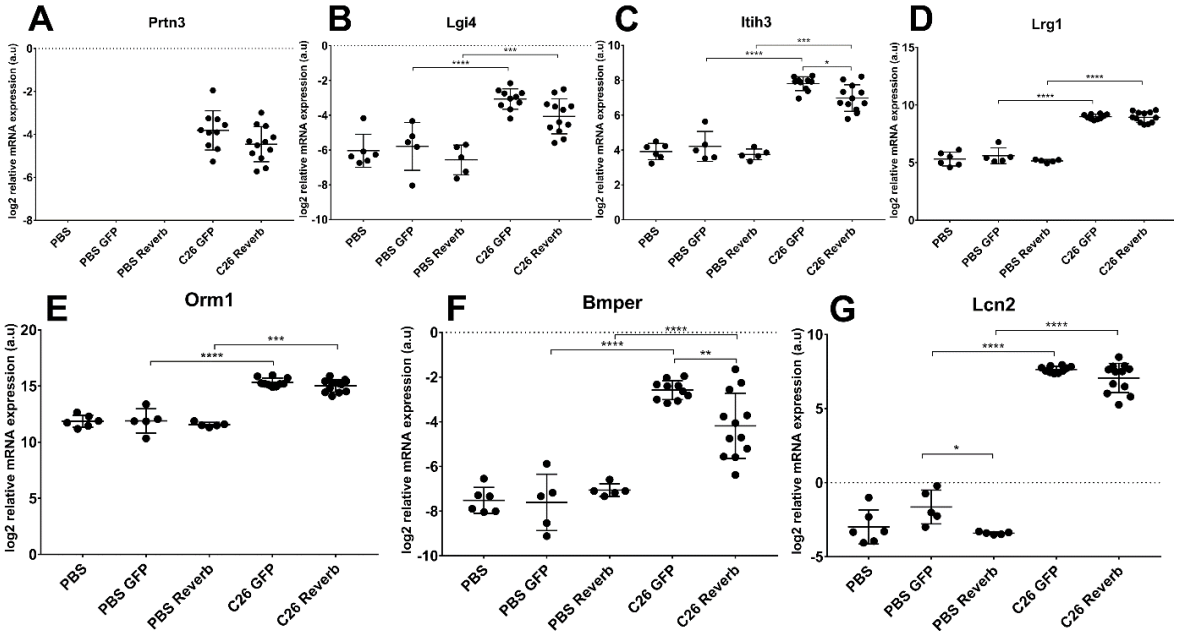

Figure 27. mRNA regulation of adipocyte-lipolysis hits upon Rev-erbα OE in C26 mice. Data are represented as log2 mean ± SD, one-way ANOVA: * p≤0.05, ** p≤0.01, *** p≤0.001, **** p≤0.0001.

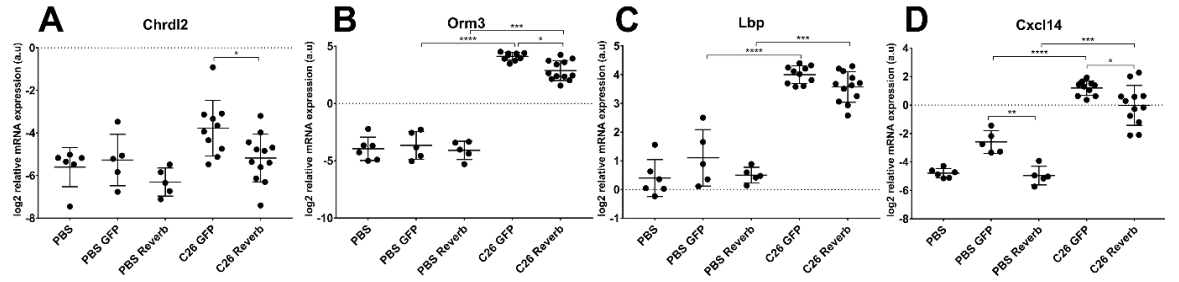

Figure 28. mRNA regulation of myotube-atrophy hits upon Rev-erbα OE in C26 mice. Data are represented as log2 mean ± SD, one-way ANOVA: * p≤0.05, ** p≤0.01, *** p≤0.001, **** p≤0.0001.

3. Discussion

3.1 Multiple liver/hepatocyte-secreted factors contribute to cachexia development

Cachexia development is associated with disturbances of several hepatic processes, such as the activation of the acute phase response, steatosis, reduced ketogenesis and inefficient utilization of energetic substrate [34]. However, to date, a direct contribution of liver-secreted factors to cachexia-associated tissue wasting has not been formally proven. The results of this thesis contribute to the pool of knowledge in regard to the consequences of hepatic dysfunction in cancer cachexia. By identifying a panel of liver/hepatocyte-secreted factors that can recapitulate cancer cachexia features *in vitro*, the data present in this thesis constitutes a first step in formally proving that the liver can have a direct role on cachexia development through secreted protein factors.

The strategy applied for the initial data set, consisting of liver-secreted factors, was to gradually narrow down the list of candidates and select the most promising one for an *in vivo* loss-of-function experiment. Although SAA 1/2 did not have an effect on adipocyte-lipolysis, its ability to reduce myotube width, coupled with its significant upregulation in the serum of cachectic mice, made it an attractive target. Therefore, as the AAV-LP1 vector has been shown to be hepatocyte-specific [72], I used a LP1-AAV-miRNA mediated approach to KD SAA 1/2 expression in hepatocytes in C26 mice. However, despite a significant downregulation of circulating and hepatic SAA 1/2 levels in tumor-bearing mice, protein levels remained extremely high as compared to a healthy state. This could, partly, explain the failure of the hepatocyte specific, AAV-mediated, SAA 1/2 KD to rescue the cachectic phenotype. Two different processes might have contributed to the insufficient reduction in SAA 1/2 levels: either the AAV-miRNA viral load was not high enough to counteract the extremely high number of copies of SAA 1/2 mRNA, or non-hepatic cells could have contributed to SAA 1/2 production under cachexia conditions. However, using a higher viral titer might be problematic since severe hepatotoxicity has been documented both in mice, as well as in nonhuman primates and piglets that were injected with high AAV titers [73, 74]. Moreover, since cachexia is a highly inflammatory state and systemic inflammation was documented to contribute to AAV clearance, it is also possible that the AAV was progressively cleared out as cachexia started developing [75].

A solution to overcome these issues could have been a hepatocyte-specific, SAA 1/2 genetic KO model, but SAA 1/2 KO models are not available on a BALB/c background [76], which is the required genetic background for the C26 model. A $Saa^{-/-}$ C57BL/6 model has been generated in the context of PDAC. While cachexia has not been addressed in this model, it was shown that SAA 1/2 did not have an effect on tumor cell proliferation or tumor weight [77], which is in contrast with the results of the SAA 1/2 KD experiment. The high variability in tumor weight, the discrepancy between tumor mass and tumor volume and the overall experimental design of the SAA 1/2 KD study, together with the findings of Lee et al, strongly indicate that SAA 1/2 does not have an effect on tumor growth. Interestingly, hepatocyte-specific deletion of STAT3 in PDAC mice abolished hepatic SAA 1/2 gene induction [77], confirming that hepatocytes are the main source of circulating SAA 1/2.

The initial strategy that led to the selection of SAA 1/2 made use of published literature in order to filter for hepatocyte-secreted factors. However, recent data generated by Sören Fisker-Schmidt using the Alb-INTACT-tumor bearing mice indicate that in early stages of cachexia, SAA 1/2 is

highly induced in hepatocytes, while in later stages SAA 1/2 expression is also upregulated in the non-parenchymal fraction (unpublished work). Indeed, although hepatocytes are the major site of SAA 1/2 production, other cells have also been shown to synthetize SAA proteins [49]. In an experimental model of amyloidosis, SAA production has been documented initially in hepatocytes, but shortly after also in Kupffer cells [78]. Therefore, our initial data set might have been confounded by the presence of factors that can be highly expressed also in non-parenchymal cells. In this respect, the subsequent identification of hepatocyte-secreted factors circumvented this issue. Overall, the results from the SAA 1/2 KD experiment suggested that, a hepatocyte-specific KD might not be sufficient to counteract the cachectic effects of highly induced liver-secreted proteins. Therefore, genetic KO models might be necessary to overcome this issue.

The *in vitro* results from the hepatocyte-secreted factors screen strengthened the view of cancer cachexia as a multi-factorial condition [8]. Over the years, multiple tumor and host-derived factors have been shown to have cachectic effects, but therapeutic strategies aimed at single factors have not proved successful [5]. Indeed, out of the initial 24 hepatocyte-secreted factors, 11 affected 3T3-L1 lipolysis or C2C12 myotube atrophy, and only one factor had effects on both read-outs. None of these candidates had major effects on tissue wasting *in vitro*, therefore pointing towards a role of the combinatorial effect of multiple factors.

Interestingly, the common factor, Lrg1 contributes to adipose tissue remodeling, as it has been reported to be induced during adipogenesis [79] and to possibly contribute to browning [80]. Moreover, Lrg1 is also an activator of TGF-β signaling [81], which is one of the best characterized pathways involved in muscle wasting in cachexia [3]. In fact, multiple of the 11 hits have been characterized as part of the TGF-β family or have been reported to interact with its members. These include Lrg1 [81], Bmper [82] and Chrdl2 [83]. Other hits, such as Lcn2 [84], Orm1 [85] and Prtn3 are known for contributing to insulin resistance [86] which could explain, at least partly, the observed effects on lipolysis.

TNFα is a potent inducer of lipolysis, so it was not surprising that TNF-CM had the strongest effect in the 3T3-L1 lipolysis screen where it was used as a positive control [87]. Remarkably, the candidates selected as adipocyte-lipolysis hits had 50-25% of the TNF-CM potency in inducing lipolysis. Although a direct comparison is not possible, by looking at the FLAG-ELISA it can be seen that Prtn3-CM, the candidate with the strongest effect on lipolysis, had similar FLAG-protein content as TNF-CM. However, Lgi4, the second strongest lipolysis inducer was secreted at much lower concentrations than TNF and still had roughly 40% of TNF-CM's effect. When recombinant protein was used, at much lower concentrations which could possibly mimic circulating levels, rTNF's effect was much stronger, rPrtn3 had no effect and rItih3 and rLrg1 had similar effects as the treatment with the respective CM. This suggests that some of the effects of candidate-CM could be attributed to the elevated concentration of proteins in the medium, or to other factors that were present in the concentrated CM. Furthermore, the presence of tags in both recombinant protein and the proteins overexpressed in HEK 293A cells might also affect protein activity. Protein aggregation during CM generation and concentration could also occur and therefore affect protein function. However, although the concentration of some proteins was very high in the candidate-CM, overall, the hits were distributed across the concentration range, and 2 out of 3 hits were confirmed with recombinant protein. This indicates that the candidate-CM can indeed be used to study the effects of secreted factors.

In the C2C12 myotube-atrophy screen, the quantification of TNF-CM was not possible, and, therefore, there was no positive control to be used as a reference. In general, strong treatments, such as Dexamethasone and C26-CM, can lead to roughly 20% decrease in C2C12 width [88, 89]. Therefore, the effects of the myotube-atrophy hits, ranging from 11-7% decrease, were more moderate, but still relevant. However, as previously mentioned, some degree of variation between different productions of CM exist, therefore the inclusion of more replicates would be needed to better address these effects. Similar to the 3T3-L1 lipolysis screening, the validation of the myotube-atrophy hits using recombinant protein would also be required.

3.2 Upstream regulators of the hepatic "cachectic program"

Although the effects of hepatocyte-secreted factors were moderate, the fact that overall, most candidates were able to induce, to some degree, adipocyte-lipolysis and/or myotube-atrophy, supports the idea that multiple hepatic factors contribute to wasting in cachexia. However, in order to be able to claim that the liver can act as an important mediator of cancer cachexia by synthesizing and releasing multiple protein factors that can contribute tissue wasting, a loss or gain-of-function experiment would be needed. Since addressing the downstream effects *in vivo* was not possible with the methods and models at hand and, also not feasible due to the large number of candidates, the upstream regulators of the new candidates were investigated. Identifying and targeting a transcriptional program would circumvent the risk of targeting individual factors whose effects might be limited.

Interestingly, most of the 11 adipocyte-lipolysis and myotube-atrophy hits are part of the APR or have been described in the context of innate immunity. The activation of the APR is well documented in cancer cachexia and it has been proposed that this increase in hepatic protein synthesis might require mobilization of skeletal muscle protein [8]. The APR could also contribute to systemic inflammation and therefore, indirectly, accelerate cachexia development. IL-1 and IL-6 have been shown to act synergistically to induce the hepatic APR through assisted loading of STAT3 on chromatin by NF-κB [69]. Interestingly, abrogation of Nf-KB and STAT3 signaling in hepatocytes abolished the activation of the APR in the liver in the context of bacterial infection [48]. Furthermore, GR has been shown to directly interact with STAT3 and drive the expression of APR proteins such as SAA 1 [67] and Hp [90]. Nf-KB and STAT3 are important regulators of the E3 ligases and autophagy genes in skeletal muscle [4], and GC-induced muscle wasting has also been reported [68]. The mechanisms driving adipose tissue wasting in cancer cachexia are less characterized, but the contribution of GC and inflammatory cytokines to lipolysis has been described [91, 92] and IL-6 mediated STAT3 activation has also recently been demonstrated to lead to 3T3-L1 lipolysis [93]. Therefore, the importance of STAT3, Nf-KB and GR activation to the regulation of the adipocyte- lipolysis and myotube-atrophy hits was addressed by treating primary hepatocytes with IL-6, IL-1β and Corticosterone. Indeed, most of the hits responded to these treatments. Interestingly, pre-mRNA levels were mostly influenced by IL-1β indicating that Nf-KB activation might be an early event in hepatic gene regulation. Synergy became more obvious for the mature mRNA levels, at least for the adipocyte-lipolysis hits, where dual treatment with IL-6 and IL-1β was the strongest inducer. This is in line with previously published data showing that STAT3 chromatin binding is very low upon IL-6 treatment alone and it only reaches maximal binding capacity once IL-1β is added and Nf-KB activated [69]. While GR activation did not seem to be important for the expression of the adipocyte-lipolysis hits, Corticosterone treatment was the most important regulator of the myotube-atrophy hits. Moreover, STAT3 and Nf-KB activation seemed to be early events while GR activation was more prominent at the 8hrs timepoint. This

observation is of particular interest since it was reported that adipose tissue lipolysis precedes skeletal muscle atrophy [16].

Intriguingly, some of these candidates are also expressed in cachexia target tissues. For instance, Orm1 and Lcn2 have been reported to be expressed by the adipose tissue [94, 95] while Lbp and Cxcl14 expression has been documented in muscle cells [96, 97]. Therefore, considering the role of STAT3, Nf-KB and GR in adipose tissue and skeletal muscle wasting, these signals could also be important for a potential autocrine effect. As such, it would be important to address whether or not the activation of the APR in the liver is a pre-requisite for the induction of these candidates in target tissues, taking into account the major contribution of the APR to systemic inflammation.

Overall, it seems that multiple transcriptional factors regulate different aspects of the cachectic hepatic program. Although knocking down Nf-KB and STAT3 was reported to abolish the APR in infection [48], the results of my experiments suggest that the induction of some hepatocyte-secreted factors responsible for tissue wasting are GR dependent. Therefore, a triple hepatocyte specific KD experiment would be the best option for addressing the contribution of the liver to cachexia development. Alternatively, parallel experiments that knock-down either GR or STAT3 and Nf-KB might provide useful molecular insight on the interrelationship between skeletal muscle atrophy and adipose tissue loss in cancer cachexia, since crosstalk between these organs has been hypothesized to further contribute to their dysfunction [98].

These experiments could not be performed in the allocated time for this thesis. However, a “proof of concept” was provided by parallel studies performed in our lab which showed that manipulation of transcriptional programs in the liver could ameliorate cachexia. To explore the mechanism underlying these effects, the regulation of cachectic hepatocyte-secreted factors was addressed in C26 mice that had restored Rev-erbα levels. The gene analysis performed on the liver samples from this experiment confirmed that the 11 adipocyte-lipolysis and myotube-atrophy hits are highly upregulated in C26 cachectic mice. Most factors were indeed downregulated upon Rev-erbα OE, showing that hepatocyte-secreted factors could be responsible, to some extent, for cachexia development.

While the genetic manipulation of these factors might provide a clear proof of the liver’s involvement in cachexia development, the success of this strategy could be complicated by the fact that some of the APR proteins also have anti-inflammatory and immunomodulatory effects, which could be problematic to address in a tumor model. Indeed, pleiotropic effects for some of the candidates have been reported. For instance, multiple glycoforms of Orm1 are generated during inflammation and present both pro- and anti-inflammatory actions [99]. Similarly, low concentrations of Lbp seem to enhance LPS induced activation of immune cells, while the acute-phase increase can inhibit LPS’ actions [100]. However, to provide a proof for the contribution of liver to cachexia, future experiments could focus on comparing transcription factors-KD phenotypes and expression profiles with the secreted-factors library. This would allow a better characterization of the hepatic transcriptional programs and the secreted factors that contribute to tissue wasting. Since hepatocytes are suggested to play a role in other cancer associated complications, such as metastatic dissemination [77] and thrombosis [35], this framework could also be employed to study the contribution of the secreted factors to other aspects of cancer cachexia, beyond tissue wasting.

The aim of this thesis was to provide evidence that supports the contribution of liver-secreted factors to the development of cancer cachexia. Two important conclusions were drawn after analyzing the first part of the work presented here. Firstly, *in vitro* functional assessment

experiments demonstrated that liver-secreted factors contribute to tissue wasting *in vitro*. Secondly, the results obtained with the SAA 1/2 KD suggested that focusing on one highly induced factor might limit the experimental strategy that can be applied in order to understand its contribution to the observed phenotype via loss-of-function experiments. Considering the magnitude of induction of many of the factors presented in this thesis, a genetic KO model would probably be required to properly assess the role of individual factors. To block potential autocrine/paracrine effects, this might need to be done at the whole-body level. These aspects might reduce the therapeutic potential of the most dramatically induced targets.

The second part of the work focused on hepatocyte-secreted factors and demonstrated that multiple factors have moderate effects on tissue wasting *in vitro*, suggesting that the identification of a "cachectic program" might be more relevant than addressing the contribution of individual factors. Indeed, STAT3, Nf-kB and GR seemed to be important for the upstream regulation of the identified secreted factors. Furthermore, the AAV-mediated restoration of Rev-erbα led to decrease expression of several of these factors, which indicates that targeting transcriptional programs important for the upregulation of cachectic factors in the liver could be a successful strategy to further clarify the role of liver-secreted factors to cancer cachexia development.

Overall, the work presented in this thesis indicates that hepatocyte-secreted factors which are upregulated in the context of cancer cachexia can lead to adipose tissue and skeletal muscle wasting *in vitro*. Taken individually, hepatocyte-secreted factors had mild effects, but in general, most factors induced adipocyte-lipolysis and myotube-width, suggesting that a potential additive/synergistic effect of multiple candidates is relevant for tissue wasting in cachexia. Moreover, the small degree of overlap between the candidates that induced adipocyte-lipolysis and myotube-atrophy indicates that distinct factors could have tissue-specific effects when it comes to wasting. As most of the factors that mediated these effects are part of the APR, this thesis also supports a direct contribution of the APR in mediating wasting in cachexia-target tissues. Further work is required to decipher potential molecular mechanism in adipose tissue and skeletal muscle wasting. These results could contribute to a better understanding of the pathophysiological mechanisms underlying cancer cachexia.

4. Material and methods

4.1 Material

Chemicals

Table 2. Chemicals

Product	Company	Catalog number
Trimethylamine N-oxide	Santa Cruz	sc-253763
3-Isobutyl-1- Methylxanthine	Sigma	I5879-250MG
Dexamethasone	Sigma	D4902-100MG
Insulin Solution, Human recombinant	Sigma	I9278-5ML
Rosiglitazone	Sigma	R2408-10MG
Primary Hepatocyte Thawing and Plating Supplements-1 kit	Life Technologies	CM3000
Primary Hepatocyte Maintenance Supplements-1 kit	Life Technologies	CM4000
TRIzol Reagent-200 mL	Life Technologies	15596018
Lipofectamine 2000	Thermo	1668019
Opti-MEM I Reduced Serum Medium	Life Technologies	31985062
FreeStyle 293 Expression Medium	Life Technologies	12338018
DMEM, high glucose, pyruvate	Life Technologies	41966052
Fetal bovine serum (FBS)	Sigma	F7524
Penicillin-Streptomycin (5,000 U/mL)	Gibco	5000956
Cell Extraction Buffer	Life Technologies	FNN0011
PhosSTOP	Roche	4906845001
cOmplete Mini, EDTA-free	Roche	11836170001
Ponceau S solution	Sigma	P7170-1L
Tween® 20	Sigma	P9416-100ML
UltraPure™ double-distilled water (ddH_2O)	Invitrogen	10977-035

Primers

Table 3. qPCR primers

Name	Company	Orientation	Sequence 5'-3'
pre-TBP	Sigma	Forward	CTCCTGTTGCAGTCACTTTCCT
		Reverse	GCAGAAGAACACTGGAGATGGT
pre-Saa	Sigma	Forward	TCTCAAAGGCATGGGCAGAG
		Reverse	TCATGTCAGTGTAGGCTCGC
pre-Fgg	Sigma	Forward	AGACTGGAATGGCAGAACCAG
		Reverse	ACCAGCTGCAAAGCTCCATT
pre-Serpin3n	Sigma	Forward	AGGCTGACCTGTCTGCAATC
		Reverse	GCACAAGCTGAACCACCAAG
pre-Prtn3	Sigma	Forward	GGCTCAGTTAGGCTTAGGGC
		Reverse	ATTGAATGCTGTGCAGTGCC

pre-Lgi4	Sigma	Forward	GCGGGTGACTGTAGGACAAG
		Reverse	CATCATCCACACCAGCGACA
pre-Itih3	Sigma	Forward	TAAGCATGGTGGGGGTTGTC
		Reverse	GTTGACTGAGGAGAACGGCA
pre-Lrg1	Sigma	Forward	TGGAAGCTTCTGCCTTCCTG
		Reverse	TGGACTCGTGTTCACTCTGC
pre-Orm1	Sigma	Forward	ACGACTTCCATGACACCTCAA
	Sigma	Reverse	ATCAAGAGGTTTCGGCATGGGT
pre-Bmper		Forward	TCTAGCCTTCTTAGCCCCGT
	Sigma	Reverse	CTCTGCGTGTTCATTCTGCC
pre-Lcn2		Forward	GCAGGTGAATGGCAGGTTTG
	Sigma	Reverse	CCCCTGCCACAAATAGCTGA
pre-Chrdl2		Forward	GGCGTCTAACCCACCTCAAA
	Sigma	Reverse	AGTTGCCTCTGTACCCGTTG
pre-Orm3	Sigma	Forward	GGTTGACACTACCGTGCCAT
		Reverse	CTATTGTAAGGTGGGTTGGGGG
pre-Lbp	Sigma	Forward	AAAGGCCTCTCTGTTCTCGC
		Reverse	GAGGTACACATCGCCTCCTG
pre-Cxcl14	Sigma	Forward	CTCCCCCAGAAACAGGACAC
		Reverse	TGTGCCCTTCCTTCACAGAC
TBP	Sigma	Forward	CTACCGTGAATCTTGGCTGTAAAC
		Reverse	AATCAACGCAGTTGTCCGTGGC
Saa 1	Sigma	Forward	GGAGTCTGGGCTGCTGAGAAAA
		Reverse	TGTCTGTTGGCTTCCTGGTCAG
Fgg	Sigma	Forward	CACCACAGAGTTTTGGCTGGGA
		Reverse	CCTGAACATGGCATAGTCCGCA
Serpin3n	Sigma	Forward	CAACCAGAGACCCTGAGGAAGT
		Reverse	AGGACATCCTCCAGGCTGTAGT
Prtn3	Sigma	Forward	ATCCACCCGAGATTCGTGCTGA
		Reverse	CTGGAAGACCTGACTGATGGTG
Lgi4	Sigma	Forward	TGTTCCTGTGCCTGACGCGATA
		Reverse	CAGGATAGCCAACTGGTCTCTG
Itih3	Sigma	Forward	CTCTTCAGCACCGATGTGACCA
		Reverse	ACCCTTCAGCAGCCCATCATTG
Lrg1	Sigma	Forward	CCAATAACTCTCTGTCCAGCACG
		Reverse	TCTTGTTTCGGTTGGCGACCAG
Orm1	Sigma	Forward	CCTTCATGCTTGCCTTTGACCTC
		Reverse	CGTGTGTGACAGCCTTCTGGAA
Bmper	Sigma	Forward	CCTGCTGTGAACGATGCAAAGG
		Reverse	ACCTCAGACTCTGTCACCACAC
Lcn2	Sigma	Forward	ATGTCACCTCCATCCTGGTCAG
		Reverse	GCCACTTGCACATTGTAGCTCTG
Chrdl2	Sigma	Forward	TGTGATGGAGCCACAGCAATGC
		Reverse	AACAGCTCCTGGGCACTGAAGA
Orm3	Sigma	Forward	CCACTGTGTCTATAACTCCAACC
		Reverse	CTCTAGCACTCTCAGGTGGAGA
Lbp	Sigma	Forward	TCCATCGGTGTCCGAGGCAAAT
		Reverse	AGGTCCACTGAAATGGTGACACC
Cxcl14	Sigma	Forward	TACCCACACTGCGAGGAGAAGA
		Reverse	CGCTTCTCGTTCCAGGCATTGT
Nr1d1	Sigma	Forward	CAGGCTTCCGTGACCTTTCTCA
		Reverse	TAGGTTGTGCGGCTCAGGAACA

Antibodies

Table 4. Antibodies

Target protein	Company	Catalog number
anti-Mouse-HRP	Thermo Fisher	61-6520
anti-Rabbit HRP	Sigma	A6154
Mouse Serum Amyloid A1/A2	R&D Systems	AF2948
FLAG	Cell Signaling	2368

Plasmids

Table 5. Plasmids

Name	Source	Backbone	Catalog number
Saa1 cDNA ORF clone	Genscript	pcDNA3.1+/C-(K)DYK vector	OMu16277
Saa2 cDNA ORF clone	Genscript	pcDNA3.1+/C-(K)DYK vector	OMu19235
Serpina3n Mouse Tagged ORF Clone	OriGene	pCMV6-Entry	Origene MR206624
Fgg Mouse Tagged ORF Clone	OriGene	pCMV6-Entry	Origene MR206950
Fgb Mouse Tagged ORF Clone	OriGene	pCMV6-Entry	Origene MR207713
Lgi4 Mouse Tagged ORF Clone	OriGene	pCMV6-Entry	Origene MR220289
Qsox1 Mouse Tagged ORF Clone	OriGene	pCMV6-Entry	Origene MR210448
Orm1 Mouse Tagged ORF Clone	OriGene	pCMV6-Entry	Origene MR202201
Prtn3 Mouse Tagged ORF Clone	OriGene	pCMV6-Entry	Origene MR222354
Igfbp1 Mouse Tagged ORF Clone	OriGene	pCMV6-Entry	Origene MR203644
Hpx Mouse Tagged ORF Clone	OriGene	pCMV6-Entry	Origene MR207345
Tnf Mouse Tagged ORF Clone	OriGene	pCMV6-Entry	Origene MR212145
Cpb2 Mouse Tagged ORF Clone	OriGene	pCMV6-Entry	Origene MR226900
Itih4 Mouse Tagged ORF Clone	OriGene	pCMV6-Entry	Origene MR212254
Orm3 Mouse Tagged ORF Clone	OriGene	pCMV6-Entry	Origene MR215822
Orm2 Mouse Tagged ORF Clone	OriGene	pCMV6-Entry	Origene MR202200
Itih3 Mouse Tagged ORF Clone	OriGene	pCMV6-Entry	Origene MR211061
Lbp Mouse Tagged ORF Clone	OriGene	pCMV6-Entry	Origene MR207709
Lrg1 Mouse Tagged ORF Clone	OriGene	pCMV6-Entry	Origene MR205144
Lcn2 Mouse Tagged ORF Clone	OriGene	pCMV6-Entry	Origene MR226233
Il1r1 Mouse Tagged ORF Clone	OriGene	pCMV6-Entry	Origene MR227508
Bmper Mouse Tagged ORF Clone	OriGene	pCMV6-Entry	Origene MR210035
Fga Mouse Tagged ORF Clone	OriGene	pCMV6-Entry	Origene MR208831
Fgl1 Mouse Tagged ORF Clone	OriGene	pCMV6-Entry	Origene MR204485
Cxcl1 Mouse Tagged ORF Clone	OriGene	pCMV6-Entry	Origene MR220966
Chrdl2 Mouse Tagged ORF Clone	OriGene	pCMV6-Entry	Origene MR206798
Cxcl14 Mouse Tagged ORF Clone	OriGene	pCMV6-Entry	Origene MR222808

miRNA SAA sequences

Table 6. Sequences of miRNAs targeting SAA

Name	Company	Orientation	Sequence 5'-3'
Saa1/2 A	Sigma	Forward	TGCTGCAGGCTGGTGAGTAGCTTCATGTTTTGGCCACTGACTGACA TGAAGCTTCACCAGCCTG

		Reverse	CCTGCAGGCTGGTGAAGCTTCATGTCAGTCAGTGGCCAAAACATG AAGCTACTCACCAGCCTGC
Saa1/2 B	Sigma	Forward	TGCTGCTTCCTTCATGTCAGTGTAGGGTTTTGGCCACTGACTGACC CTACACTCATGAAGGAAG
		Reverse	CCTGCTTCCTTCATGAGTGTAGGGTCAGTCAGTGGCCAAAACCCTA CACTGACATGAAGGAAGC
Saa1/2 C	Sigma	Forward	TGCTGACCCTTGTGGGATACACACATGTTTTGGCCACTGACTGACA TGTGTGTCCCACAAGGGT
		Reverse	CCTGACCCTTGTGGGACACACATGTCAGTCAGTGGCCAAAACATG TGTGTATCCCACAAGGGTC
Saa1/2 D	Sigma	Forward	TGCTGTTACCCTCTCCTCCTCAAGCAGTTTTGGCCACTGACTGACTG CTTGAGGGAGAGGGTAA
		Reverse	CCTGTTACCCTCTCCCTCAAGCAGTCAGTCAGTGGCCAAAACTGCT TGAGGAGGAGAGGGTAAC
Saa1/2 E	Sigma	Forward	TGCTGAGTCCAGGAGGTCTGTAGTAAGTTTTGGCCACTGACTGAC TTACTACACCTCCTGGACT
		Reverse	CCTGAGTCCAGGAGGTGTAGTAAGTCAGTCAGTGGCCAAAACTTA CTACAGACCTCCTGGACTC
Saa1 F	Sigma	Forward	TGCTGAAGAATTCCTGAAAGGCCTCTGTTTTGGCCACTGACTGACA GAGGCCTCAGGAATTCTT
		Reverse	CCTGAAGAATTCCTGAGGCCTCTGTCAGTCAGTGGCCAAAACAGA GGCCTTTCAGGAATTCTTC
Saa1 G	Sigma	Forward	TGCTGAGTATTTGTCAGGCAGTCCAGGTTTTGGCCACTGACTGACC TGGACTGTGACAAATACT
		Reverse	CCTGAGTATTTGTCACAGTCCAGGTCAGTCAGTGGCCAAAACCTG GACTGCCTGACAAATACTC
Saa2 F	Sigma	Forward	TGCTGAAGAATTCCTGAAAGCTCTCTGTTTTGGCCACTGACTGACA GAGAGCTCAGGAATTCTT
		Reverse	CCTGAAGAATTCCTGAGCTCTCTGTCAGTCAGTGGCCAAAACAGA GAGCTTTCAGGAATTCTTC
Saa2 G	Sigma	Forward	TGCTGAGTATTTGGCAGGCAGTCCAGGTTTTGGCCACTGACTGAC CTGGACTGTGCCAAATACT
		Reverse	CCTGAGTATTTGGCACAGTCCAGGTCAGTCAGTGGCCAAAACCTG GACTGCCTGCCAAATACTC

Cytokines and recombinant proteins

Table 7. Cytokines and recombinant proteins

Cytokine/rec protein	Company	Catalog no.
Apo-SAA1, rec. Human	PeproTech	300-53-1000
rmLipocalin-2 CF; 50 µg	R&D Systems	1857-LC-050
Recombinant protein of human proteinase 3 (PRTN3)	Biocat	TP720488-OR
Inter-a-Trypsin Inhibitor Heavy Chain H3/ITIH3 Protein(C-6His)	Biomol	E-PKSH032658.10
Recombinant Human LRG1 protein	Abcam	ab185867-10ug
IL-6, rec. Murine	PeproTech	216-16-10
IL-1 beta, rec. Murine	PeproTech	211-11B-10
TNF-alpha, rec. Murine	Peprotech	315-01A-5

Kits

Table 8. Kits

Kit	Manufacturer	Catalog Reference

Pierce™ BCA protein assay kit	Thermo Scientific	23227
Trans-Blot Turbo RTA Transfer Kit, nitrocellulose, midi	Bio-Rad Laboratories	1704271
RNeasy Plus Mini Kit (50)	Qiagen	74134
QuantiTect Reverse transcription (400)	Qiagen	205314
TaqMan Gene Expression Master Mix-2 x 5 mL	Applied Biosystems	4369514
PowerUp SYBR Green Master Mix	Applied Biosystems	A25741
EndoFree Plasmid Mega Kit (5)	Qiagen	12381
QIAQUICK GEL EXTRACTION KIT (50)	Qiagen	28704
HiSpeed Plasmid Midi Kit (25)	Qiagen	12643
FREE GLYCEROL REAGENT	Sigma-Aldrich	F6428-40ML
GLYCEROL STANDARD SOLUTION, 25 MG-ML	Sigma-Aldrich	G7793-5ML
DYKDDDDK-Tag Detection ELISA Kit	Biomol	Cay501560-96
Mouse Serum Amyloid A Quantikine ELISA Kit	R&D Systems	MSAA00
SAA Human ELISA Kit-96 assays	Life Technologies	KHA0011
Mouse Lipocalin-2/NGAL Quantikine ELISA Kit	R&D Systems	MLCN20
Human Lipocalin-2/NGAL Quantikine ELISA Kit	R&D Systems	DLCN20
Mouse Serpin E1/PAI-1 DuoSet ELISA	R&D Systems	DY3828-05
Human Total Serpin E1/PAI-1 Quantikine ELISA Kit	R&D Systems	DTSE100
Ancillary Kit 2; 1 Kit	R&D Systems	DY008
MitoTracker Red CMXRos	LIFE Technologies	M7512
MitoTracker Green FM	LIFE Technologies	M7514

Instruments

Table 9. Instruments

Device	**Company**
-20 °C Freezer	Liebherr
-80 °C Freezer Innova U101	Eppendorf
0.2-2.5 µL Pipette Research plus	Eppendorf
1-10 µL Pipette Research plus	Eppendorf
2-20 µL Pipette Research plus	Eppendorf
20-200 µL Pipette Research plus	Eppendorf
100-500 µL Pipette Research plus	Eppendorf
4 °C Fridge Lgex-3410-22A	Liebherr
Analytical scale AX124M	Ohaus
Bacteria incubator HeraTherm	Thermo Scientific
Cell counter Countess 2	Life technologies
Cell incubator HeraCell150i	Thermo Scientific
Centrifuge 5427R	Eppendorf
Centrifuge 5910R	Eppendorf
Centrifuge Microfuge 20	Beckmann Coulter
Centrifuge Microfuge 20R	Beckmann Coulter
Chemidoc	Bio-Rad

Ice machine ZBE 110-35	Ziegra
Laboratory scale AX5202M	Ohaus
Laminar flow HeraSafe KS	Thermo Scientific
Magnetic stirrer RMS-10HS	Phoenix Instrument
Microscope Eclipse TS2	Nikon
Multipette® E3 multistep pipette	Eppendorf
Nanodrop 2000	Thermo Scientific
PCR Cycler Mastercycler X50s	Eppendorf
Pipetboy Easypet 3	Eppendorf
Plate centrifuge	Axygen
Varioskan LUX plate reader	Thermo Scientific
qPCR machine Quantstudio 6 flex	ABS
Shaker	Edmund Bühler GmbH
Shaker SM-30	Edmund Bühler GmbH
Thermomixer C	Eppendorf
Tuberoller RS-TR05	Phoenix Instrument
Turbo blotter	Bio-Rad
Vacuum N811KN.18	KNF
Vortexer Genie 2	Scientific Ind
Voyager 0.5-12.5 µL, 12 channel electrical pipette	Integra
Voyager 0.5-12.5 µL, 8 channel electrical pipette	Integra
Waterbath Aqualine AL 25	Lauda
Xplorer®, 8 channel, 15 – 300 µL electrical pipette	Eppendorf
Xplorer®, 8 channel, 5 – 100 µL electrical pipette	Eppendorf

Consumables

Table 10. Consumables

Consumable	Company	Catalog reference
BIOCOAT Collagen I 12-well-Platten	VWR International	734-0295
Cell culture plates 150X25mm	Falcon	5000740
6 Well Clear Flat Bottom TC-Treated Multiwell Cell Culture Plate	Falcon	353046
12 Well Clear Flat Bottom TC-Treated Multiwell Cell Culture Plate	Falcon	353043
24 Well Clear Flat Bottom TC-Treated Multiwell Cell Culture Plate	Falcon	353047
96 Well Clear Flat Bottom TC-Treated Multiwell Cell Culture Plate	Falcon	353072
96 Well Plates, transparent	Fisher Scientific	10124721
0.2 mL non-skirted low profile 96-well PCR plate	Thermo Scientific	00464225
Adhesive PCR Plate Seals-100 sheets	Life Technologies	AB0558
Amersham Protran 0.45 NC nitrocellulose western blotting membranes, 300 cm x 4 cm	GE Healthcare	10600002
Cell scraper 25 cm, sterile	Sarstedt	83.1830
Cell strainer, nylon, single packed, 100 µm	Fisher Scientific	11517532
Cellstar® 10 mL, serological pipette, sterile	Greiner Bio-One	607180/10ml
Cellstar® 2 mL, serological pipette, sterile	Greiner Bio-One	710180/2ml
Cellstar® 25 mL, serological pipette, sterile	Greiner Bio-One	760180/25ml

Cellstar® 5 mL, serological pipette, sterile	Greiner Bio-One	606180/5ml
Cellstar® 50 mL, serological pipette, sterile	Greiner Bio-One	768180/50ml
Combitips Advanced 0.2 mL	Eppendorf	5431800
Combitips Advanced 10.0 mL biopur	Eppendorf	5431823
Combitips Advanced 5.0 mL biopur	Eppendorf	5431822
Conical tube 15 mL	Falcon	352096
Conical tube 50 mL	Falcon	352070
Pierce™ Protein Concentrator PES, 3K MWCO, 5-20 mL	Thermo Scientific	88525
Corning Syringe Filters, 0.45 µm	Sigma-Aldrich	CLS431220-50EA
Countess™ cell counting chamber slide	Invitrogen	C10228
Delicate task wipes	Kimtech	7558
Eppendorf Tubes® 5.0 mL	Eppendorf	0030119380
Extra thick blot paper	Bio-Rad	1703966
Filter Midisart®2000 0.45 µm	Sartorius	17804
Filtertips TipOne 0.1-10 µL	Starlabs	5000828
Filtertips TipOne 1-20 µL	Starlabs	5000829
Filtertips TipOne 1-200 µL	Starlabs	5000830
Filtertips TipOne 100-1000 µL	Starlabs	5001148
LONG filter sterile tips 12.5 µL	Integra	#4405
MicroAmp™ optical 384-well reaction plate with barcode	ABS	4309849
MicroAmp™ optical adhesive film	ABS	4311971
Norm-Ject® 10 mL syringe	VWR	4100-000V0
Round gel loading tips 200 µL	Santa Cruz	Sc-201732
Safe Lock tubes 1.5 ml	Eppendorf	0030120086
Safe Lock tubes 2.0 ml	Eppendorf	0030120094
Weighing boats PS, black, antistatic, 140 x 140mm, 250 mL	Schubert und Weiss	5900800
Weighing boats PS, black, antistatic, 85 x 85 mm, 100 mL	Schubert und Weiss	5900791
Novex WedgeWell 4-20% Tris-Glycine Mini Gels	Life Technologies	XP04202BOX

Primer-Blast NCBI

4.2 Methods

Cell culture

General cell culture conditions

All experiments with cells were performed under sterile conditions. Cells were incubated at 37°C, 5% CO_2 and 95% humidity. Prior to use, media and all additives were warmed to 37°C. The types of media that were used are listed in Table 11.

Table 11. Media used for cell culture

Name	Medium	Serum	Antibiotic	Additives
3T3-L1 culture	DMEM (4.5g/L glucose)	10% FBS	1% P/S	-
3T3-L1 differentiation	DMEM (4.5g/L glucose)	10% FBS	1% P/S	See Table 1
C2C12 culture	DMEM (4.5g/L glucose)	10% FBS	1% P/S	-
C2C12 differentiation	DMEM (4.5g/L glucose)	2% FBS	1% P/S	-
C26 culture	DMEM (4.5g/L glucose)	10% FBS	1% P/S	
HEK293 culture	DMEM (4.5g/L glucose)	10% FBS	1% P/S	
Primary hepatocyte culture	DMEM (4.5g/L glucose)	10% FBS	1% P/S	-
Freezing media	DMEM (4.5g/L glucose)	10% FBS	1% P/S	10% DMSO

3T3-L1: cell culture, differentiation, and lipolysis assay

3T3-L1 fibroblasts were cultured in 15cm dishes containing 20mL media (Table 11). To avoid diminishing their differentiation potential, cells were never grown beyond the 11^{th} passage and a 70% confluency. For passaging, the media was removed from the cells, the plate was washed once with 1xPBS and the cells were detached from the cell culture dishes with Trypsin. Cells were then centrifuged at 2000rpm for 3min and re-suspended in 10mL media.

For the experiments in 2.1Liver-secreted factors screen, $1x10^4$ cells were seeded in 12 well plates and differentiated as stated in Table 1 (Protocol 1). For the experiments in Hepatocyte-secreted factors screen, $3x10^3$ cells were seeded in 96 well plates and differentiated as stated in Table 1 (Protocol 2).

Lipolysis was measured after 24hrs of treatment (recombinant protein or candidate-CM) as free glycerol content of the media according to instructions from the company (F6428, Sigma).

C2C12: cell culture, differentiation, and atrophy assay

C2C12 myoblasts were cultured as the 3T3-L1 cells. For the experiments in the Liver-secreted factors screen, $1x10^4$ cells were seeded in 12 well plates and differentiated for 48hrs. Myotubes were treated for 48hrs, imaged in bright-field and approximately 100 myotubes per condition were quantified. For the experiments in the Hepatocyte-secreted factors screen, cells were seeded in 24 well plates, differentiated for 72hrs and treated for 48hrs. Myotubes were stained with Mitotracker Green (250nM, 30min) and then imaged and quantified.

C26: cell culture, CM generation and CCK8 assay

C26 cells were cultured as the 3T3-L1 cells. To study the viability of cells upon the tested treatments, the Cell Counting Kit-8 (CCK-8) assay (Sigma Aldrich) was used. This assay is based on

the conversion of a highly water-soluble tetrazolium salt, called WST-8, to a water-soluble formazan dye, in the presence on an electron carrier. In living cells, WST-8 is reduced to an orange colored product thorough the activity of dehydrogenases. The amount of colored product is directly proportional to the number of living cells and can be determined by spectrophotometry at 450nm.

For this assay, cells were seeded in 96 well plates. 10µL of CCK-8 reagent were added and the plate was incubated at 37°C. Absorbance was read after 30min and 1hr.

For C26-CM generation cells were seeded in 15cm dishes. When cells reached 80% confluency fresh media was added and collected, filtered and frozen 24hrs later.

HEK293A transfection and candidate-CM generation

6 x 10^6 HEK293 A cells were seeded in 15cm dishes 24hrs prior to transfection and were transfected at 70% confluency. Cells were transfected with ready-to-use cDNA expression plasmids (see Table 5) obtained from OriGene. 20µg of plasmid DNA were mixed with 40µL Lipofectamine 200 in 4mL OptiMEM. The mixture was incubated for 15 - 20min at RT and subsequently added to the cells dropwise. Medium was changed 24 h after transfection and conditioned medium was produced as described in Figure 15A. For the concentration of candidate-CM Filters (Pierce,20ml, 3K) were washed once with 70% Et-OH 15min at 4000xg and twice with PBS. Media (20ml) was collected and filtered to remove cells (0.22µm) and then loaded on the columns and spun 3hrs at 4°, 4000g. Volumes were adjusted to 2mL with the flow-through and topped up with 15ml DMEM phenol free, SFM, 1% P/S and spun at 4°, 4000g until they reached a final volume of 2mL. Candidate-CM was aliquoted and snap frozen in liquid N2. 1% fresh FBS was added to the candidate-CM before using it to treat adipocytes and myotubes.

Primary hepatocytes: culture and treatment

8-12 weeks old male C57BL/6N mice were perfused with collagenase to isolate primary hepatocytes [101]. Under anesthesia, mice were cut open and the liver was perfused via vena cava first for 10min with an EGTA-containing buffer, afterwards with a buffer containing collagenase for 10 -12min (both buffers on HEPES/KH base). After perfusion, the liver was collected in a buffer containing BSA, filtered through a 100nm pore size sieve and re-suspended in the buffer after centrifugation. Cells were plated on BioCoat collagen-coated plates (Corning) in seeding media (Williams E Medium + CM3000 Sigma). After 1-2hrs, media was changed to maintenance media (Williams E Medium + CM4000 Sigma) and 6hrs later to mild starvation media (DMEM -glucose, -phenol red, -glutamine, +5mM glucose, 1% FBS and 1% P/S). Cells were treated next day for either 2 or 8hrs with IL-6 (100ng/mL), Il-1β (100ng/mL) and Corticosterone (1µM).

LP1-AAV-miR SAA 1/2 KD *in vivo*

All animal studies were performed in accordance with German animal welfare legislation and in specific pathogen-free conditions in the animal facility of the Helmholtz Center, Munich, Germany. Protocols were approved by the Institutional Animal Welfare Officer (Tierschutzbeauftragter), and necessary licenses were obtained from the state ethics committee and government of Upper Bavaria. 8 weeks old male BALB/c mice purchased from the Jackson laboratory were maintained on a 12-h light/12-h dark cycle, in a specific pathogen-free animal facility with a climate-controlled environment and were fed a regular rodent chow ad libitum.

1 week prior to the start of the experiment mice were assigned into 3 groups and matched for BW and body composition: PBS (6 mice), AAV_LP1_miR Saa1/2 (10 mice) and AAV_LP1_miR Ctrl (10

mice). The respective AAVs were injected via tail vein and 4 weeks later 1x 10^5 C26 cells were subcutaneously implanted into the 2 AAV groups. Prior to the injections, BW and body composition was measured again and these data were used to calculate BW loss during experiment and % change in fat mass and lean mass at the end of the experiment.

The humane endpoint was defined as 10% BW loss. Mice were weighed every day and tumor sizes were measured every second day. Once one mouse, from either group, reached the 10% BW loss point, another mouse from the opposite group was also sacrificed. This mouse was paired based on BW loss. If none of the mice from the opposite group had reached a similar BW loss then a mouse with similar BW and composition, and preferably similar tumor size was selected. Some mice had to be sacrificed due to tumor size/aspect and one mouse from both tumor groups has been excluded from the analysis since they had to be sacrificed because of the tumor aspect shortly after the experiment began.

Mice were sacrificed by cervical dislocation and blood was collected into Serum-gel tubes (SAI). Tissues were weighed and snap frozen in liquid nitrogen.

Molecular biology & biochemistry

RNA isolation from cultured cells

Cell suspensions were centrifuged, supernatant was discarded and 1mL QIAzol (Qiagen) was added to the pellets that were subsequently transferred to RNase free tubes. The resulted lysates were incubated at RT for 5min after which 200µL chloroform were added. The mixtures were briefly vortexed and then centrifuged for 15min at 13000rpm, 4°C. The upper RNA containing phase was then mixed with 500µL of isopropanol and incubated at RT for 10min, followed by a 15min centrifugation step at 13000rpm, 4°C. The supernatant was discarded, and the pellet was washed with 1mL of 75% ethanol. The pellet was left to dry at RT and then dissolved in 30µL DNase/RNase free water. The samples were stored at -80°C until further use.

RNA isolation from tissues

Liver pieces were lysed with TRIzol using a tissue lyser. 200µL of chloroform were added and tubes were vortexed for 30sec then incubated 15min at RT and spin 10.000g for 10min at 4°C. 400µL of the upper phase were transferred to a 1.5mL tube and placed on ice. 240µL 96% EtOH was added and the contents were briefly vortex, and briefly spun down. The contents of the tubes were transferred to an EconoSpin column, spin 13.000g for 30 sec at RT. The columns were washed 2x with RPE buffer and then spun dry. The RNA was eluted in RNAse-free H_2O and stored at -80°C.

Determination of RNA concentration

To measure the RNA concentration, a NanoDrop ND-1000 spectrophotometer was used. Following the machine calibration, the absorbance of 1µL of the sample was measured at 260nm. The quality of the RNA was assessed by the 260/280 and 260/230 ratios, which indicate the presence of protein and chemical contaminants.

cDNA synthesis from mRNA

For the cDNA synthesis the QuantiTect ® Reverse Transcript Kit, by Qiagen, was used. 500ng-1µg of RNA were used as template and the reverse transcription was performed according to the manufacturer's instructions. The resulted cDNA was diluted 5-10x with DNase/RNase free water and stored at -20°C.

Quantitative RT-PCR

Quantitative detection of transcripts levels was achieved by using either the TaqMan® Gene Expression Assay (Applied Biosystems) or PowerUp SYBR Green (Applied Biosystems)

TaqMan

2.5µL cDNA were mixed with 7.5µL master mix containing 5µL 2x TaqMan® Gene Expression Master Mix, 2µL DNase free water and 0.5µL TaqMan® Probe per reaction.

SYBR green

2.5µL cDNA were mixed with 7.5µL master mix containing 5µL 2x PowerUp SYBR Green Master Mix, 0.5µL Primer Mix (5µM) and 2µL DNase free water per reaction.

Water was used as negative control and samples containing no reverse transcriptase served as controls for genomic DNA contamination. 10µL/well of this mixture were loaded on a MicroAmp Optical 96 well reaction plate and qRT-PCR was performed using the QuantStudio 6 Flex Real-Time PCR system (Thermo Fisher). Data was analyzed using the $2^{\Delta\Delta}$Ct method.

Dot blot analysis

1µL of protein lysates was spotted in triplicates on a nitrocellulose membrane (0.45µM). The membrane was allowed to dry for 10-15min, rinsed 4x with d2H_2O and blocked for 1hr. The membranes were then blocked in 5% skimmed milk in TBS-T for 1hr and incubated at 4°C overnight with the primary antibody in 5% skimmed milk TBS-T or 5% BSA as per supplier's instructions. The immunoblots were then washed 3x with TBS-T for 10min each and incubated with secondary antibody conjugated to horse radish peroxidase (HRP) at a dilution of 1:5.000 in 5% BSA or 5% skimmed milk for 1hr. The immunoblots were washed again and the ECL™ Western Blotting Detection Reagent was applied on them to visualize the chemiluminescence using the BioRad Chemidoc MP imaging system and afterwards quantified using Image Lab (Bio-Rad).

ELISA

Serum and liver ELISA

Mouse and human Elisa kits (see Material, Kits) were used for the quantification of SAA 1/2, Lcn2 and PAI-1 from serum samples. Serum samples were diluted as shown in Table 12 and the manufacturer's instructions were followed.

Table 12. Murine and human serum dilutions

	Mouse		**Human**	
	Control	Cachexia	Control	Cachexia
SAA 1/2	1:200	1:20000 (C26) 1:2000 (APC)	1:200	1:300 (CRC) 1:1000 (PDAC)
LCN2	1:100	1:2000 (C26) 1:2000 (APC)	1:25	1:50 (CRC) 1:50 (PDAC)
PAI-1	1:200	1:200 (C26)	1:25	1:25 (CRC) 1:25 (PDAC)

FLAG ELISA

To verify if the overexpressed proteins were secreted in the media. FLAG ELISA (Cayman Chemicals) has been performed on concentrated candidate-CM according to the manufacturer's instructions.

Generation of LP1-AAV-miR SAA 1/2

The miRNA targeting SAA1/2 were first cloned into a pcDNA6.2-GW/EmGFP-miR vector, and subsequently subcloned into a pdsAAV2-LP1-GFPmut-miR vector, which specifically targets the miRNA expression in the hepatocytes.

Initial miRNA-expression vector:

To generate the miRNA against SAA1/2, the "BLOCK-iT™ Pol II miR RNAi Expression Vector Kits" (Invitrogen, Catalog nos. K4935-00, K4936-00, K4937-00, K4938-00) was used. The single-stranded complementary miRNA-oligos were selected using Invitrogen´s RNAi designer (www.invitrogen.com/rnai), annealed and inserted into the pcDNA6.2-GW/EmGFP-miR vector (Gateway®-adapted expression vector for the expression of miRNA in mammalian cells under control of Pol II promoters) according to manufacturer's protocol. Annealing was performed by mixing equal volumes of the equimolar oligonucleotides in a microtube, together with the 10X ligation buffer provided in the kit. The tube was incubated at 95°C for 5min and allowed to slowly cool down at RT. Subsequently the resulting double stranded DNA was mixed together with the linearized pcDNA6-2-GW/EmGFP-miR vector and T4 ligase enzyme and was incubated for 5min at RT. The reaction was then used to transform TOP10 chemically competent *E.coli* bacteria. 2µL of the ligation was mixed into a vial of bacteria, and after 5min incubation on ice, the cells were heat-shocked for 30sec at 42°C. The cells were supplemented with 250µL of SOC medium and allowed to recover for 1 hour, shaking at 37°C. They were then plated on agar plates containing the specific antibiotics O/N. Several colonies were picked, amplified and the plasmids were purified with a mini-prep kit (Qiagen). They were sent for sequencing and the appropriate clones were selected for the following step.

Subcloning of miRNA dsDNA construct into pdsAAV2-LP1-GFPmut-miR vector:

Both vectors were digested with SalI and BglII. They were run in a 1% agarose gel, and the relevant bands were purified using a Gel Extraction MiniElute kit from Qiagen. From the pcDNA6.2-GW/EmGFP-miR reaction, the fragment corresponding to the dsDNA mirSAA1/2 was purified (insert), using the Qiagen MiniElute kit whereas the entire linearized vector was purified from the into pdsAAV2-LP1-GFPmut-miR reaction, using QIAquick gel extraction kit. The insert was ligated with the linear vector, at a 5:1 ratio. Specifically, the two DNA fragments were mixed with 5X ligation buffer and Ligase enzyme and incubated for 1hr at RT. A negative control reaction, was included by mixing the linearized plasmid with water instead of insert. Following ligation, SURE 2 Supercompetent cells (Stratagene) were transformed with pdsAAV2 constructs. The cells were thawed on ice and (100µL) and 2µL of 1,22M beta-mercaptoethanol was added. The cells were swirled gently every 2min while on ice for 10min. They were aliquoted into 50µL, and 2µL of ligation reaction was added. They were swirled gently and kept on ice for 30min. The cells were then heat-shocked at 42°C for 30sec and transferred back to ice for 2min. 200µL of preheated SOC medium was added and after a recovery phase of 1 hour at 37°C (shaking horizontally in a bacteria shaker) they were plated on an Ampicillin containing agar plate. Several colonies were picked and after amplification with a Miniprep kit, were sequenced to make sure there were no mutations. One of the clones was then amplified by Megaprep and a restriction test of intact inverted terminal repeats (ITRs) was performed. The pdsAAV2-LP1-GFPmut-miR Control and pdsAAV2-LP1-GFPmut-miR SAA1/2 vectors were shipped to the company Vigene, together with pDGΔVP, an adenoviral helper plasmid and p5E18 VD2/8-mut6, a plasmid with a mutation in a capsid protein which results in improved *in vivo* liver infection. The AAV particles were delivered 4 weeks later.

Annex

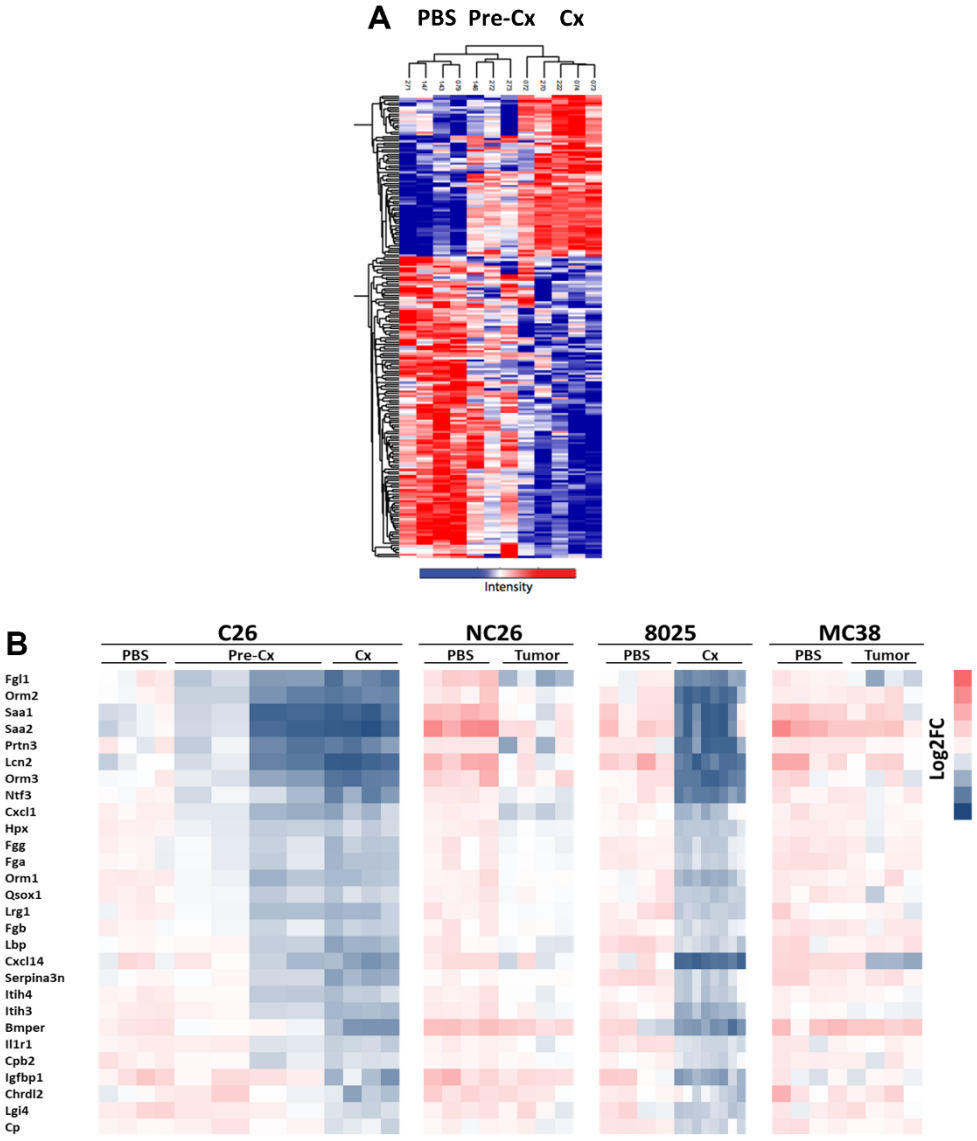

Annex 1. (A) Heatmap representation of secreted factors which are differentially regulated during cachexia development in C26 tumor-bearing mice versus PBS healthy controls. Abbreviations: Pre-Cx, pre-cachectic C26 animals; Cx. Cachectic C26 animals. Pre-Cx was defined as absence of BW loss, while Cx was defined as BW ≥10%. **(B)** Hepatocyte-derived factors are upregulated in cachectic (C26, CRC; 8025, PDAC) versus non-cachectic mouse models (NC26 and MC38, CRC). Log2FC of the twenty-eight candidates identified through RNA-seq and C26 serum proteome integration in the hepatocytes of tumor-bearing mice.

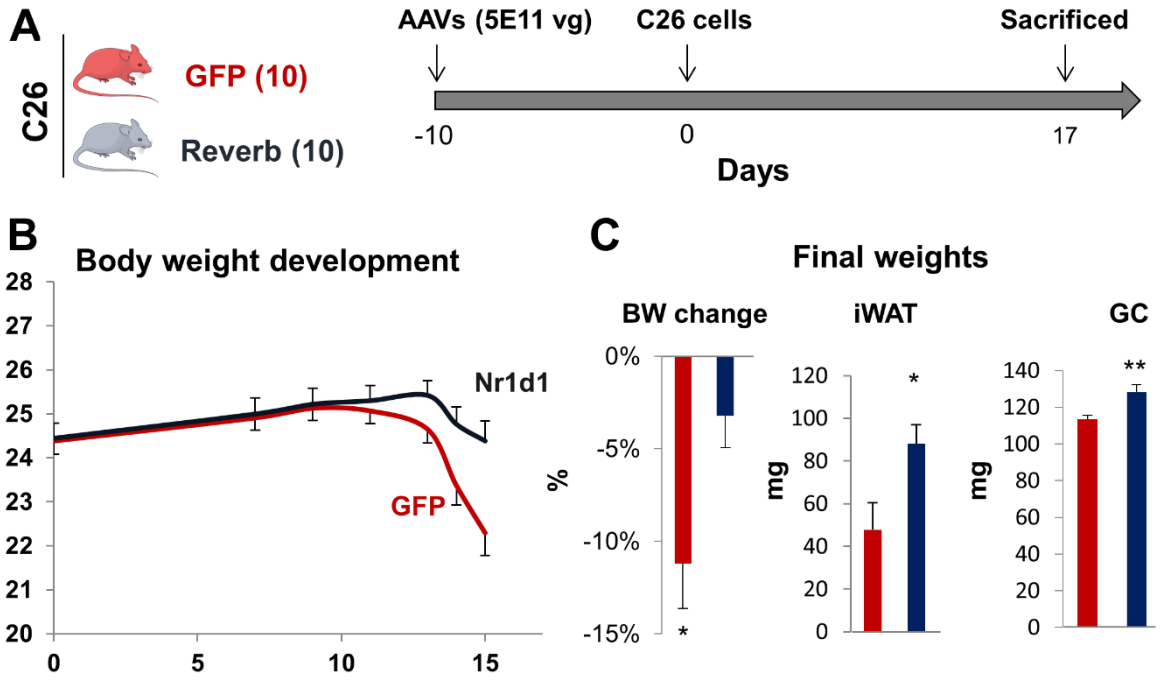

Annex 2. Hepatocyte specific restoration of Rev-erbα using the LP1-AAV system protects C26 mice from cachexia. (A) Schematics of experimental set-up. 10 days prior to C26 subcutaneous implantation, mice were injected with LP1-AAV-GFP or LP1-AAV-NR1D1 (Reverb). Mice were sacrificed based on BW loss **(B)** Body weight development (grams) over time (days). **(C)** BW loss, iWAT and GC mass in C26 GFP vs Reverb OE mice. Data are represented as mean ± SD, t.test: * p≤0.05, ** p≤0.01.

Publications

Data presented in this thesis pertaining to the *in vitro* effects of SAA 1/2 on tissue wasting and the *in vivo* data of the SAA 1/2 KD experiment were presented in the 12th international Conference on Cachexia, Sarcopenia and Muscle Wasting organized by the Society on Sarcopenia, Cachexia and Muscle Disorders in December 2019. The abstract 2-05, of which I was the first author, was published in the J Cachexia Sarcopenia Muscle. 2019 Dec; 10(6): 1378–1435

References

1. WHO, *Cancer fact sheet*. 2018: https://www.who.int/en/news-room/fact-sheets/detail/cancer.
2. Fearon, K., et al., *Definition and classification of cancer cachexia: an international consensus.* Lancet Oncol, 2011. **12**(5): p. 489-95.
3. Argiles, J.M., et al., *Cancer cachexia: understanding the molecular basis.* Nat Rev Cancer, 2014. **14**(11): p. 754-62.
4. Baracos, V.E., et al., *Cancer-associated cachexia.* Nat Rev Dis Primers, 2018. **4**: p. 17105.
5. Advani, S.M., et al., *Pharmacological management of cachexia in adult cancer patients: a systematic review of clinical trials.* BMC Cancer, 2018. **18**(1): p. 1174.
6. Porporato, P.E., *Understanding cachexia as a cancer metabolism syndrome.* Oncogenesis, 2016. **5**: p. e200.
7. Friesen, D.E., V.E. Baracos, and J.A. Tuszynski, *Modeling the energetic cost of cancer as a result of altered energy metabolism: implications for cachexia.* Theor Biol Med Model, 2015. **12**: p. 17.
8. Fearon, K.C., D.J. Glass, and D.C. Guttridge, *Cancer cachexia: mediators, signaling, and metabolic pathways.* Cell Metab, 2012. **16**(2): p. 153-66.
9. Mueller, T.C., et al., *Molecular pathways leading to loss of skeletal muscle mass in cancer cachexia--can findings from animal models be translated to humans?* BMC Cancer, 2016. **16**: p. 75.
10. Sandri, M., *Protein breakdown in muscle wasting: role of autophagy-lysosome and ubiquitin-proteasome.* Int J Biochem Cell Biol, 2013. **45**(10): p. 2121-9.
11. Sartori, R., et al., *Smad2 and 3 transcription factors control muscle mass in adulthood.* Am J Physiol Cell Physiol, 2009. **296**(6): p. C1248-57.
12. Fitzwalter, B.E. and A. Thorburn, *FOXO3 links autophagy to apoptosis.* Autophagy, 2018. **14**(8): p. 1467-1468.
13. Miyamoto, Y., et al., *Molecular Pathways: Cachexia Signaling-A Targeted Approach to Cancer Treatment.* Clin Cancer Res, 2016. **22**(16): p. 3999-4004.
14. Silva, K.A., et al., *Inhibition of Stat3 activation suppresses caspase-3 and the ubiquitin-proteasome system, leading to preservation of muscle mass in cancer cachexia.* J Biol Chem, 2015. **290**(17): p. 11177-87.
15. Egerman, M.A. and D.J. Glass, *Signaling pathways controlling skeletal muscle mass.* Crit Rev Biochem Mol Biol, 2014. **49**(1): p. 59-68.
16. Fouladiun, M., et al., *Body composition and time course changes in regional distribution of fat and lean tissue in unselected cancer patients on palliative care--correlations with food intake, metabolism, exercise capacity, and hormones.* Cancer, 2005. **103**(10): p. 2189-98.
17. Das, S.K., et al., *Adipose triglyceride lipase contributes to cancer-associated cachexia.* Science, 2011. **333**(6039): p. 233-8.
18. Stephens, N.A., et al., *Intramyocellular lipid droplets increase with progression of cachexia in cancer patients.* J Cachexia Sarcopenia Muscle, 2011. **2**(2): p. 111-117.
19. Beals, J.W., et al., *Obesity Alters the Muscle Protein Synthetic Response to Nutrition and Exercise.* Front Nutr, 2019. **6**: p. 87.

20. Hafidi, M.E., et al., *Adipogenesis: A Necessary but Harmful Strategy.* Int J Mol Sci, 2019. **20**(15).

21. Petruzzelli, M. and E.F. Wagner, *Mechanisms of metabolic dysfunction in cancer-associated cachexia.* Genes Dev, 2016. **30**(5): p. 489-501.

22. Agustsson, T., et al., *Mechanism of increased lipolysis in cancer cachexia.* Cancer Res, 2007. **67**(11): p. 5531-7.

23. Wang, H., et al., *Unique regulation of adipose triglyceride lipase (ATGL) by perilipin 5, a lipid droplet-associated protein.* J Biol Chem, 2011. **286**(18): p. 15707-15.

24. Sengenes, C., et al., *Involvement of a cGMP-dependent pathway in the natriuretic peptide-mediated hormone-sensitive lipase phosphorylation in human adipocytes.* 2003(0021-9258 (Print)).

25. Bonetto, A., et al., *The Colon-26 Carcinoma Tumor-bearing Mouse as a Model for the Study of Cancer Cachexia.* J Vis Exp, 2016(117).

26. Aulino, P., et al., *Molecular, cellular and physiological characterization of the cancer cachexia-inducing C26 colon carcinoma in mouse.* BMC Cancer, 2010. **10**: p. 363.

27. Bonetto, A., et al., *STAT3 activation in skeletal muscle links muscle wasting and the acute phase response in cancer cachexia.* PLoS One, 2011. **6**(7): p. e22538.

28. Schafer, M., et al., *Ataxin-10 is part of a cachexokine cocktail triggering cardiac metabolic dysfunction in cancer cachexia.* Mol Metab, 2016. **5**(2): p. 67-78.

29. Puppa, M.J., et al., *Gut barrier dysfunction in the Apc(Min/+) mouse model of colon cancer cachexia.* Biochim Biophys Acta, 2011. **1812**(12): p. 1601-6.

30. Baracos, V.E., *Bridging the gap: are animal models consistent with clinical cancer cachexia?* Nat Rev Clin Oncol, 2018. **15**(4): p. 197-198.

31. Michaelis, K.A., et al., *Establishment and characterization of a novel murine model of pancreatic cancer cachexia.* J Cachexia Sarcopenia Muscle, 2017. **8**(5): p. 824-838.

32. Talbert, E.E., et al., *Modeling Human Cancer-induced Cachexia.* Cell Rep, 2019. **28**(6): p. 1612-1622 e4.

33. Fong, Y., et al., *Cachectin/TNF or IL-1 alpha induces cachexia with redistribution of body proteins.* Am J Physiol, 1989. **256**(3 Pt 2): p. R659-65.

34. Schmidt, S.F., et al., *Cancer Cachexia: More Than Skeletal Muscle Wasting.* Trends Cancer, 2018. **4**(12): p. 849-860.

35. Reddel, C.J., et al., *Increased thrombin generation in a mouse model of cancer cachexia is partially interleukin-6 dependent.* J Thromb Haemost, 2017. **15**(3): p. 477-486.

36. Rohm, M., et al., *Energy metabolism in cachexia.* EMBO Rep, 2019. **20**(4).

37. Tsoli, M., et al., *Activation of thermogenesis in brown adipose tissue and dysregulated lipid metabolism associated with cancer cachexia in mice.* Cancer Res, 2012. **72**(17): p. 4372-82.

38. Rohm, M., et al., *An AMP-activated protein kinase-stabilizing peptide ameliorates adipose tissue wasting in cancer cachexia in mice.* Nat Med, 2016. **22**(10): p. 1120-1130.

39. Trefts, E., M. Gannon, and D.H. Wasserman, *The liver.* Curr Biol, 2017. **27**(21): p. R1147-R1151.

40. Vekemans, K. and F. Braet, *Structural and functional aspects of the liver and liver sinusoidal cells in relation to colon carcinoma metastasis.* World J Gastroenterol, 2005. **11**(33): p. 5095-102.

41. Peixoto da Silva, S., et al., *Cancer cachexia and its pathophysiology: links with sarcopenia, anorexia and asthenia.* J Cachexia Sarcopenia Muscle, 2020.

42. Goncalves, M.D., et al., *Fenofibrate prevents skeletal muscle loss in mice with lung cancer.* Proc Natl Acad Sci U S A, 2018. **115**(4): p. E743-E752.

43. Gulhar, R., M.A. Ashraf, and I. Jialal, *Physiology, Acute Phase Reactants*, in *StatPearls*. 2020: Treasure Island (FL).

44. Gruys, E., et al., *Acute phase reaction and acute phase proteins.* J Zhejiang Univ Sci B, 2005. **6**(11): p. 1045-56.

45. Rafferty, M., et al., *Reprioritisation of Liver Export Protein Synthesis in Patients with Decompensated Alcoholic Liver Disease.* J Hepatol Gastroint Dis 2016. **2**(3).

46. Fearon, K.C., et al., *Elevated circulating interleukin-6 is associated with an acute-phase response but reduced fixed hepatic protein synthesis in patients with cancer.* Ann Surg, 1991. **213**(1): p. 26-31.

47. Ueki, R., et al., *Role of Elevated Fibrinogen in Burn-Induced Mitochondrial Dysfunction: Protective Effects of Glycyrrhizin.* Shock, 2016. **46**(4): p. 382-9.

48. Quinton, L.J., et al., *Hepatocyte-specific mutation of both NF-kappaB RelA and STAT3 abrogates the acute phase response in mice.* J Clin Invest, 2012. **122**(5): p. 1758-63.

49. Sack, G.H., Jr., *Serum amyloid A - a review.* Mol Med, 2018. **24**(1): p. 46.

50. Uhlar, C.M. and A.S. Whitehead, *Serum amyloid A, the major vertebrate acute-phase reactant.* Eur J Biochem, 1999. **265**(2): p. 501-23.

51. Passey, S.L., et al., *Serum Amyloid A Induces Toll-Like Receptor 2-Dependent Inflammatory Cytokine Expression and Atrophy in C2C12 Skeletal Muscle Myotubes.* PLoS One, 2016. **11**(1): p. e0146882.

52. Jha, M.K., et al., *Acute Phase Protein Lipocalin-2 Is Associated with Formalin-induced Nociception and Pathological Pain.* Immune Netw, 2013. **13**(6): p. 289-94.

53. Li, C. and Y.R. Chan, *Lipocalin 2 regulation and its complex role in inflammation and cancer.* Cytokine, 2011. **56**(2): p. 435-41.

54. Abella, V., et al., *The potential of lipocalin-2/NGAL as biomarker for inflammatory and metabolic diseases.* Biomarkers, 2015. **20**(8): p. 565-71.

55. Gomez-Chou, S.B., et al., *Lipocalin-2 Promotes Pancreatic Ductal Adenocarcinoma by Regulating Inflammation in the Tumor Microenvironment.* Cancer Res, 2017. **77**(10): p. 2647-2660.

56. Feng, M., et al., *Lipocalin2 suppresses metastasis of colorectal cancer by attenuating NF-kappaB-dependent activation of snail and epithelial mesenchymal transition.* Mol Cancer, 2016. **15**(1): p. 77.

57. Rehwald, C., et al., *The iron load of lipocalin-2 (LCN-2) defines its pro-tumour function in clear-cell renal cell carcinoma.* Br J Cancer, 2020. **122**(3): p. 421-433.

58. Xu, M.J., et al., *Liver is the major source of elevated serum lipocalin-2 levels after bacterial infection or partial hepatectomy: a critical role for IL-6/STAT3.* Hepatology, 2015. **61**(2): p. 692-702.

59. Cesari, M., M. Pahor, and R.A. Incalzi, *Plasminogen activator inhibitor-1 (PAI-1): a key factor linking fibrinolysis and age-related subclinical and clinical conditions.* Cardiovasc Ther, 2010. **28**(5): p. e72-91.

60. Boncela, J., et al., *Acute phase protein alpha 1-acid glycoprotein interacts with plasminogen activator inhibitor type 1 and stabilizes its inhibitory activity.* J Biol Chem, 2001. **276**(38): p. 35305-11.

61. Iwaki, T., T. Urano, and K. Umemura, *PAI-1, progress in understanding the clinical problem and its aetiology.* Br J Haematol, 2012. **157**(3): p. 291-8.

62. Devaraj, S., D.Y. Xu, and I. Jialal, *C-reactive protein increases plasminogen activator inhibitor-1 expression and activity in human aortic endothelial cells: implications for the metabolic syndrome and atherothrombosis.* Circulation, 2003. **107**(3): p. 398-404.

63. Mo, A., et al., *Epigenomic Signatures of Neuronal Diversity in the Mammalian Brain.* Neuron, 2015. **86**(6): p. 1369-84.

64. Tang, J., et al., *Construction of a general albumin promoter reporter system for real-time monitoring of the differentiation status of functional hepatocytes from stem cells in mouse, rat and human.* Biomed Rep, 2017. **6**(6): p. 627-632.

65. Rose, A.J., et al., *Molecular control of systemic bile acid homeostasis by the liver glucocorticoid receptor.* Cell Metab, 2011. **14**(1): p. 123-30.

66. Miyake, T., J.C. McDermott, and A.O. Gramolini, *A method for the direct identification of differentiating muscle cells by a fluorescent mitochondrial dye.* PLoS One, 2011. **6**(12): p. e28628.

67. Su, Q. and G. Weindl, *Glucocorticoids and Toll-like receptor 2 cooperatively induce acute-phase serum amyloid A.* Pharmacol Res, 2018. **128**: p. 145-152.

68. Schakman, O., et al., *Glucocorticoid-induced skeletal muscle atrophy.* Int J Biochem Cell Biol, 2013. **45**(10): p. 2163-72.

69. Goldstein, I., et al., *Synergistic gene expression during the acute phase response is characterized by transcription factor assisted loading.* Nat Commun, 2017. **8**(1): p. 1849.

70. Gueugneau, M., et al., *Increased Serpina3n release into circulation during glucocorticoid-mediated muscle atrophy.* J Cachexia Sarcopenia Muscle, 2018. **9**(5): p. 929-946.

71. Bugge, A., et al., *Rev-erbalpha and Rev-erbbeta coordinately protect the circadian clock and normal metabolic function.* Genes Dev, 2012. **26**(7): p. 657-67.

72. Nathwani, A.C., et al., *Self-complementary adeno-associated virus vectors containing a novel liver-specific human factor IX expression cassette enable highly efficient transduction of murine and nonhuman primate liver.* Blood, 2006. **107**(7): p. 2653-61.

73. Hinderer, C., et al., *Severe Toxicity in Nonhuman Primates and Piglets Following High-Dose Intravenous Administration of an Adeno-Associated Virus Vector Expressing Human SMN.* Hum Gene Ther, 2018. **29**(3): p. 285-298.

74. Chandler, R.J., et al., *Genotoxicity in Mice Following AAV Gene Delivery: A Safety Concern for Human Gene Therapy?* Mol Ther, 2016. **24**(2): p. 198-201.

75. Breous, E., et al., *Inflammation promotes the loss of adeno-associated virus-mediated transgene expression in mouse liver.* Gastroenterology, 2011. **141**(1): p. 348-57, 357 e1-3.

76. Eppig, J.T., et al., *The International Mouse Strain Resource (IMSR): cataloging worldwide mouse and ES cell line resources.* Mamm Genome, 2015. **26**(9-10): p. 448-55.

77. Lee, J.W., et al., *Hepatocytes direct the formation of a pro-metastatic niche in the liver.* Nature, 2019. **567**(7747): p. 249-252.

78. Uchino, F., et al., *Experimental amyloidosis. Role of the hepatocytes and Kupffer cells in amyloid formation.* Appl Pathol, 1985. **3**(1-2): p. 78-87.

79. Birsoy, K., et al., *Analysis of gene networks in white adipose tissue development reveals a role for ETS2 in adipogenesis.* Development, 2011. **138**(21): p. 4709-19.

80. Bostrom, P., et al., *A PGC1-alpha-dependent myokine that drives brown-fat-like development of white fat and thermogenesis.* Nature, 2012. **481**(7382): p. 463-8.

81. Wang, X., et al., *LRG1 promotes angiogenesis by modulating endothelial TGF-beta signalling.* Nature, 2013. **499**(7458): p. 306-11.

82. Moser, M., et al., *BMPER, a novel endothelial cell precursor-derived protein, antagonizes bone morphogenetic protein signaling and endothelial cell differentiation.* Mol Cell Biol, 2003. **23**(16): p. 5664-79.

83. Oren, A., et al., *hCHL2, a novel chordin-related gene, displays differential expression and complex alternative splicing in human tissues and during myoblast and osteoblast maturation.* Gene, 2004. **331**: p. 17-31.

84. Yan, Q.W., et al., *The adipokine lipocalin 2 is regulated by obesity and promotes insulin resistance.* Diabetes, 2007. **56**(10): p. 2533-40.

85. Ramsay, T.G., L. Blomberg, and T.J. Caperna, *alpha 1-acid glycoprotein inhibits lipogenesis in neonatal swine adipose tissue.* Animal, 2016. **10**(5): p. 812-20.

86. Toonen, E.J., et al., *Activation of proteinase 3 contributes to Non-alcoholic Fatty Liver Disease (NAFLD) and insulin resistance.* Mol Med, 2016. **22**.

87. Kawakami, M., et al., *Human recombinant TNF suppresses lipoprotein lipase activity and stimulates lipolysis in 3T3-L1 cells.* J Biochem, 1987. **101**(2): p. 331-8.

88. Chen, L., et al., *Matrine improves skeletal muscle atrophy by inhibiting E3 ubiquitin ligases and activating the Akt/mTOR/FoxO3alpha signaling pathway in C2C12 myotubes and mice.* Oncol Rep, 2019. **42**(2): p. 479-494.

89. Archer-Lahlou, E., C. Lan, and R.T. Jagoe, *Physiological culture conditions alter myotube morphology and responses to atrophy treatments: implications for in vitro research on muscle wasting.* Physiol Rep, 2018. **6**(12): p. e13726.

90. Arambasic, J., et al., *Association of the glucocorticoid receptor with STAT3, C/EBPbeta, and the hormone-responsive element within the rat haptoglobin gene promoter during the acute phase response.* IUBMB Life, 2010. **62**(3): p. 227-36.

91. Xu, C., et al., *Direct effect of glucocorticoids on lipolysis in adipocytes.* Mol Endocrinol, 2009. **23**(8): p. 1161-70.

92. Feingold, K.R., et al., *Stimulation of lipolysis in cultured fat cells by tumor necrosis factor, interleukin-1, and the interferons is blocked by inhibition of prostaglandin synthesis.* Endocrinology, 1992. **130**(1): p. 10-6.

93. Hu, W., et al., *Lung cancer-derived extracellular vesicles induced myotube atrophy and adipocyte lipolysis via the extracellular IL-6-mediated STAT3 pathway.* Biochim Biophys Acta Mol Cell Biol Lipids, 2019. **1864**(8): p. 1091-1102.

94. Sun, Y., et al., *The Acute-Phase Protein Orosomucoid Regulates Food Intake and Energy Homeostasis via Leptin Receptor Signaling Pathway.* Diabetes, 2016. **65**(6): p. 1630-41.

95. Sun, W.Y., et al., *Lipocalin-2 derived from adipose tissue mediates aldosterone-induced renal injury.* JCI Insight, 2018. **3**(17).

96. Wong, H.R., et al., *Induction of lipopolysaccharide-binding protein gene expression in cultured rat pulmonary artery smooth muscle cells by interleukin 1 beta.* Am J Respir Cell Mol Biol, 1995. **12**(4): p. 449-54.

97. Hromas, R., et al., *Cloning of BRAK, a novel divergent CXC chemokine preferentially expressed in normal versus malignant cells.* Biochem Biophys Res Commun, 1999. **255**(3): p. 703-6.

98. Argiles, J.M., et al., *Inter-tissue communication in cancer cachexia.* Nat Rev Endocrinol, 2018. **15**(1): p. 9-20.

99. Hochepied, T., et al., *Alpha(1)-acid glycoprotein: an acute phase protein with inflammatory and immunomodulating properties.* Cytokine Growth Factor Rev, 2003. **14**(1): p. 25-34.

100. Gutsmann, T., et al., *Dual role of lipopolysaccharide (LPS)-binding protein in neutralization of LPS and enhancement of LPS-induced activation of mononuclear cells.* Infect Immun, 2001. **69**(11): p. 6942-50.

101. Zellmer, S., et al., *Transcription factors ETF, E2F, and SP-1 are involved in cytokine-independent proliferation of murine hepatocytes.* Hepatology, 2010. **52**(6): p. 2127-36.